Optimization and control of feed and transfer pumps

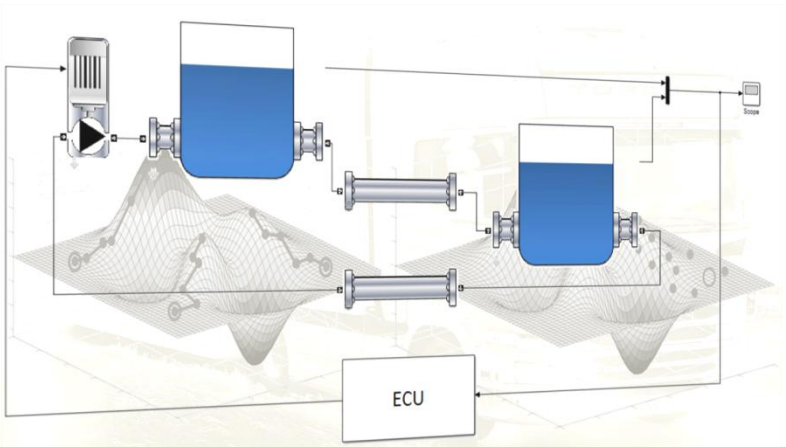

Carlos Jorques Moreno

LUND UNIVERSITY

SCANIA

Department of Automatic Control

Msc Thesis
ISRN LUTFD2/TFRT--5956--SE
ISSN 0280-5316

Department of Automatic Control
Lund University
Box 118
SE-221 00 LUND
Sweden

Printed in Sweden by Media-Tryck
Lund 2014

Abstract

A new low pressure fuel system implementation for Scania's trucks is being investigated. The main challenge consists in exchanging the mechanical pump with electrical pumps. The electrical pumps must then be controlled to supply exactly the demanded amount of fuel at the required pressure. System redundancy allows a lot of degrees of freedom influencing the final performance.

This thesis studies the factors influencing system's performance to design a controller that enhances its behavior. The physical basis of the elements in the system are investigated and stated with that purpose.

The system is analyzed and the output pressure and tank level are controlled by a LQG regulator giving successful results in reference tracking. Integral action is included for disturbance rejection and the states are estimated to overcome quantifications and noise from the signals. The disturbance rejection performance is improved by extending the regulator with a Smith Predictor for time delay compensation and including information about the engine mass-flow demand. The control actions are minimized by the tuning of the controller in order to extend component's life. The controller includes different modes for when an external action should be input e.g., when a diagnosis test must be run.

The optimization of free set-points is discussed and holistic criteria from experience is set. The result is that the system endurance is enhanced by running only two pumps when one does not provide higher efficiency. Results show that different pumps should be chosen in the final design for an improvement of the global efficiency.

Future work will consist in implementing the resulting controller in the real system built with actuators selected accordingly to the optimization results.

Acknowledgements

This thesis was developed in Scania AB at the Powertrain Combustion Control Software department (NESC), under Ola Stenlåås supervision, during the spring of 2014 for the Department of Automatic Control at Lund University.

I would like to express my gratitude to all the effort my superior at Scania, Ola, put on my work and all his support by continuous revision, comments and engagement through my learning process while developing my Master Thesis, always pushing me harder to do my best and helping me to focus on what was important for a successful project. In the same way, I want to thank you Sussana Jacobsson supervision, who kept following all my work and guided me with her help. Nonetheless, I want to thank all the people in NESC department at Scania for their help and good patience and support, especially Patrik Ederstål for his confidence on my work, and my mates at the department, André Ellenfjärd for his close collaboration while developing my project, Marcus Winroth for his help with fluid mechanics and good comments on the thesis, and Duca Cosmin for his continuous support.

I am very grateful to my examinator in Lund, Tore Hägglund, for his patient in answering questions and guiding me through the thesis formalities, and to my professors in Lund that taught me the knowledge to run this project, especially Anders Robertsson, Gunnar Lindstedt and Karl-Erik Årzén. I would like to appreciate the labor of my professor in Valencia, Juan José Pérez. I want to show appreciation to the assistance from my international coordinators in Valencia, Arantxa Querol Monforte, and in Lund, Christina Grossmann.

A very special thanks to the people who had encourage me to continue hard working even when things did not go very well, Knut Mårtensson whose support completely changed my working experience in Sweden, and my good friend Violeta de Lama, who have always listen to my success and failures during developing this project and who has been a big support. Also, I want to thank you all my friends in Valencia, Lund and Stockholm, who made living this experience abroad as feeling at home.

And the most important, I want to show my appreciation and gratitude to all my family, who always believed in my success, encouraged me to keep working hard with my failures, and support me taking difficult decisions.

Carlos Jorques Moreno

Södertälje, June 2014

Nomenclature

Symbol	Description	Unit
A	Area	[m^2]
c	Speed of sound in the medium	[m/s]
$C(s)$	Regulator transfer function	
C_v	Specific heat capacity	[J/(Kg·K)]
$d(t)$	Disturbance signal	[·]
D	Pipe internal diameter	[m]
$\frac{d}{dt}$	Total time derivative	[·/s]
$\frac{D}{Dt}$	Material time derivative	[·/s]
e	Specific energy	[J/kg]
e_x	Surface thickness	[m]
E	Young's modulus	[Pa]
$\boldsymbol{E}\{\}$	Variance operator	
f, f_D	Darcy friction factor	[-]
$f(t)$	Function over time	[·]
$f'(t)$	Derivative of a function over time	[·/s]
g	Gravity constant acceleration	[m/s^2]

Symbol	Description	Unit
$G(s)$	System's transfer function	
H, h	Absolute piezometric height	[m]
h_c	Convection proportional constant	[]
h_τ	Sampling time interval	[s]
Δh	Piezometric height difference	[m]
I	Current	[A]
J	Cost function	[-]
k	Piezometric height losses coefficient	[s^2/m]
k_{cond}	Thermal conductivity	[W/(m·K)]
K	Bulk's modulus	[Pa]
$Kest$	Kalman filter gain	
K_h	Piezometric height pump gain	[m/RPM]
K_P	Pressure to flow pump gain	[m/P^2]
K_q	RPM to flow pump gain	[m^3/(s·RPM)]
l	Pipe length	[m]
L	State-feedback gain	
$\tilde{L}$	Discrete state-feedback gain	
m	Fuel mass	[Kg]
$\dot{m}$	Fuel mass-flow	[Kg/s]
$\overrightarrow{M_L}$	Linear momentum as a vector magnitude	[N·m]
N	Pumps RPM	[RPM]
N_0	Nominal RPM for maximum pump efficiency	[RPM]
P, p	Absolute pressure	[Pa]
P_0	Nominal relative pressure for maximum pump efficiency	[Bar]
P_{amb}	Ambient pressure	[Pa]
ΔP	Pressure diference	[Pa]

Symbol	Description	Unit
q	Volumetric flow	[m^3/s]
$\dot{Q}_f$	Heat generated by the pumps	[W]
$\dot{Q}_H, \dot{q}_H$	Heat flow	[W]
r	Pipe losses coefficient	[s^2/m]
$r(t)$	Reference signal	[·]
R^2	Coefficient of determination	
Re	Reynolds's number	[-]
$\boldsymbol{s}$	Laplace variable	
$\boldsymbol{s}'$	Approximation of Laplace variable	
$S(s)$	Sensitivity transfer function	
t	Time	[s]
T_S	Temperature at the surface	[°C]
T_∞	Temperature far away from the surface	[°C]
$T(s)$	Complementary sensitivity transfer function	
ΔT	Temperature difference	[°C]
$u(t)$	Control action signal	[·]
U	Overall heat transfer coefficient	[$W/(m^2 \cdot K)$]
U_{eq}	Equivalent overall heat transfer coefficient	[$W/(m^2 \cdot K)$]
v	Flow mean velocity	[m/s]
v	Measurement noise	[·]
v_0	Bias velocity for filter's piezometric height	[m/s]
V	Volts	[V]
$\vec{V}$	Flow velocity vector	[m/s]
w	Internal state noise	[·]
$\dot{W}$	Work power into the control volume	[J/s]
$\dot{W}_f$	Work power done by the flow	[J/s]

Symbol	Description	Unit
x	Longitudinal-axis variable	[m]
$x(t)$	States signal	[·]
$\hat{x}(t)$	Estimated states	[·]
$y(t)$	Output signal	[·]
z	Physical flow height	[m]
$\boldsymbol{z}$	Discrete time variable	
$\forall$	Volume	[m^3]
$\forall_p$	Pump's internal volume	[m^3]
γ	Specific weight	[N/m^3]
τ	Time delay	[s]
Γ	Discrete control action to next states matrix	
Φ	Discrete state to next state matrix	
∇	Gradient operator	
η	Energetic efficiency	[-]
η_{vol}	Volumetric efficiency	[-]
μ	Dynamic fluid viscosity	[Pa·s]
μ_0	Nominal pump efficiency	[-]
μ_N	Pump efficiency gain from the RPM term	[RPM^{-2}]
μ_P	Pump efficiency gain from the pressure term	[Bar^{-2}]
ρ	Fluid density	[Kg/m^3]
ω	Frequency	[Hz]
ϵ	Fitting error	[·]
ν	Poisson's ratio	[-]
$\frac{\partial}{\partial t}$	Partial time derivative	[·/s]
$\frac{\partial}{\partial x}$	Partial derivative respect to the longitudinal-axis variable	[·/m]

Abbreviations

FP	Feed-pump
LQG	Linear Quadratic Gaussian regulator
LPH	Liters per hour
LSQ	Least Squares Quadratic
MT	Main-tank
RPM	Revolutions per minute
TP	Transfer-ump
TT	Tech-tank
XPI	Extreme Pressure Injection

Sub-index

cond	Referred to conduction heat transfer
conv	Referred to convection heat transfer
CS	Control surface
C∀	Control volume
eng	Engine
f	filter
flow	Referred to the fuel flow
heat	Referred to the heat flow
i	Numerical index
in	Into the system
out	Out of the system
q	Referred to the volumetric flow
T	Total

List of figures

Figure 1: Scania's fuel system. 20
Figure 2: Scania's fuel system with pump redundancy 21
Figure 3: Control volume for a pipe. 30
Figure 4: Tank control volume 31
Figure 5: Pump control volume 32
Figure 6: Simulink screen-shot used to simulate the system in the rig 33
Figure 7: Screw pump inside. 34
Figure 8: Manufacturer characteristics curves for a pump 35
Figure 9: Flow vs. Pressure and efficiency curves from manufacturer datasheet at different RPM's 36
Figure 10: Theoretical Flow vs. Pressure and efficiency curves fitted from manufacturer datasheet at different RPM's 39
Figure 11: Error for the efficiency model adjusted with parabolic LSQ curve fitting 39
Figure 12: Efficiency curves at a different speeds of two pumps working in parallel at 2 bar. 41
Figure 13: Efficiency curves at a different speeds of two pumps working in parallel at 6 bar. 41
Figure 14: Simplified system diagram for hydraulics modeling of the transfer sub-system 42
Figure 15: Simplified system diagram for hydraulics modeling of the feed sub-system. 43
Figure 16: Time plot for pumps' RPM and the tanks' levels 48
Figure 17: Experimantal correlation between pumps' RPM and flow. 49

Figure 18: Piezometric height provided by the pumps..... 50
Figure 19: Piezometric height loss of the main-filter and pre-filter..... 52
Figure 20: 3D plot for the transfer-pump Efficiency vs. RPM and Pressure 54
Figure 21: 3D plot for the feed-pump Efficiency vs. RPM and Pressure..... 55
Figure 22: 3D plots for the error of pumps efficiency fitting..... 56
Figure 23: Time plots for the temperature evolution of the main-tank. 58
Figure 24: Temperature difference self-evolution of the Main-tank. 59
Figure 25: Temperature difference self-evolution of the Tech-tank. 60
Figure 26: Pie charts for the transfer- and feed-pumps energy balance. 61
Figure 27: Optimal path for two parallel pumps handling 72
Figure 28: Closed-loop diagram for LQ designed state-feedback..... 78
Figure 29: Closed-loop for LQG controller 80
Figure 30: Closed-loop structure diagram for LQG control and IMC from Smith Predictor 81
Figure 31: Closed-loop for LQG controller with delay compensation from IMC of Smith-Predictor form and reference tracking by integral action 82
Figure 32: Effects to the control action and system output when limited control action is not accounted 82
Figure 33: Closed-loop diagram for LQG controller with delay compensation from IMC of Smith-Predictor form and reference tracking by augmented state integral action and antiwindup and bumpless transfer mode 83
Figure 34: Step response of the used pressure sensor 87
Figure 35: Optimal selector for handling two equal parallel pumps 88
Figure 36: Overview of the whole controller structure 89
Figure 37: Sensitivity and Complementary sensitivity functions Bode plots. 92
Figure 38: Cross-coupled sensitivity and complementary senstivity functions ... 93
Figure 39: Bode plots for the transfer functions between the Tech-tank level reference and the pressure reference to the control actions. 94
Figure 40: Temperature evolution over time for different constant fuel mass inside the Tech-tank 95
Figure 41: Temperature controller by generating the Tech-tank level reference . 96
Figure 42: Output pressure reference tracking for positive and negative steps of one bar in simulation 103
Figure 43: Output pressure reference tracking for positive and negative steps of one bar..... 104

Figure 44: Output pressure reference tracking for positive and negative steps of one bar with optimal handling 106
Figure 45: Pressure output when the pump start-up is not handle smoothly 106
Figure 46: Output pressure reference tracking for ±1.5 bar steps in simulation. 108
Figure 47: Output pressure reference tracking for ±1.5 bar steps 109
Figure 48: Output pressure reference tracking for ±1.5 bar steps with optimal handling 110
Figure 49: Output pressure disturbance rejection 112
Figure 50: Output pressure disturbance rejection with optimal pumps handling 113
Figure 51: Output pressure reference tracking and Tech-tank level 114
Figure 52: Output pressure disturbance rejection and Tech-tank level 115
Figure 53: Tech-tank and Main-tank level measurement in simulation with the estimation overlaid for ±10% level steps 116
Figure 54: Tech-tank and Main-tank level measurement in the rig with the estimation overlaid for ±10% level steps 117
Figure 55: Tech-tank level tracking 118
Figure 56: Tech-tank level tracking with optimal handling 119
Figure 57: Tech-tank temperature reference tracking 121
Figure 58: Temperature trakcing at different set points. 122

Contents

1. Introduction 19

1.1 Fuel system 19

1.2 Fuel system rig's layout 21

1.3 Statement of purpose 22

1.4 Document structure 22

2. System description 24

2.1 Fluid mechanics background 24

2.2 Heat transfer background 28

2.3 Equations for system's components 29

2.4 System simulation environment 33

3. Modeling experiments 34

3.1 Modeling of the pumps 34

3.2 Modeling of system's hydraulics 42

3.3 Pumps efficiency modeling 53
3.4 Modeling of heat transfer coefficients 56
3.5 Energy balance of the pumps 61
4. System model 63
4.1 Equations overview 63
4.2 Model for control 65
5. System optimization 67
5.1 Parallel pumps optimization 67
5.2 Pumps endurance 72
5.3 Tech-Tank level 74
6. Controller design 76
6.1 Controller requirements 76
6.2 Controller structure design 77
6.3 Feedback from estimated states 78
6.4 Disturbance rejection 81
6.5 Controller tuning 83
6.6 Controller overview 88
6.7 Tech-tank level reference generator 95
7. Controller implementation 97

7.1 Sampling time 97

7.2 Controller discretization 98

7.3 Time delays in discrete time 100

7.4 Real-time considerations 101

8. Results 102

8.1 Pressure control 102

8.2 Level control 116

8.3 Temperature control 120

9. Discussion and conclusions 123

9.1 Discussions 123

9.2 Conclusions 124

10. Recommendations and future work 127

11. Bibliography 129

Appendix A: Derivation of fluid mechanics equations 131

Reynolds's transport theorem 131

Mass conservation 132

Linear momentum conservation 135

Energy equation 137

Appendix B: *Simulink*® hydraulics library implementation 140

Numerical solution to ODE's 140

Implementation of system's components 143

Simulink® structure 156

Discussion 157

Appendix C: *Simulink*® hydraulics library examples 158

Example 1: Sudden opening of a constant height tank 158

Example 2: Sudden connection of two variable height tanks 160

Example 3: Connection of three tanks 163

Example 4: Transfer from one tank to another with a pump 165

1. Introduction

This chapter is an introduction where the fuel system is presented, the main intention with it and the reasons why it should be analyzed.

1.1 Fuel system

The fuel system, in cars or trucks, consists of the components that feed the fuel from the tank to the engine. Depending on the engine configuration, this can be done at low pressure (such as in systems based on carburetors) or high pressure (i.e., injection systems).

The usual solution was to use the engine shaft power to run a mechanical pump that moved the fuel to the engine. Due to its lack of controllability, the design was oversized and the overflow was sent back to the tank.

Modern cars have already moved towards systems where mechanical pumps have been replaced with electric ones. This approach brings more freedom in working at different steady-states designed to be optimal. The pumps used for fuel and oil circuits are usually of positive displacement, e.g., screw type. The reasons why are [1], [2]:

- It works at different flow rates providing a constant pressure.
- It is small enough to fit in the reduced available space.
- It has small vibrations and turbulence due to its axial and continuous flow.
- It has high efficiency for a viscous fluid (e.g., diesel).

Despite of modern cars, trucks usually still use a fuel system working with oversized mechanical pumps. In addition to the initial approach where one pump is used, this fuel system includes two pumps and an extra tank, which will further be called ‘Tech-tank’.

The intention of this intermediate tank is to act as a buffer where pre-filtered fuel is accumulated. Hence, two fuel sub-systems are included: one low-pressure pumping system from the fuel tank, further called ‘Main-tank’, which includes a pre-filter; and a higher pressure pumping from the tech-tank to the engine, which includes the main filter. Therefore, two electrical pumps are used: one moving fuel from the main-tank to the Tech-tank, which will further be called ‘Transfer-pump’ and another moving the fuel from the tech-tank to the engine, further called ‘Feed-pump’.

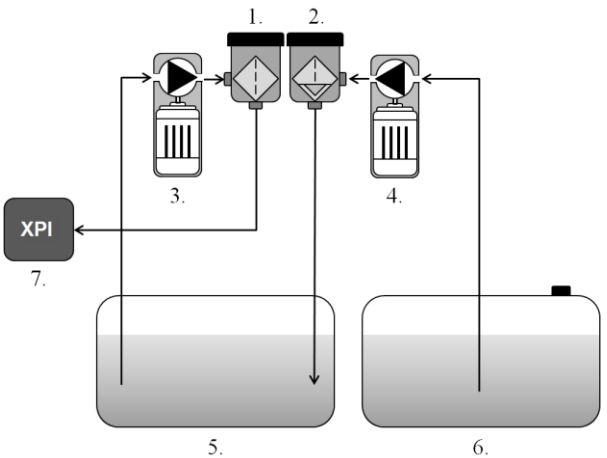

Figure 1: Scania’s fuel system: a transfer-pump (4) moves the fuel from the main-tank (6) through a pre-filter (2) to the tech-tank (5). This components integrate the ‘transfer-sub system’. Then, a feed-pump (3) push the fuel from the tech-tank trhough the main-filter (1) to the XPI (7). This second half is the ‘feed-subsystem’.

Component redundancy

Scania’s quality policy states that the pumps have to run without faulty behavior for minimum certain amount of working hours. That is not possible by means of

using only two pumps for the transfer- and feed- fuel systems. Therefore, pump redundancy is required and included in Scania's fuel system.

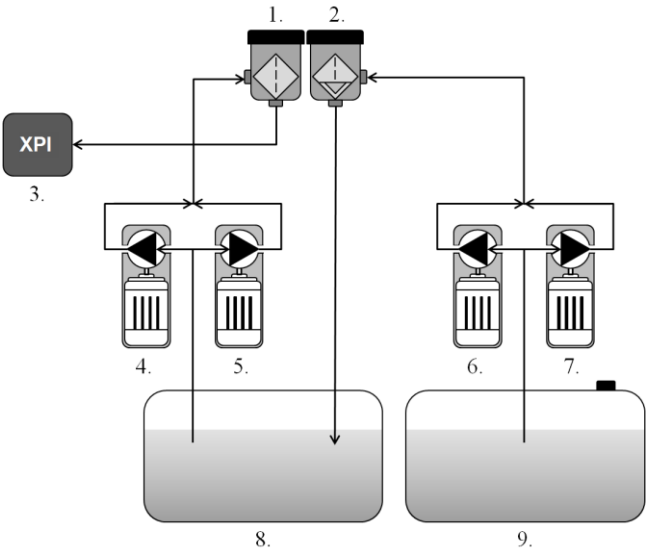

Figure 2: Scania's fuel system with pump redundancy. Two transfer-pumps in parallel (6 and 7) move the fuel from the main-tank (9) through a pre-filter (2) to the tech-tank (8). This components integrate the 'tansfer-subsystem'. Then, two feed-pumps in parallel (4 and 5) push the fuel from the tech-tank trhough the main-filter (1) to the XPI (3). This second half is the 'feed-subsystem'.

1.2 Fuel system rig's layout

The main fuel system layout was presented in Figure 2. Even though it can still suffer future modifications in the real implementation, a more detailed layout of the system includes flows-back to the tech-tank or main-tank and different sensors. Even though the sensors can be different, the overall system behavior is explained from this system's layout. Only an extra design will be considered, and it is with the feed-pumps placed inside the tech-tank, which mainly affects the fuel inside the Tehc-tank temperature.

1.3 Statement of purpose

With pump redundancy, the fuel system becomes much more complex. Furthermore, the handling of four pumps has many degrees of freedom influencing the system's behavior. These are some examples:

- Run the redundant pumps only when the others fail.
- Run all the pumps in parallel, which may allow using reduced-sized pumps.
- Use the tech-tank as a buffer and run the transfer-pumps at maximum in intervals to keep the tech-tank within lower and upper level limits.

These examples illustrates the complex the system can be handled. And the system can become more complex if other considerations are taken, e.g., if temperature control though recirculation is accounted.

Hence, a throughout study should be done. The purpose of this project is: *how should the fuel system be **designed** and **controlled** to behave optimally?* And the question that should first be answered: *How should **optimality** be defined?*

The outcomes of this Master Thesis are:

- Define suitable optimality criteria.
- Design the system according to these criteria, i.e., set a criterion for proper selection of transfer and feed pumps.
- Define optimal criteria to define the behavior of the system.
- Derive a controller to accomplish the optimal behavior.
- Implement the controller and test it in a rig.
- Set the conclusions from the experimental results and recommendations for implementing the system in the trucks.

1.4 Document structure

The procedure for the fuel system study was presented in this chapter.

In ***Chapter 2.*** , the system is depicted and the equations that describe the components' behavior are studied from the mechanical point of view, which is reviewed in order to understand the limitations imposed on this system description approach. The equations are used to build a simulation environment in *Simulink*® that will be further used to compare different system layouts and controller implementations.

In ***Chapter 3.*** , the rig where the real system runs is described. Modeling experiments are designed and run in the system's rig to obtain real data for fitting the models in Chapter 2, for every single component of interest (pumps calibration, pipes loses, filters loses and tank's heat transfer). The equations are analyzed so that differences can be explained.

In ***Chapter 4.*** , a suitable and simple model from the experimental conclusions is finally chosen for the controller design. An extension of the model is discussed for diagnosis purposes.

In ***Chapter 5.*** , the optimal handling of the system is discussed in order to support the controller requirements.

In ***Chapter 6.*** , the controller is design to overcome the different problems in the real system and make it behave as required. Different control structures are discussed in accordance to system constraints, sensors, actuators, disturbances and uncertainties.

In ***Chapter 7.*** , the controller is adapted and discretized for its implementation. Related problems are commented too.

In ***Chapter 8.*** , the overall results are discussed and recommendations of the system design are depicted for components selection and handling.

Chapter 9. consists in the discussion of the project results.

In ***Chapter 10. ,*** the final recommendations and future work are commented.

2. System description

In this chapter the equations that model the system behavior are studied. The system is first presented and the required theory is discussed. Secondly, the fluid hydraulics background is reviewed and applied to system's components. Finally, the derived equations are applied to the different components of the system and the Simulink® model for simulation is showed.

2.1 Fluid mechanics background

To give an overall behavior of the system, the differential form of the fluid mechanics equations for the continuous medium [3] are formulated from the Euler's perspective instead of the Lagrangian, typically used in the classical mechanics [3]. This uses the concept of control volume and the Reynolds transport theorem is applied to the differential equations, see Appendix A for more details. The results are suitable integral equations to be applied in the system's components where the control volume is properly defined.

Further on, lower-case letters will refer to magnitudes per mass unit (i.e., 'e' refers to the energy per mass unit), while capital letters refers to the magnitudes for the whole control volume (i.e., 'E' is the total energy in that volume).

Fluid model for fuel

As a previous step for the derivation of the equations, some assumptions for the fuel as a fluid should be considered.

The fluid mechanics theory is enough to explain the fuel behavior in the system due to the fact that its thermodynamic state (density, pressure and temperature) only changes in a reduced interval with constant properties. Hence, the fuel is considered a ***viscous incompressible fluid*** with constant properties within the temperature range, this is, constant density ρ and constant specific heat capacity C_v at a constant volume, which is typically the case for closed pipes fully filled circuits, where the volume is constant and limited by its geometry.

The flow is considered ***quasi-stationary one-dimensional flow***. This means, its properties are only studied in one geometrical dimension (along the pipe) and it is considered to have homogeneous properties in the cross-section, i.e., the velocity depending on the pipe radius is considered constant. These considerations derive how the friction losses analysis is done: as a viscous fluid, it generates fiction losses that will be studied from the Darcy-Weisbach [3] experimental formulation. This will be explained in next section.

The summary of the properties that defines and describes the fuel behavior as a fluid are:

- ***Density, ρ***. Defined at a normal pressure (1atm) and temperature (25°C), and considered constant within the working range. The units used are Kg/m^3.
- ***Dynamic viscosity, μ***. Defined at a normal pressure (1atm) and temperature (25°C), and considered constant within the working range and linear since the fluid is considered Newtonian. The units used are Pa·s.
- ***Poisson's ratio, v.*** It relates the deformation in the other two dimensions when a material is compressed in one direction. It is dimensionless and it usually varies between 0 and 0,5.
- ***Young's modulus, E***. It relates the elastic deformation with the force applied to one direction. The units used are Pa.
- ***Bulk's modulus, K***. It relates the volume change when uniform compression is applied. The units used are Pa.
- ***Specific heat capacity, C_v***. It is the energy required for a one Kelvin degree increasing in temperature for one unit mass of material. The units used are J/(Kg·K).

Darcy-Weisbach equation

The usual way for accounting the fluid's viscous effects in hydraulic systems is by means of the Darcy-Weisbach formulation. This is an empirical formula that relates the loss of pressure to the friction along a pipe. This formulation uses a quasi-one-dimensional flow where only the mean velocity is used. That is consistent with the previous assumptions.

The general formula for pipe with a circular cross section (as the ones used in trcuks), is [3]:

$$\Delta P = f_D \cdot \frac{l}{D} \cdot \rho \cdot \frac{v^2}{2} \tag{2.1}$$

Where *l* is the length of the pipe, *D* is its diameter, ρ is the fluid's density and *v* is the mean velocity in the cross section of the pipe. f_D is Darcy's friction factor, further on called *f*. Its value can be obtained in different ways, and it is dependent as well on the flow velocity. Different experimental formulas have been derived [3] as well as the extended graphical method of Moody's chart [3]. In this study, the formula used is the Swamee-Jain because it is straight forward to obtain the friction factor without iterations:

$$f = 0.25 \cdot \left[log_{10} \left(\frac{\varepsilon}{3.7D} + \frac{5.74}{Re^{0.9}} \right) \right]^{-2} \tag{2.2}$$

In this equation, ε is the roughness height (m), D pipe's diameter and Re Reynolds's number. This equation is suitable for turbulent flows.

Reynolds's number is used, among other things, to distinguish between laminar or turbulent flow. It is computed for a circular pipe as [3]:

$$Re = \frac{\rho D \cdot v}{\mu} \tag{2.3}$$

The flow is usually turbulent for *Re>4000* and laminar for *Re<2300*. For values between them, the flow is said to be transition flow, and the value of the friction factor can be very uncertain depending on flow conditions and fluid. In

that case, the friction factor will be interpolated from the Swamee-Jain formulation for turbulent flow and the value for laminar flow, which is computed as:

$$f = \frac{64}{Re} \tag{2.4}$$

Fluid mechanics equations

The equations from the incompressible Navier-Stokes equations [1] (see Appendix A for detailed derivation of the equations) are:

- **Mass conservation:** the change in the mass equals the difference between the mass-flows in and out:

$$\frac{dm}{dt} = \sum \dot{m}_{in} - \sum \dot{m}_{out} \tag{2.5}$$

- **Continuity equation,** where *c* is the speed of sound in the medium:

$$0 = \frac{\partial p}{\partial t} + \rho c^2 \frac{\partial v}{\partial x} \tag{2.6}$$

- **Momentum conservation**, including the dissipation term from the Darcy-Weisbach equation:

$$0 = \frac{\partial v}{\partial t} + v\frac{\partial v}{\partial x} + \frac{1}{\rho}\frac{\partial p}{\partial x} + g\frac{\partial z}{\partial x} + \frac{f v|v|}{2D} \tag{2.7}$$

- **Energy conservation,** combining the previous equations plus the thermal energy:

$$e = C_v \Delta T + \frac{P}{\rho} + \frac{1}{2}v^2 + gz \tag{2.8}$$

$$\begin{aligned} &\frac{d}{dt}\int \left(C_v T + \frac{P}{\rho} + \frac{1}{2}v^2 + gz\right)\rho d\forall = \\ &= \dot{Q_H} + \dot{W} - \dot{m}_{in} f \frac{L}{2D} v^2 + \sum \dot{m}_{in} e_{in} - \sum \dot{m}_{out} e_{out} \end{aligned} \tag{2.9}$$

2.2 Heat transfer background

The energy equation includes a heat flux term that was assumed to be known. In this section, the global objective is to review the theory around the estimation of the heat transfer. Since mainly the heat transfer in the tanks will be considered, the overlying theory will focus on conduction through a thick surface and convection on a surface. Therefore, pipes will be considered adiabatic and any other source of thermal energy will be directly estimated e.g., the pumps or flow back the XPI system.

Conduction through a surface

The heat flux goes through the tank walls by means of conduction mechanism. The considered cases are one dimensional in the normal axis to the wall. Hence, Fourier's law is set for one dimensional conduction in a planar medium with constant properties and no heat generation. The heat flux can be computed for a material with k_{cond} material, simply with one-dimensional Fourier's law for a unitary area:

$$\dot{q}_{H_{cond}} = -\frac{k_{cond}}{e_x}\Delta T \tag{2.10}$$

Convection

Only the simplest case of convection will be considered. From this approach, the convection law comes from Newton's cooling law:

$$\dot{q}_{H_{conv}} = h_c \cdot (T_S - T_\infty) \tag{2.11}$$

The main problem here is to estimate the convection coefficient *h*. This is estimated by using different formulation depending on the type of convection and flow regime: natural or forced convection, laminar or turbulent flow [4].

If a multilayer system is studied, the heat flux across all its surfaces can be expressed from the overall heat transfer coefficient, computed as:

$$U = \frac{1}{\frac{1}{h_{c_{in}}} + \sum_{i=1}^{n} \frac{e_i}{k_i} + \frac{1}{h_{c_{out}}}} \tag{2.12}$$

And therefore, the total heat flux is computed as:

$$\dot{Q}_H = U \cdot A \cdot \Delta T \tag{2.13}$$

This is used to account for all the heat transfer modes. In this case, conduction in the film layer is neglected as well as radiation, due to the low temperatures at with the system operates.

2.3 Equations for system's components

Pipes

The connections of the pumps and the tanks are done with pipes. The flow transients are explained by the water-hammer model. In this approach, the continuity and momentum conservation equations from their differential formulation are the main equations used. The boundary conditions must be obtained from where the pipe or pipe branch are connected, and will be different depending on if it is a tank, open valve, etc.

- Continuity and momentum conservation for a pipe:

$$0 = \frac{\partial p}{\partial t} + \rho c^2 \frac{\partial v}{\partial x} \tag{2.14}$$

$$0 = \frac{\partial v}{\partial t} + v\frac{\partial v}{\partial x} + \frac{1}{\rho}\frac{\partial p}{\partial x} + g\frac{\partial z}{\partial x} + \frac{f}{2D}v|v| \tag{2.15}$$

This pair of equations forms a system of PDE that will be further solve by the method of characteristics (see Appendix B).

- Energy conservation. The heat exchange in pipes is neglected against the heat flow in the tanks and pumps, so the energy equation turns to the well-known Bernoulli's equation [3]:

$$\left(\frac{p_{out}}{\rho}+\frac{1}{2}v_{out}^2\ +gz_{out}\right)+\frac{fL}{2D}v|v|=\left(\frac{p_{in}}{\rho}+\frac{1}{2}v_{in}^2\ +gz_{in}\right) \tag{2.16}$$

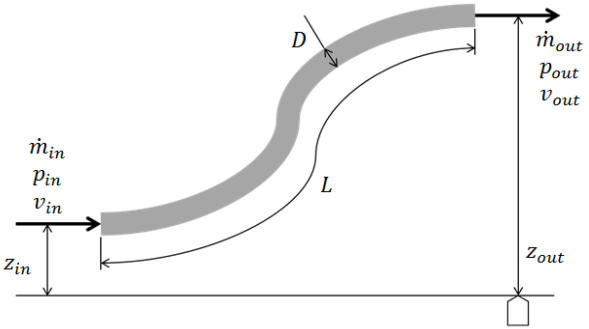

Figure 3: Control volume for a pipe. Only one input and one output flow are considered. The pipe properties and flow parameters are indicated.

Tanks

The properties inside the tanks are considered homogeneous i.e., constant temperature and density in the whole volume. In this approach, a constant area is considered and the pressure is determined by the atmosphere pressure as they are considered opened. In addition, an external source of heat is considered, that is a consequence of the temperature difference between the fluid in the tank and the temperature of tank's surroundings.

- Mass conservation:

$$\dot{m}=\sum_{i_{in}=1}^{n_{in}}\dot{m}_{i_{in}}-\sum_{i_{out}=1}^{n_{out}}\dot{m}_{i_{out}} \tag{2.17}$$

- Tank level:

$$\dot{z}=\frac{\dot{m}}{A\cdot\rho} \tag{2.18}$$

- Pressure boundary condition, due to the fact that tanks are opened:

$$P=P_{amb}\cong 1bar \tag{2.19}$$

- Conservation of energy. The flow energy in and out the tank is neglected against the potential, and the inputs are assumed to be always higher than the tank level, therefore the energy equation reduces to a thermal balance:

$$mC_v \cdot \dot{T} = \dot{Q}_H + \sum_{i_{in}=1}^{n_{in}} \dot{m}_{i_{in}} C_v \left(T_{i_{in}} - T\right) - \sum_{i_{out}=1}^{n_{out}} \dot{m}_{i_{out}} C_v \left(T_{i_{out}} - T\right) \qquad (2.20)$$

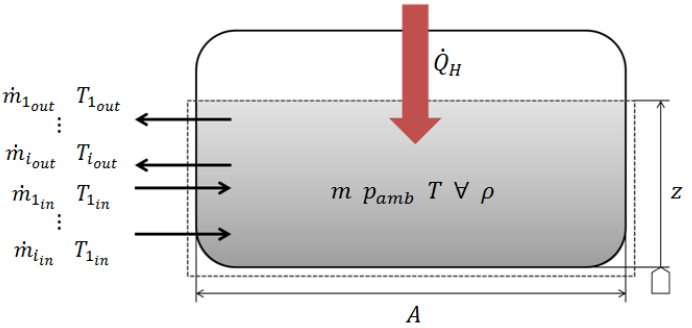

Figure 4: Tank control volume limited by dashed line. Undetermined number of inputs and outputs are shown as well as tank's fluid parameters. A heat flow is represented by a solid arrow into tank's fluid. Geometric properties of the tank are indicated.

The heat flux is considered positive when goes into the tank and negative otherwise. The equation (2.13) is used for its computation. Therefore, the overall heat transfer coefficient (2.12) must be first computed from the multilayer heat system. It is not worthwhile to compute it theoretically as it will have big errors as the conditions in the real system may suffer big changes e.g., stopped truck vs. truck running on a highway. Hence, the heat into the tank is left and only its influence on Tech-tank fuel's temperature is accounted as a disturbance.

Pumps

Every pump can be studied from the same point of view, even if they have different power. The pumps are of the positive displacement type, which means that the output pressure is selected by the flow circuit, while is the mass flow what can be controlled from the motor speed i.e., RPM.

The pumps are considered as a quasi-stationary process, this is, it does not contain any variable mass within it: all input mass flow is the same as output. However, this flow changes depending on pump speed. The equations applied to the pump as a control volume are:

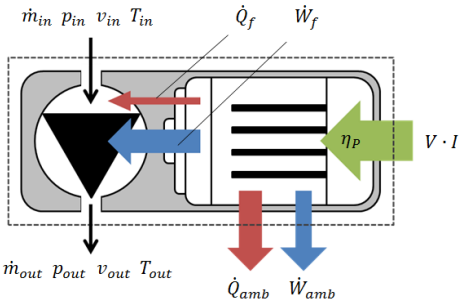

Figure 5: Pump control volume, determined by the dashed line. Flow inputs and outputs parameters are depicted. Energy balanced is showed in solid arrows: electrical energy is put into the system and it is transformed to heat and work to the fluid and to the ambient.

- Mass conservation:

$$\dot{m}_{in} = \dot{m}_{out} = \dot{m} \tag{2.21}$$

- Conservation of energy. The mass-flow in and out has to be the same from the mass continuity principle if there is no accumulation inside the pump. The pump sets the flow velocity, and the circuit determines the pressure drop necessary to get that velocity, which determines the required energy. Therefore, the equation can be decoupled in the thermal and hydraulics effects:

$$\dot{m} C_v \Delta T = \dot{Q}_f \tag{2.22}$$

$$\dot{m} \frac{\Delta p}{\rho} = \dot{W}_f \tag{2.23}$$

The actual flow q and the RPM N, are related by the volume displaced at each revolution, which is determined experimentally. The electrical energy that is converted into flow energy (i.e., efficiency), the heat to the fluid and heat to the surroundings are determined experimentally as well (see section 3.1 for more details).

2.4 System simulation environment

With the simulation environment created from the previous equations (see Appendix B for more details) a *Simulink*® model is used to simulate the fuel system. The library allows to build different hydraulic system topologies. Despite of its limitations, the results shows properly and accurate results that validate the library for further modeling of different systems (see Appendix C for some example). The model used for the system, that matches the one on the rig, is shown in Figure 6:

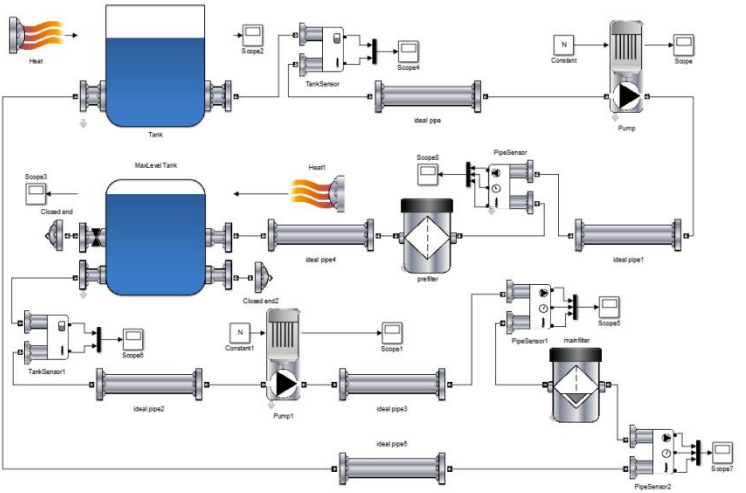

Figure 6: Simulink screen-shot used for different systems simulations. In the picture the different blocks used and how to connect them is shown.

The parameters used for the simulation should be adapted to match the experimental results. This is done by proper parameter setting of the component's blocks.

3. Modeling experiments

In this chapter, the theory from previous chapter is used to explain the experimental behavior. Firstly, the pumps are modeled from the datasheet. Experiments are then designed to model experimentally the pumps, the tanks and the hydraulic circuits.

3.1 Modeling of the pumps

The working characteristics of a positive displacement pump are, in an ideal case:

- Flow proportional to the rotor speed according to the volume it has.
- Pressure determined by the hydraulic circuit.

Figure 7: Screw pump indside. The case holds the screews that moves the fluid along them increasing its pressure. The axe torque is generated by a brushless DC motor. (Source: http://www.knoll-mb.de/).

The approach for modeling the pumps will be: first, to analyze the data from the datasheets model, generate a suitable model and then compare this model to the experimental results, obtained from adequate experiments in the rig, explained in section 3.2

Pump characteristics

In order to obtain a model, the steady-state pump characteristic is first analyzed. The manufacturer of the pumps is Nichols Portland. The provided characteristic curves are shown below [2].

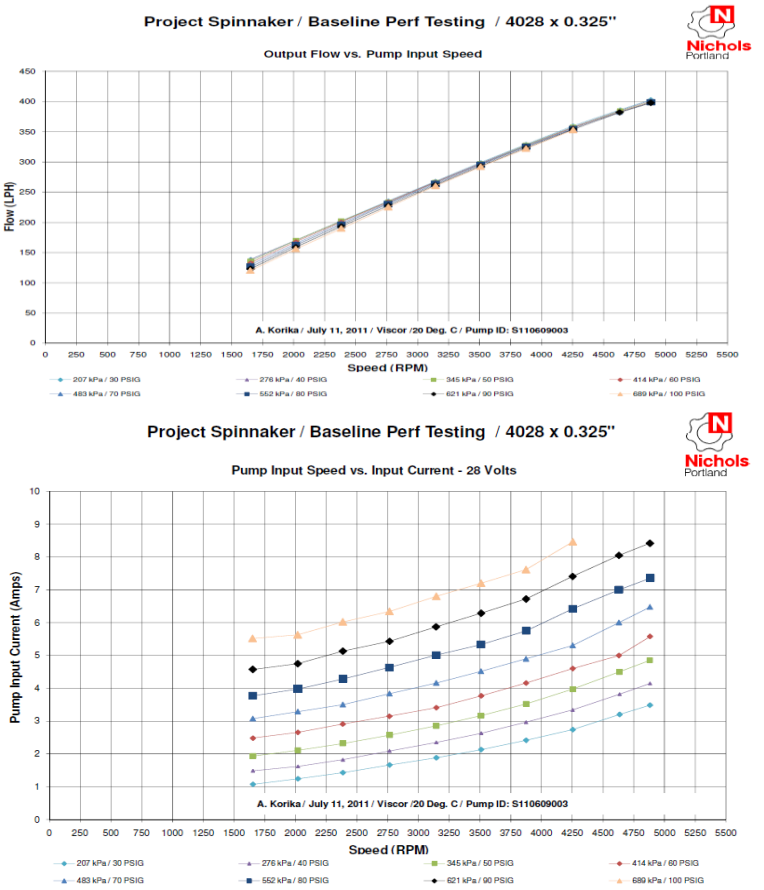

Figure 8: Manufacturer characteristics curves for a positive displacement pumps [2]. The first graph shows the flow (LPH) against the pump RPM working at different pressure difference between inlet and outlet. The second graph shows the consumed current for the same RPM and at different pressures difference.

For an efficiency analysis, the efficiency curves should be obtained. Hence, the data from the manufacturer is extracted and used to calculate those points.

From the graphs, the points (RPM, flow, and input current) at the different pressures are used to generate the map (Flow, Pressure) for each RPM, and the efficiency is calculated according to:

$$\eta = \frac{q \cdot \Delta P}{V \cdot I} \tag{3.1}$$

With the flow (q) in m^3/s, pressure difference (ΔP) in Pa, voltage (V) in volts and the current (I) in amperes. As the pump curves work with volumetric flow, it will still use it. The resulting points and curves for the real pump are shown in Figure 9:

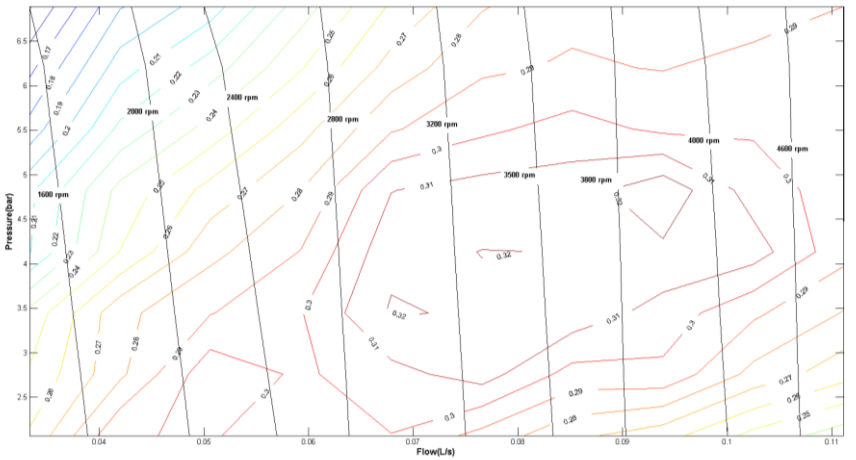

Figure 9: Flow vs. Pressure and efficiency curves from manufacturer datasheet at different RPM's.

As can be seen, the efficiency depends on the working point (Q, ΔP) and it is set by the pump speed for the flow and the hydraulic circuit for the pressure.

Theoretical modeling of one pump

If considering an ideal positive displacement pump, the equations that model its behavior are:

$$P = cnt \tag{3.2}$$

$$q_{pump} = \eta_{vol} \cdot \forall_p \cdot \frac{1}{60} \cdot N \tag{3.3}$$

Where q_{pump} is the volumetric flow in m^3/s, $\forall_p$ the displaced volume in m^3 for a full loop, and N is the pump speed in rpm. η_{vol} is the volumetric efficiency.

However, this model does not explain the losses due to the pressure difference that the pump supplies. In addition, the volume of the pump is not depicted in the datasheet, so a linear-in-parameters equation can be extrapolated from the experimental data. A simple way for fitting the theoretical curve to the real one is by using the least squares method (LSQ), which can be applied algebraically due to its linearity. The linear-in-parameters model is:

$$q_{pump} = K_{q_{Pump}} \cdot N + K_{P_{Pump}} \cdot \Delta P^2 \tag{3.4}$$

The algebraic solution is:

$$\begin{bmatrix} K_{q_{Pump}} \\ K_{P_{Pump}} \end{bmatrix} = \begin{bmatrix} N_1 & P_1^2 \\ \vdots & \vdots \\ N_n & P_n^2 \end{bmatrix}^{\dagger} \cdot \begin{bmatrix} Q_1 \\ \vdots \\ Q_n \end{bmatrix} \tag{3.5}$$

In this equation, $A^{\dagger}$is the Moore-Penrose pseudoinverse [5] matrix:

$$A^{\dagger} = (A^T \cdot A)^{-1} \cdot A^T \tag{3.6}$$

The LSQ method gives, for one pump according to the datasheet:

$$K_{q_{Pump}} = 2.354 \cdot 10^{-5} \frac{l/s}{rpm} \tag{3.7}$$

$$K_{P_{Pump}} = -6.961 \cdot 10^{-5} \frac{l/s}{bar^2} \tag{3.8}$$

For the efficiency theoretical modeling, the surface is modeled as a elliptic paraboloid, which can approximate the real pump efficiency with sufficient accuracy. This model, almost linear-in-parameters, is:

$$\eta = \mu_N \cdot (N - N_0)^2 + \mu_P \cdot (\Delta P - P_0)^2 + \mu_0 \tag{3.9}$$

Here, N_0 and P_0 determines the vertex of the paraboloid, which can be obtained from the maximum efficiency in the experimental curves, i.e., $N_0 = 3800$ *RPM* and $P_0 = 4.14$ *bar*. Hence, a linear-in-parameters equation can be fitted with the same algebraic LSQ procedure. The values obtained are:

$$\mu_N = -2.2677 \cdot 10^{-8} \tag{3.10}$$

$$\mu_P = -5.995 \cdot 10^{-3} \tag{3.11}$$

$$\mu_0 = 0.31867 \tag{3.12}$$

In summary, the pump is characterized by the next equations:

$$q_{pump} = 2.35 \cdot 10^{-5} \cdot N - 6.96 \cdot 10^{-5} \cdot \Delta P^2 \tag{3.13}$$

$$\eta = -2.27 \cdot 10^{-8}(N - 3800)^2 - 5.99 \cdot 10^{-3}(\Delta P - 4.14)^2 + 0.32 \tag{3.14}$$

With the flow q_{pump} in m^3/s, N in RPM, ΔP in Pa and the efficiency in modulus one, i.e., $\eta \in [0,1]$. These expressions will further allow to work from an analytical point of view in order to obtain the expressions for two pumps.

The plot of these equations gives the theoretical curves for the used pump:

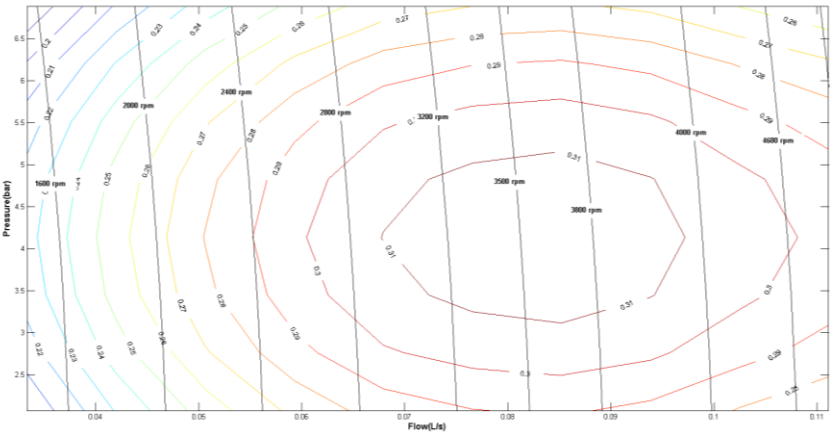

Figure 10: Theoretical Flow vs. Pressure and efficiency curves fitted from manufacturer datasheet at different RPM's. Equations (3.13) and (3.14).

In order to determine the errors of the real and theoretical curves, the error is computed:

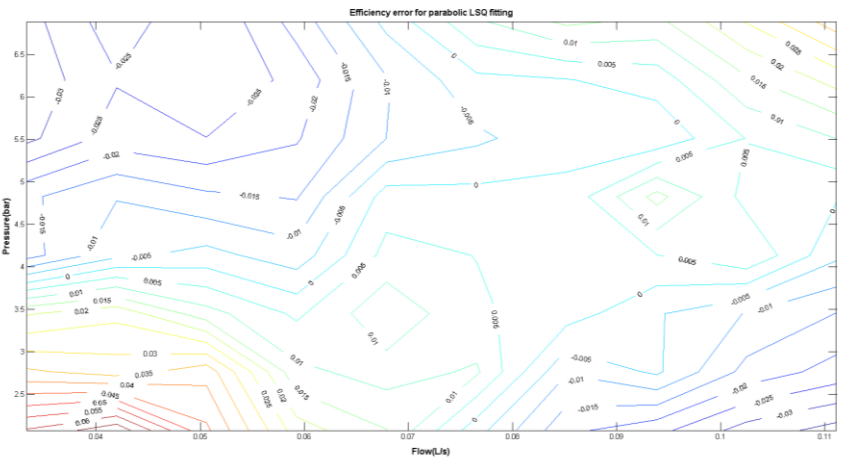

Figure 11: Error for the efficiency model adjusted with parabolic LSQ curve fitting

The total square error is:

$$\epsilon^2 = \iint_{S=(q,P)} E(q,P)^2 \cdot dq \cdot dP = 0.0205 \tag{3.15}$$

It is small enough to consider the parabolic approximation valid. Moreover, taking the max norm of the error matrix:

$$\|\epsilon\| = max\{|e_{ij}|\} = 0.06 \tag{3.16}$$

It shows that the biggest error is small enough as well.

Modeling of two pumps in parallel

For two pumps working in parallel, the compatibility equations are, the sum of the flow of both pumps, equally output pressure, and the efficiency:

$$q_T = q_1 + q_2 \tag{3.17}$$

$$\Delta P_T = \Delta P_1 = \Delta P_2 \tag{3.18}$$

$$\eta_T = \frac{q_1 \cdot \Delta P_1}{q_T \cdot \Delta P_T} \cdot \eta_1 + \frac{q_2 \cdot \Delta P_2}{q_T \cdot \Delta P_T} \cdot \eta_2 = \frac{q_1}{q_T} \cdot \eta_1 + \frac{q_2}{q_T} \cdot \eta_2 \tag{3.19}$$

The flow of each pump can be computed with equation (3.13) and its efficiency with (3.14).

The plots showing the behavior of two pumps working in parallel according to these equations are, for a given pressure:

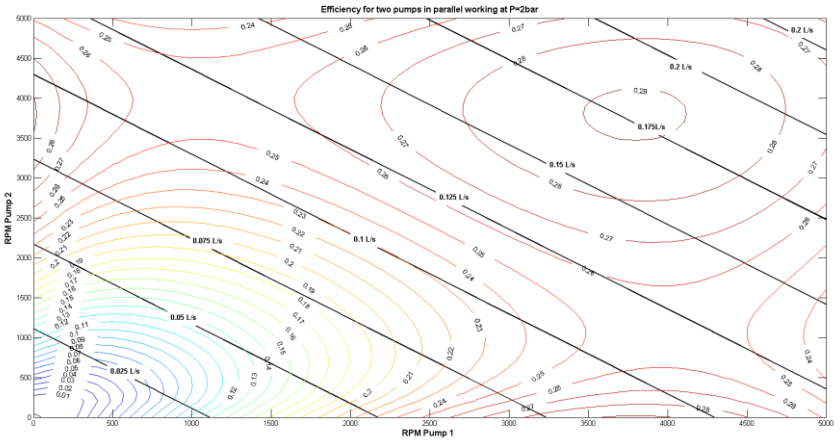

Figure 12: Efficiency curves at a different speeds of two pumps working in parallel at 2 bar.

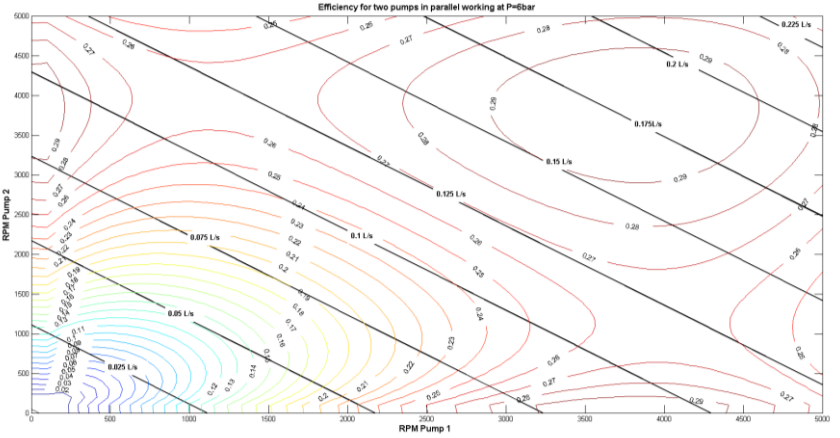

Figure 13: Efficiency curves at a different speeds of two pumps working in parallel at 6 bar.

As can be seen in Figure 12 and Figure 13, the efficiency level curves depend on the pressure the pumps work at. However, the shape is the same, so the optimization problem can be solved in the same way for a given flow and pressure.

3.2 Modeling of system's hydraulics

In this section the model of the pipes, conducts and filters is derived from the hydraulics point of view. A first theoretical model is derived in order to decide the proper experiments due to be run on the rig and from the experimental results the model is adjusted.

Theoretical model

The overall hydraulic circuit can be decoupled in two as a transfer sub-system, Figure 14, plus a feed sub-system, Figure 15. In the following diagrams pump redundancy is avoided.

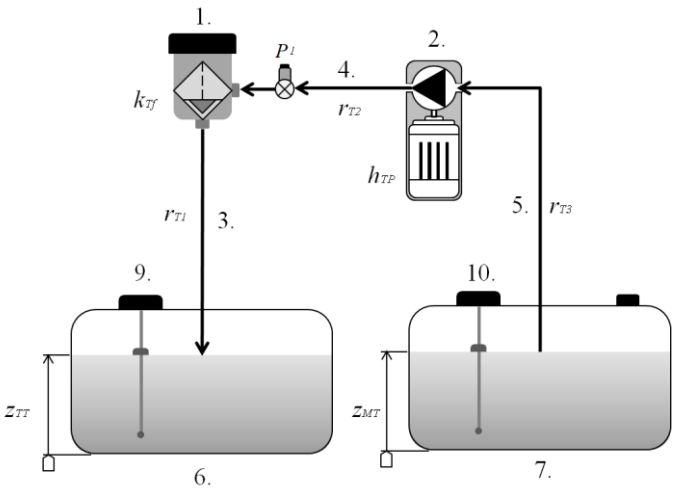

Figure 14: Simplified system diagram for hydraulics modeling of the transfer sub-system: the fluid is moved from the Main-tank (7) at a level z_{MT} through a pipe (5) which losses coefficient is r_{T1} by the Transfer-pump (2) which inputs a flow energy of h_{TP}. The Transfer-pump is connected by another pipe (4) with r_{T2} losses coefficient to a pre-filter (1) that inputs losses according to its k_{Tf} coefficient and finally another pipe (3) with r_{T3} losses coefficient connects the filter to the Tech-tank (6) with a fuel level z_{TT}. The actual system equals this one with an extra Transfer-pump for redundancy. A sensor measures the pressure before the pre-filter (8) and sensors in the tanks measures their level and temperature (9 and 10).

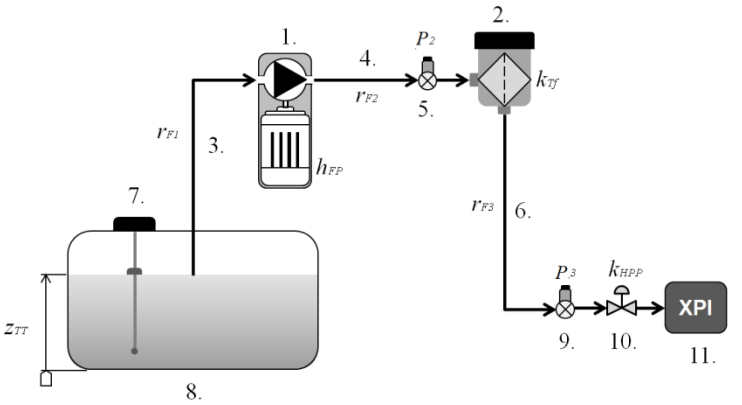

Figure 15: Simplified system diagram for hydraulics modeling of the feed sub-system: the fluid is moved from the Tech-tank (8) at a level z_{TT} through a pipe (3) which losses coefficient is r_{F1} by the Feed-pump (1) which inputs a flow energy of h_{FP}. The Feed-pump is connected by another pipe (4) with h_{F2} losses coefficient to a filter (2) that inputs losses according to its k_{Ff} coefficient and finally another pipe (6) with r_{F3} losses coefficient connects the filter to the High Pressure System (11) modeled as a valve (10) of k_{HPP} losses coefficient. The actual system equals this one with an extra Feed-pump for redundancy. A sensor measures the pressure before the main-filter (5) and another before the HPP (9). A sensor in the Tech-tank measures its level and temperature (7).

Assumptions in this modeling approach are:

- The pipes are ideal and no flow transients are considered.
- All the pipes are equal and have the same diameter.
- All the local height losses are assumed to be on the filters, so pipe branching and pipe connections are neglected and all their losses will be summarized on the filter losses coefficient.

The different coefficients and parameters should be estimated from the experimental data:

- Pipe losses coefficients, from the friction factors.
- Filters local losses.
- Flow velocity, from the pump flow.

Estimation approach

From Bernoulli's equation (2.16), the complete energy balance has to include the local losses of the filter and the piezometric height gain done by the pump. If that is included and the energy balance is done all along the components for both sub-systems, the resulting equations are:

$$z_{MT} + \left(r_{T1} + r_{T2} + r_{T3} + k_{Tf}\right) \cdot v^2 = z_{TT} + h_{TP} \tag{3.20}$$

$$k_{XPI} \cdot v^2 + \left(r_{F1} + r_{F2} + r_{F3} + k_{Ff}\right) \cdot v^2 = z_{MT} + h_{FP} \tag{3.21}$$

Pipes' losses can be estimated from the Darcy-Weisbach (2.1) equation in its piezometric height formulation:

$$\Delta h = f \cdot \frac{l}{D} \cdot \frac{v^2}{2g} \tag{3.22}$$

On the other hand, the friction factor can be estimated as well for turbulent or laminar flow with equations (2.2) and (2.4). However, the roughness height is harder to estimate than the friction factor indeed. In addition, the formulas are always approximations. Therefore, in this modeling approach it would be the friction factor the estimated parameter.

The local losses due to the filters have to be estimated as well from the experiments, since even though there are approximations formulas, the required parameters are harder to estimate than the coefficient itself.

About the pumps height, it cannot be directly measured, and they can only be obtained by isolation in equations (3.20) and (3.21).

At the same time, the flow velocity should be estimated from the pump equation (3.4) and the pipe diameter.

Many variables should be therefore estimated. However, using different sensors at middle points of the system allows to split the systems in smaller subsystems where fewer coefficients needs to be estimated, which makes it possible to know the approximated value for every coefficient.

The accessed variables from different sensors are shown in Figure 14: pressure sensor before the pre-filter (8), called '*Pressure sensor 1'* and the tank level sensors (9) and (10); and in Figure 15: Pressure sensors before (8), '*Pressure sensor 2'*, and after the main-filter (9), '*Pressure sensor 3',*and the Tech-tank level sensor (10). The equations (3.20) and (3.21) can therefore be split in:

$$\frac{P_1}{\rho g} + (r_{T1} + r_{T2}) \cdot v^2 = \left[z_{TT} + \frac{P_{amb}}{\rho g}\right] + h_{TP} \tag{3.23}$$

$$\left[z_{MT} + \frac{P_{amb}}{\rho g}\right] + r_{T3} \cdot v^2 + k_{Tf} \cdot v^2 = \frac{P_1}{\rho g} \tag{3.24}$$

$$\frac{P_2}{\rho g} + (r_{F1} + r_{F2}) \cdot v^2 = \left[z_{MT} + \frac{P_{amb}}{\rho g}\right] + h_{FP} \tag{3.25}$$

$$\frac{P_3}{\rho g} + k_{Ff} \cdot v^2 = \frac{P_2}{\rho g} \tag{3.26}$$

$$k_{HPP} \cdot v^2 + r_{F3} \cdot v^2 = \frac{P_3}{\rho g} \tag{3.27}$$

All the pipes are built with the same material and have the same diameter; therefore the friction factor can be estimated as all the pipes were only one as long as the sum of their lengths:

$$f \cong \frac{\sum h_i}{\sum L_i} \cdot \frac{2D}{v^2} \tag{3.28}$$

In addition, the flow velocity can be estimated by the mean flow from the tanks level variation over a measured time interval:

$$\bar{q} \cong \frac{A \cdot \Delta z}{\Delta t} \tag{3.29}$$

If the RPM are constant over the time needed to bring the tank from a low level to a high one, and that time is big enough, the mean flow is a good

approximation of the flow at that RPM. Once this flow is properly estimated from the previous equation, the flow velocity would be estimated as:

$$v \cong \sqrt{\frac{4\bar{q}}{\pi D^2}} \tag{3.30}$$

Experiments description

- **Flow estimation experiment**

  In first place, the flow at different RPM's will be estimated from the tank levels established variation (i.e., fixed Δz) during certain amount of time by equation (3.29). In order to do that, the experiments consist in setting the Tech-tank at a lower level, while the Main-tank is set at an upper level. These levels are arbitrarily decided, but they should be different enough so the pumps are running during enough time. Then, the transfer-pumps are turned on until the Tech-tank reaches the same upper level and the Main-tank reaches the lower one. The feed-pumps are turned off meanwhile. After that, the same is done but running the feed-pumps whiles the transfer pumps are set off. The speed at the pumps run goes from 1300 RPM (manufacturer's internal controller set this as the minimum value for running them) until 4500 RPM (upper RPM limit from the manufacturer) by steps of 100 RPM alternatively: first transfer-pumps, then feed-pumps, as explained. This step size is selected so that few range needs to be interpolated, which are a source of uncertainty increased by the natural non-linearity's of the system.

- **Transfer-subsystem experiment**

  This experiment is wanted to estimate the friction factor of the pipes, the local height losses of the pre-filter and the pump height. The procedure is to run only one transfer-pump at different RPM, providing a known flow velocity within the pipes from the previous estimation and equation (3.30). The tank level should remain constant. The easiest way achieving that is by setting the pipe out from the pre-filter to the Tech-tank back again to the Main-tank.

The RPM's will go from 1300 RPM to 4500 RPM in steps of 100 RPM, but without shutting off the pump, so different velocities and losses can be obtained at steady-state. This steady-state is assumed to be fully reached after 10 seconds, which will be the time between RPM steps.

The consumed current is measured as well to estimate the pump consumption at different RPM, which is provided by the controller included within the pumps.

The same procedure is done with the other transfer-pump and finally both transfer-pumps working at a time, in order to describe possible non-linearity due to system's couplings

- **Feed-subsystem experiment**

The experiments are the same as for the transfer-subsystem, and therefore the pipe back to the main-tank is put to the tech-tank. However, it is repeated for different positions of the valve after the main-filter in order to simulate the different pressures from the High Pressure system. This will affect the XPI coefficient, which is function of the fuel demanding pressure as well.

The pump consumption depends on the required pressure difference ΔP, which is modified by the valve position.

Experimental data

The data from the tests explained above is following plotted. Time plots to estimate the pumps flow are:

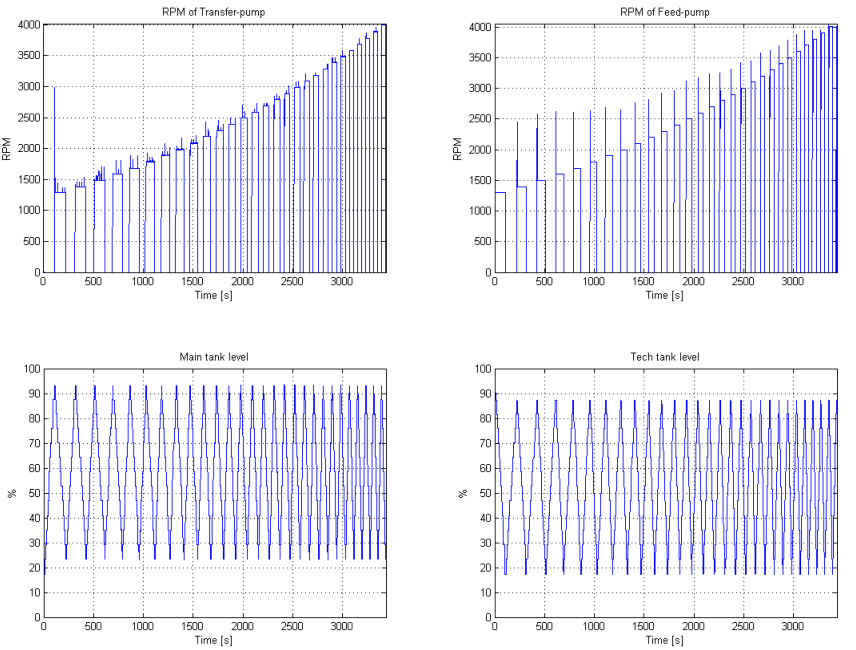

Figure 16: Time plot for pumps' RPM and the tanks' levels. At the left side, the transfer-pump RPM's are shown in the upper plot and the corresponding Main-tank level on the lower plot. The same is on the right side for the Feed-pump and Tech-tank. As shown, the pumps are started alternatively for filling up and emptying the tanks between two set levels. Note that there is an optical bias: the flow is linear with RPM's but it seems quadratic due to the time interval while running at same RPM's is decreasing in every step.

From equations (3.29) and (3.30) the flow is estimated and its relation from the RPM is computed. This relation and the line that fits the real curve are shown in Figure 17 for the Transfer- and Feed-pumps. The real values can be explained by a linear function that minimizes the total square error, which results are:

Transfer-pump: $$\dot{q}_{TP}(L/min) \approx 7 \cdot 10^{-4} \cdot N(rpm) \quad (3.31)$$

Feed-pump: $$\dot{q}_{FP}(L/min) \approx 8 \cdot 10^{-4} \cdot N(rpm) \quad (3.32)$$

The coefficients of determination of these adjustments are:

Transfer-pump: $R^2 \approx 0.99$ (3.33)

Feed-pump: $R^2 \approx 0.99$ (3.34)

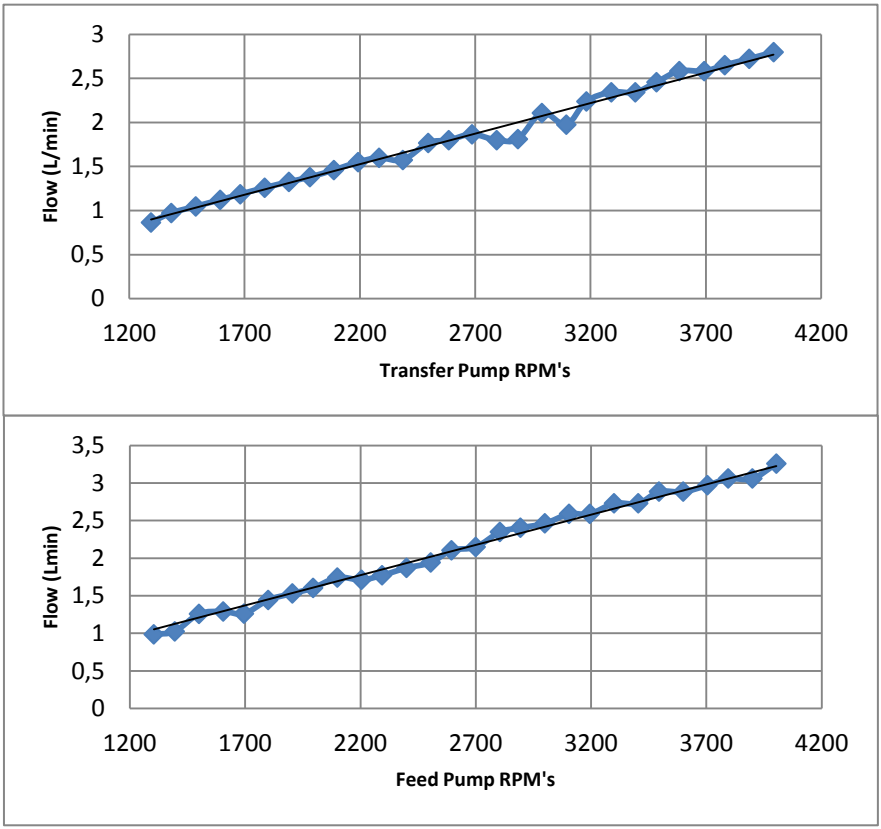

Figure 17: Experimantal correlation between transfer-pump RPM's and flow (upper plot) and for feed-pump RPM and flow (lower plot).

These results are further used to estimate the flow velocity from the pumps' RPM. The experimental data is not shown as their time plots. Instead, the piezometric height vs. flow velocity is used for meaningful modeling of the circuit in steady-state.

Next plots show this relation for the piezometric height the pumps have to provide. The different curves are obtained for running one or two pumps and for different demanded pressures (in the case of the feed-pumps):

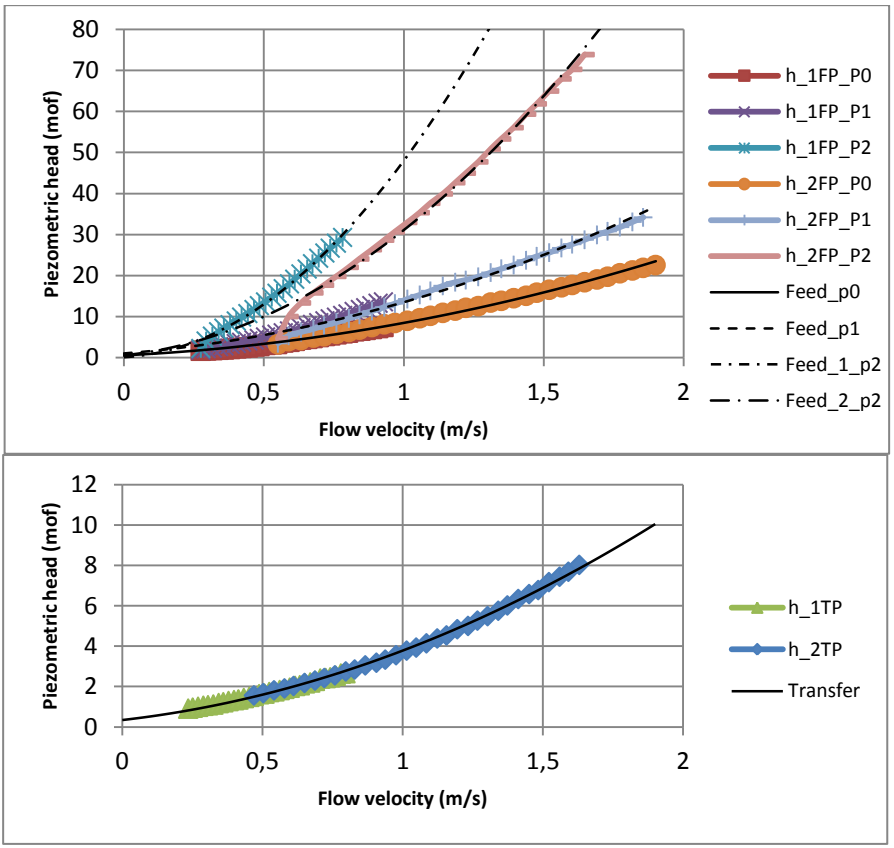

Figure 18: Piezometric head provided by the pumps in relation with the flow velocity they provide at different demanded pressures (selected by the output ball-valve possitions, P0, P1 and P2, from fully opend to partially closed) for the feed-pumps (upper plot) and the transfer-pumps (lower plot). The model fitting the real data is overlayed.

The curve that explains this behavior is for both, transfer- and feed-pumps, a displaced parabola:

$$\Delta h_{pump} = K_{hPump} \cdot (v + v_0)^2 \tag{3.35}$$

Where Δh_{pump} is the provided piezometric height in meters of fuel (mof) and the velocity is in m/s. The curves fitting the real values are in the previous plots as well. In some cases, the results for one or two pumps running at a time are explained with the same equation at different pressures, i.e., different output ball-valve positions: this is the case of the transfer-pumps and the feed-pumps for the output valve at position P0 (full open) and slightly closed (P1). For much closed positions (P2) different parameters are needed for one and two pumps.

The values of the parameters that minimize the total square error are:

Table 1: Parameter values for pumps' piezometric head fitting

	K_{hPump}	v_0
Feed-pumps_ p0	4	0.3
Feed -pumps_p1	7	0.4
One Feed-pump_p2	44	0.0
Two Feed-pumps_p2	23	0.2
Transfer-pumps	2	0.4

It can be seen that an extra velocity should be added in order to get the experimental curve. This term comes from the losses the pumps have, and it is smaller as the pressure increases. The reason is that, even though the values of the velocity are smaller, the gain increases more, giving higher losses for higher pressures. The differences in the gain are due to how much pressure the circuit demands. By modifying the valve position, the demanded pressure increases for a certain flow. However, it can be seen that it is independent on the flow velocity (note: in the case of the position 2, it was not exactly the same for one and two pumps).

If same analysis is done for the height loss in the filters, the results are:

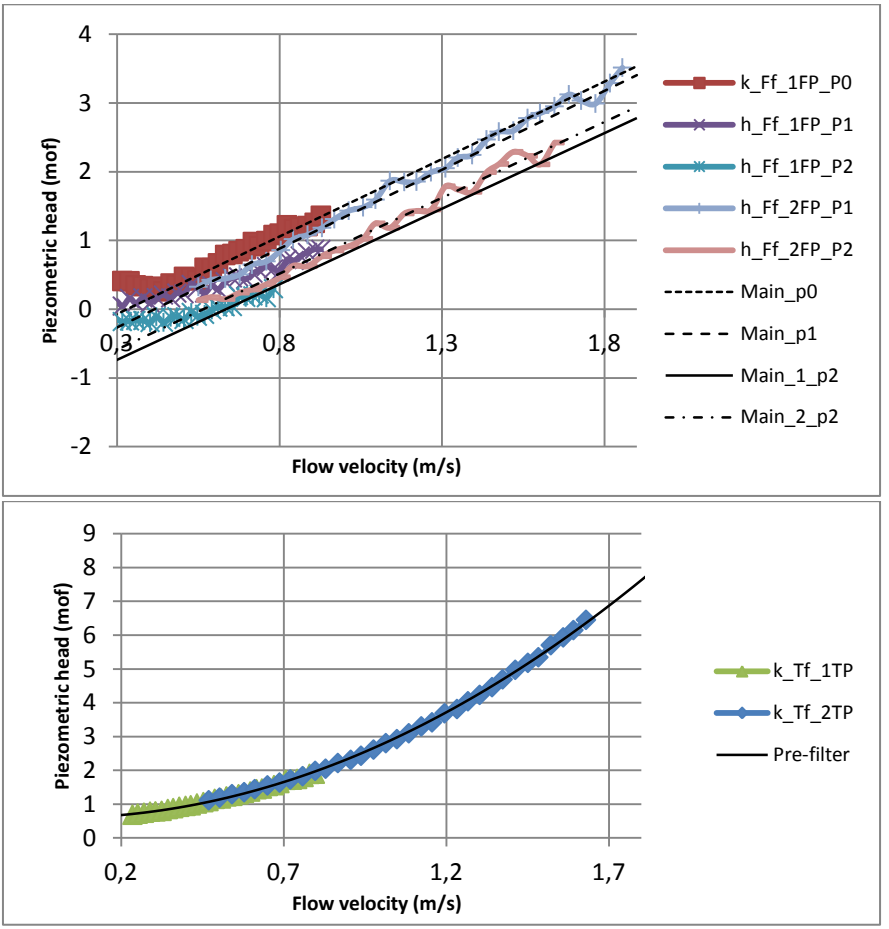

Figure 19: Piezometric height loss of the main-filter (upper plot) and pre-filter (lower plot) in relation with the flow velocity they provide at different demanded pressures pressures (selected by the output ball-valve possitions, P0, P1 and P2, from fully opend to partially closed). The model fitting the real data is overlayed.

In this case, the models have different structure for the main filter and the pre-filters: a linear function can be used to explain the main-filter's behavior (as an analogy from the Kozeny-Carman equation [6]) while the pre-filters can be done as a valve. The equations and the parameter values, that minimize the total square error, are:

$$\Delta h_{main-filter} = K_{h_{main-filter}} \cdot v + h_0 \quad (3.36)$$

$$\Delta h_{pre-filter} = K_{h_{pre-filter}} \cdot v^2 + h_0 \quad (3.37)$$

Table 2: Parameter values for filters' piezometric head fitting

	Kh_{filter}	h_0
Main-filter p0	2.253358	-0.745
Main-filter p1	2.295881	-0.95437
Main-filter_1_p2	2.2	-1.4
Main-filter_2_p2	2.207668	-1.24881
Pre-filter	2.173073	0.588515

For the main-filter, the losses are equally proportional independently on the valve position (and hence the output pressure demand) but it affects the initial head loss. Note that its sign is negative, which means that it has more energy than the provided by the pump. This can be explained by the initial filter level and internal pressure accumulated when initially filled, that is released if the flow is not enough. As the demanded pressure increases, its internal pressure increases and therefore this term becomes bigger in magniute.

For the pre-filter, its behavior is very similar as the transfer-pump piezometric height. In fact, it is this demanded pressure from the filter what the transfer-pumps supply. However, in this case, the transfer-pumps have to overcome the initial filter level and pressure, and therefore the positive sign in the constant.

3.3 Pumps efficiency modeling

The same experimental data from the previous section can be used to compute the pump's efficiency according to (3.1). The fitting function is the same as (3.9).

The experiments are limited for the different pressures the system requires at a certain flow velocity. In the case of the feed-pumps, different pressure can be obtained by changing the output valve. It is not the same for the transfer-pumps,

where different pressures cannot be handled easily in the rig. The data is shown in the following figures:

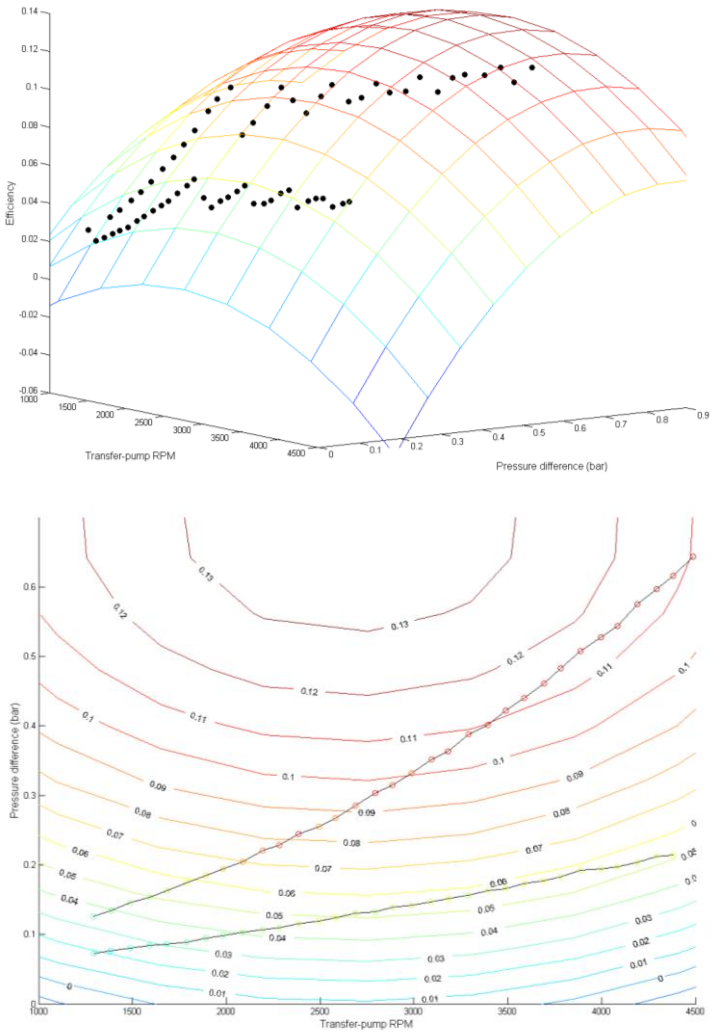

Figure 20: 3D plot for the transfer-pump Efficiency vs. RPM and Pressure of the real data and the fitting surface (up). The same data is presented in a contour plot (down) with the efficiency values and the real data coloured depending on the efficiency value.

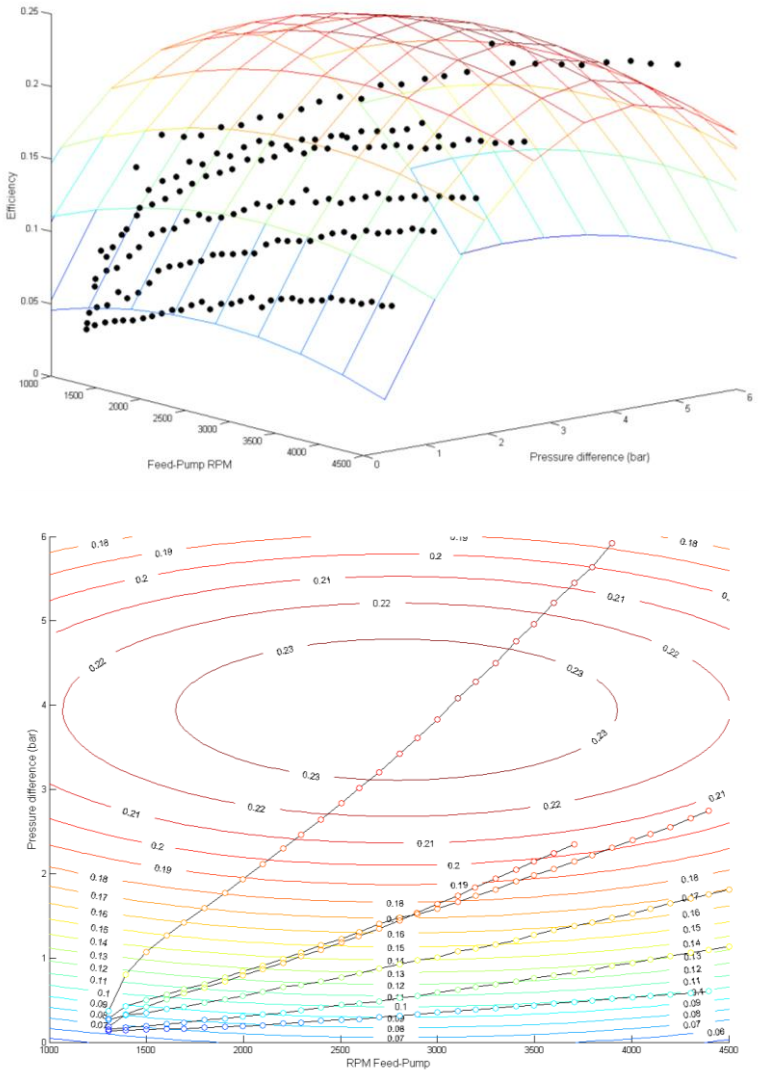

Figure 21: 3D plot for the feed-pump Efficiency vs. RPM and Pressure of the real data and the fitting surface (up). The same data is presented in a contour plot (down) with the efficiency values and the real data coloured depending on the efficiency value.

Hence, by LSQ minimization, the fitting curves match the model in equation (3.9) with a coefficient of determination of:

$$\text{Transfer-pump:} \quad R^2 = 0.99 \tag{3.38}$$

$$\text{Feed-pump:} \quad R^2 = 0.96 \tag{3.39}$$

The errors are following shown:

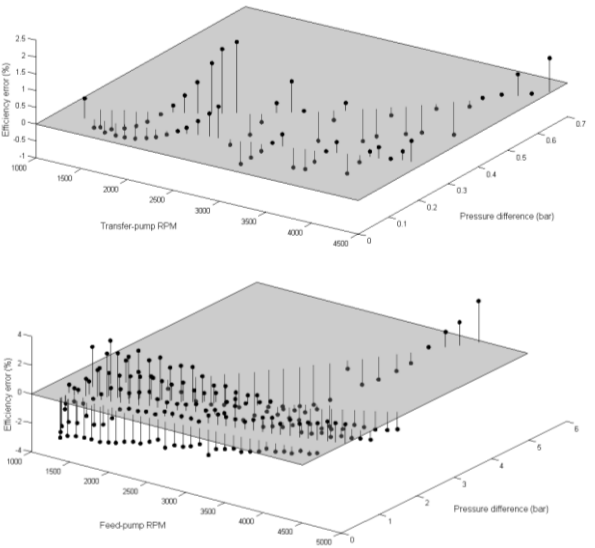

Figure 22: 3D plots for the error (in percentage) between real data and the fitted curve of the transfer-pump efficiency (upper plot) and feed-pump efficiency (lower plot), depending on pump's RPM and Pressure difference (in Bars).

The results show that for the Transfer-pump the efficiency model is only valid in the working range, which is within a very limited pressure difference. For the Feed-pumps this range is bigger as they will work in that wider range.

3.4 Modeling of heat transfer coefficients

All the parameters required to estimate the convection thermal coefficients are very arduous to compute and they have big approximation errors indeed.

Therefore, it turns better an experimental approximation from the heat transfer dynamics. For this purpose, the system is reduced and simplified as a lumped system [7], and therefore Newton´s cooling law explains its dynamic behavior by making equals equations (2.13) and (2.20) with no extra flows going into or out the tank (free temperature evolution):

$$mC_v \cdot \frac{d(\Delta T)}{dt} = -U_{eq} \cdot A_{total} \cdot \Delta T \tag{3.40}$$

$$\Delta T(t) = \Delta T_0 \cdot e^{-\frac{t}{\tau}} \tag{3.41}$$

$$\tau = \frac{(\rho \forall) C_v}{U_{eq} \cdot A_{total}} = t|_{\Delta T = \Delta T_0 - 0.63\Delta T_0} \tag{3.42}$$

The experiment consists therefore in leaving the tank filled with a known amount of fuel at a known initial temperature until it cools down to the ambient temperature. From that first order system, the time constant is estimated and the total overall heat transfer coefficient computed for the whole tank. If results are required to be closer to real conditions, more on-line experiments (i.e., truck running) must be performed, however, the rig is currently inside a lab.

From those results, the heat into the fuel from the pumps can be estimated too. Considering an equilibrium state, the heat into the fuel from the pumps and out the fuel due to convection in the tank, should be equals at a certain equilibrium temperature. Since the convection heat is known from the previous results, the heat from the pumps is known. The problem with this approach is that it takes too long to achieve the equilibrium state; therefore, a dynamic modeling is more suitable. The dynamic equation is in this case:

$$mC_v \cdot \frac{d(\Delta T)}{dt} = q_{pump} - U_{eq} \cdot A_{total} \cdot \Delta T \tag{3.43}$$

It can be expressed as a transfer function:

$$G_{RPM\to\Delta T}(s) = \frac{\frac{K_{RPM,q}}{mC_v}}{s + \frac{U_{eq}\cdot A_{total}}{mC_v}} \tag{3.44}$$

The procedure consists in, from the ambient temperature, run the pump with recirculation of the fuel back to the same tank, and leave it running until a big enough temperature difference has been reached, or until the equilibrium is reached. From the results, the pump heat is estimated from the particular solution of the differential equation (3.43).

To model the pump heat as a function of the RPM's, the experiment is repeated at different RPM's. The chosen ones are: 3500 RPM and 4000 RPM, which are enough to show this relation.

Experimental data

The time plots for the temperature modeling are:

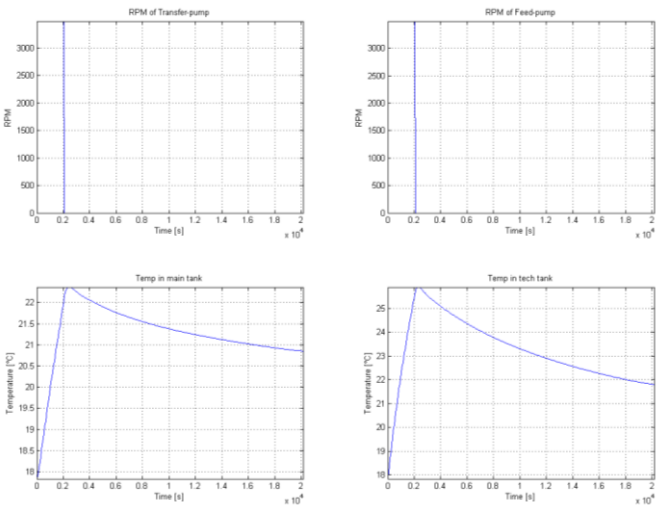

Figure 23: Time plots for the temperature evolution of the main-tank run by the transfer-pumps (left) and tech-tank run by the feed-pumps (right) with the pumps RPM while recirculating the flow back to the same tank in each case.

As can be seen, the temperature conditions differ while running the experiment: the final temperature when cooling down is around 20.5°C while at the beginning of the experiments it was 17.7°C. This should be considered in the modeling.

The experimental data is separated in two phases: heat up and cool down. For the first case, the heat comes from the pumps and its dynamic behavior is modeled as a transfer function (3.44). The best fitting gives:

Transfer-pump $$G_{RPM\to\Delta T}(s) = \frac{6\cdot 10^{-7}}{s + 6\cdot 10^{-5}} \quad (3.45)$$

Feed-pump $$G_{RPM\to\Delta T}(s) = \frac{1.5\cdot 10^{-6}}{s + 3\cdot 10^{-4}} \quad (3.46)$$

The cooling down is a free-evolution system that can be modeled as (3.41). The initial temperature difference is directly computed by estimating the final temperature, while the time constant can be computed graphically. However, by means of minimum total square error, this non-linear fitting is optimal for:

Main-tank $$\Delta T_{MT}(t) = 1.7\cdot e^{-\frac{t}{11000}} \quad (3.47)$$

Tech-tank $$\Delta T_{TT}(t) = 4.9\cdot e^{-\frac{t}{11000}} \quad (3.48)$$

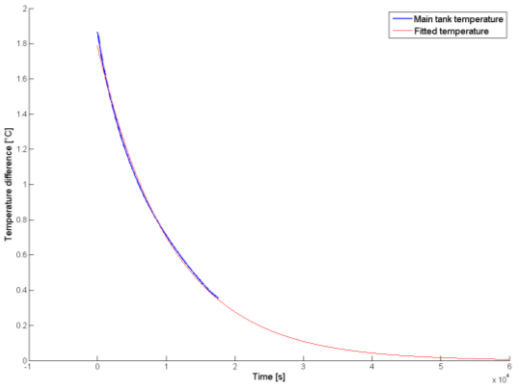

Figure 24: Temperature difference self-evolution of the Main-tank and the model fitting the real data.

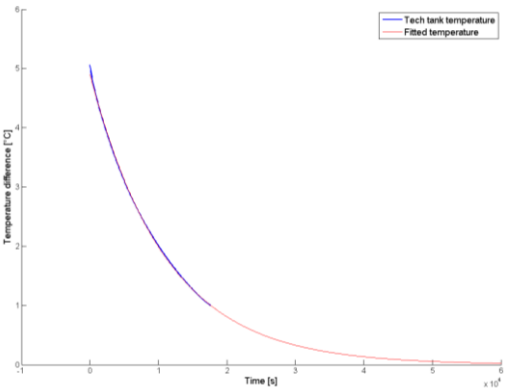

Figure 25: Temperature difference self-evolution of the Tech-tank and the model fitting the real data.

From this experimental data, the overall heat transfer coefficient for internal natural and forced convection and the heat gain of the transfer- and feed-pumps can be extracted:

Table 3: Overal heat-transfer coefficient for natural and forced internal convection

	Natural	Forced internal
Ueq Tech-tank J/K/m^2	0.3	0.1
Ueq Main-tank J/K/m^2	0.3	0.5

Table 4: Heat gain for the pumps

Transfer-Pump heat gain (Watt/RPM)	0.003
Feed-Pump heat gain (Watt/RPM)	0.006

Analyzing these results, the heat out of the tanks can be neglected when no wind or movement is considered (adiabatic tanks), despite the fact that this is not the real conditions the tanks will work at. Hence, real conditions should be considered for the heat transfer modeling, which will be left as a temperature disturbance of the tank. There is, however, one result still valid, and this is the heat the pumps supply to the fuel. Even though its influence in tank's temperature can be neglected, the result is used for the energy balance in next section.

3.5 Energy balance of the pumps

From the previous experiments, an energy balance can be done for the pumps working at 3500 RPM and full opened valve. The results are better shown in a pie graph:

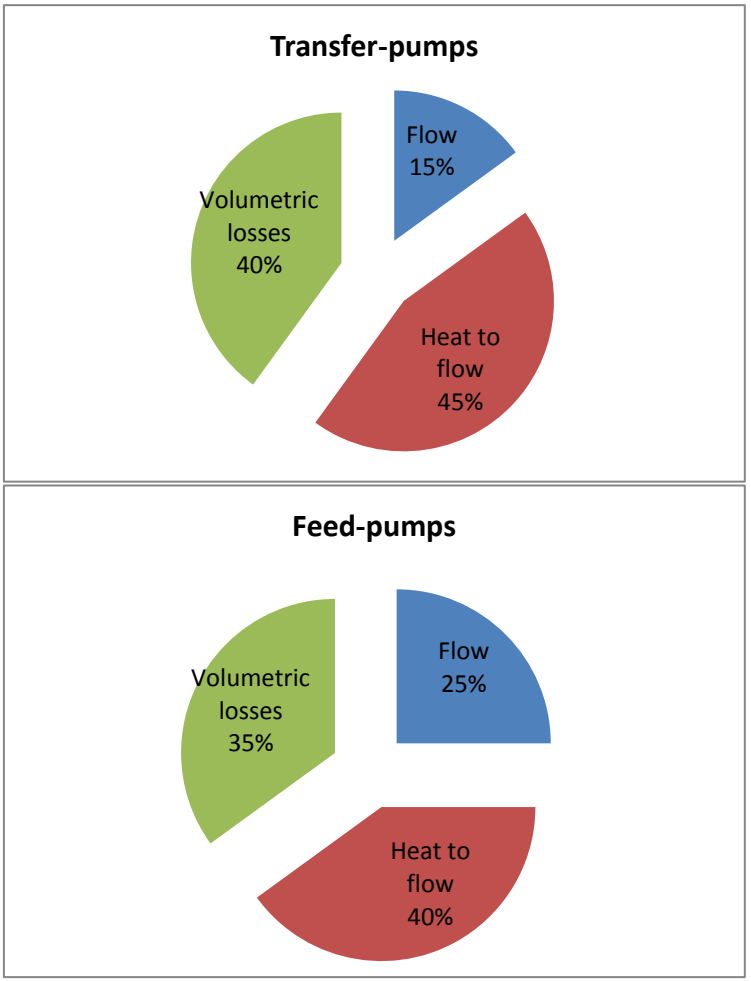

Figure 26: Pie charts for the transfer- and feed-pumps energy balance at 3500 RPM and no pressure demand.

For this balance, the different energies involved were computed as:

$$E_{electrical}(J) = I(A) \cdot V \tag{3.49}$$

$$E_{flow}(J) = q(m^3/s) \cdot \Delta P(Pa) = E_{electrical} \cdot \eta(N, \Delta P) \tag{3.50}$$

$$E_{heat}(J) = K_{h_{pump}} \cdot N(RPM) \tag{3.51}$$

$$E_{volumetric\ losses}(J) = E_{electrical} - E_{flow} - E_{heat} \tag{3.52}$$

Attending at these results, it arises that the selected pumps are not very efficient for the purposes of the system. However, this may be due to the fact that fuel pumps are subject to high contamination and its reliability is against its performance. Even though, more suitable pumps, in terms of efficiency, must be considered and selected so that where the main system's working point matches the highest pump efficiency. In addition, the parallel pumps interaction affects the global system's efficiency. This is discussed in section 5.1

4. System model

In this chapter a derivation of suitable models for the diagnosis and control purposes are derived from the theoretical equations and experimental results.

4.1 Equations overview

The equations used for modeling the whole system are following stated.

Transfer-subsystem

- **Transfer-pumps flow**

Pump 1 $$q_{TP_1} = K_{q_{TP}} \cdot N_{TP_1} \tag{4.1}$$

Pump 2 $$q_{TP_2} = K_{q_{TP}} \cdot N_{TP_2} \tag{4.2}$$

- **Transfer-subsystem flow velocity**

$$v_T = \frac{q_{TP_1} + q_{TP_2}}{A_{pipe}} \tag{4.3}$$

- **Transfer-pumps pressure**

$$\Delta P_{TP} = \gamma \cdot K_{h_{TP}} \cdot \left(v_T + v_{0_{TP}}\right)^2 \tag{4.4}$$

- **Transfer-pumps efficiency**

Pump 1 $$\eta_{TP_1} = K_{N_{TP}}\left(N_{TP_1} - N_{0_{TP}}\right)^2 + K_{p_{TP}}\left(\Delta P_{TP} - p_{0_{TP}}\right)^2 + \eta_{0_{TP}} \quad (4.5)$$

Pump 2 $$\eta_{TP_2} = K_{N_{TP}}\left(N_{TP_2} - N_{0_{TP}}\right)^2 + K_{p_{TP}}\left(\Delta P_{TP} - p_{0_{TP}}\right)^2 + \eta_{0_{TP}} \quad (4.6)$$

- **Transfer-pumps current**

Pump 1 $$I_{TP_1} = \frac{q_{TP_1} \cdot \Delta P_{TP}}{V \cdot \eta_{TP_1}} \quad (4.7)$$

Pump 2 $$I_{TP_2} = \frac{q_{TP_2} \cdot \Delta P_{TP}}{V \cdot \eta_{TP_2}} \quad (4.8)$$

Feed-subsystem

- **Feed-pumps flow**

Pump 1 $$q_{FP_1} = K_{q_{FP}} \cdot N_{FP_1} \quad (4.9)$$

Pump 2 $$q_{FP_2} = K_{q_{FP}} \cdot N_{FP_2} \quad (4.10)$$

- **Feed-subsystem flow velocity**

$$v_F = \frac{q_{FP_1} + q_{FP_2}}{A_{pipe}} \quad (4.11)$$

- **Feed-pumps pressure**

$$\Delta P_{FP} = \gamma \cdot K_{h_{FP}}(p_{out}) \cdot \left(v_F + v_{0_{FP}}(p_{out})\right)^2 \quad (4.12)$$

Components

- **Pressure sensor 1**

$$P_1 = P_{atm} + \gamma \cdot \left[z_{MT} - (k_{p1} + k_{p2}) \cdot v_T\right] + P_{TP} \quad (4.13)$$

- **Pressure sensor 2**

$$P_2 = P_{atm} + \gamma \cdot \left[z_{TT} - (k_{p4} + k_{p5}) \cdot v_F\right] + P_{FP} \quad (4.14)$$

- **Pressure sensor 3**

$$P_3 = P_2 - \gamma \cdot \left[k_{MF} \cdot v_F + h_{PF_0}(p_{out})\right] = p_{out} \tag{4.15}$$

- **Tanks levels**

Main-tank
$$\dot{z}_{MT} = -\frac{1}{A_{MT}} \cdot \left[q_{TP_1} + q_{TP_2}\right] \tag{4.16}$$

Tech-tank
$$\dot{z}_{TT} = \frac{1}{A_{TT}} \cdot \left[\left(q_{TP_1} + q_{TP_2}\right) - q_{eng}\right] \tag{4.17}$$

- **Tanks temperatures**

Main-tank
$$\Delta\dot{T}_{MT} = 0 \tag{4.18}$$

Tech-tank
$$\Delta\dot{T}_{TT} = \frac{1}{z_{TT} \cdot A_{TT}} \cdot \left[\left(q_{TP_1} + q_{TP_2}\right)(T_{MT} - T) + \left(q_{FP_1} + q_{FP_2} - q_{eng}\right)(T_{XPI} - T)\right] \tag{4.19}$$

4.2 Model for control

A model used to design a control algorithm must be representative of the plant, but never too complex, since the more complex it is, the more sensitive to variations. It should include the controlled variables and the actuators effects on them. With a state-space representation, the internal states can be represented (whilst it is not the case for a transfer function) and if them can be accessed, a state-feedback regulator become much reliable. Otherwise, a kind of observer can be used to estimate the not accessible states.

In this case, the variables to be controlled are the output pressure and the Tech-tank level. Hence, the non-linear equations are (4.15) and (4.17). By substitution, they can be expressed only by the variables of interest. In addition, Tech-tank fuel mass and mass flow are used, which gives more generality in case different pumps were used. The final equations are, expressed in *Kg/s* and *bar*:

$$\dot{m}_{TT} = \dot{m}_{TP} - \dot{m}_{FP} + (\dot{m}_{FP} - \dot{m}_{eng}) \tag{4.20}$$

$$P_3 = P_{atm} + \gamma \cdot 10^{-5} \cdot \left[\frac{\Delta m_{TT}}{\rho A_{TT}} + K_{h_{FP}} \cdot \left(\frac{\dot{m}_{FP}}{\rho A_{pipe}} + v_{0_{FP}} \right)^2 - (k_{p4} + k_{p5} + k_{MF}) \cdot \frac{\dot{m}_{FP}}{\rho A_{pipe}} - h_{PF_0} \right] \tag{4.21}$$

The second equation is non-linear and therefore it should be linearized. The equilibrium point is where the regulation takes place:

$$\dot{m}_{TT_{eq}} = 0 \tag{4.22}$$

$$P_{3_{eq}} = 6\ bar \tag{4.23}$$

$$\dot{m}_{FP_{eq}} = \dot{m}_{FP}|_{P_3 = 6bar} \tag{4.24}$$

$$\dot{m}_{TP_{eq}} = \dot{m}_{eng} \tag{4.25}$$

Hence, the structure of the linearized system is:

$$\begin{bmatrix} \Delta\dot{m}_{TT} \\ \Delta\ddot{m}_{FP} \end{bmatrix} = \boldsymbol{A} \cdot \begin{bmatrix} \Delta m_{TT} \\ \Delta\dot{m}_{eng} \end{bmatrix} + \boldsymbol{B} \cdot \begin{bmatrix} \Delta\dot{m}_{TP} \\ \Delta\dot{m}_{FP} \end{bmatrix}$$
$$\begin{bmatrix} \Delta m_{TT} \\ \Delta P \end{bmatrix} = \boldsymbol{C} \cdot \begin{bmatrix} \Delta m_{TT} \\ \Delta\dot{m}_{eng} \end{bmatrix} + \boldsymbol{D} \cdot \begin{bmatrix} \Delta\dot{m}_{TP} \\ \Delta\dot{m}_{FP} \end{bmatrix} \tag{4.26}$$

5. System optimization

In this chapter, different considerations are accounted to set an optimization criterion that is solved for the handling of two parallel pumps. For the pumps endurance and Tech-tank level there is not an explicit optimization problem to be solve, but some guidelines are discussed.

5.1 Parallel pumps optimization

For an optimum long term efficiency of two pumps working in parallel, the steady-state should be analyzed. The efficiency of one pump depends on the flow and the pressure it handles. However, for two pumps it depends also in the interaction between them in order to provide the required flow.

The steady-state optimization criterion is the energy the pumps consume. Since the flow and pressure are assumed to be given, it is therefore the efficiency of the whole pumps-in-parallel system what should be optimized. The expression used has been obtained in the previous chapter, equations (3.13) and (3.14) for one pump model and (3.18) and (3.19) for two parallel pumps model.

Even though the optimization function is analytic, the optimization problem becomes non-linear due to the constraints on the pump speed i.e., RPM. The setup is therefore:

$$\max_{N1,N2} \eta = \frac{q_1}{q_T} \cdot \eta_1 + \frac{q_2}{q_T} \cdot \eta_2$$

$$\text{such that:} \quad \begin{matrix} q_T = q_1 + q_2 \\ 0 < \binom{N_1}{N_2} < 5000 \end{matrix} \tag{5.1}$$

In order to express those equations in terms of the optimization parameters, the variables should be N_1 and N_2. The problem is therefore:

$$\max_{N1,N2} \eta =$$

$$\frac{K_q \cdot N_1 + K_P \cdot \Delta P_T{}^2}{q_T} \cdot (\mu_N \cdot (N_1 - N_0)^2 + \mu_P \cdot (\Delta P_T - P_0)^2 + \mu_0) +$$

$$+ \frac{K_q \cdot N_2 + K_P \cdot P_T{}^2}{q_T} \cdot (\mu_N \cdot (N_2 - N_0)^2 + \mu_P \cdot (\Delta P_T - P_0)^2 + \mu_0) \tag{5.2}$$

$$\text{such that:} \quad \begin{matrix} q_T = K_q \cdot (N_1 + N_2) + 2 \cdot K_P \cdot \Delta P_T{}^2 \\ 0 < \binom{N_1}{N_2} < 5000 \end{matrix}$$

Due to the first equality, the problem can be solved explicitly if no constraints are considered. However, it may be solved easily if the symmetry of the surface is considered.

Since the addition of the two efficiency curves is done equally, the total efficiency is therefore a symmetric curve in respect of the line $N_1 = N_2$. This means that the first derivative of the total efficiency is zero in that line, for every pressure and total flow:

Proof:

First, the total efficiency is computed. Calling:

$$q = m \cdot N + n \tag{5.3}$$

$$\eta = a \cdot N^2 + b \cdot N + c \tag{5.4}$$

Where:

$$\begin{gathered} \eta = a \cdot N^2 + b \cdot N + c \\ m = K_q \qquad\qquad n = K_P \cdot \Delta P^2 \\ a = \mu_N \qquad\qquad b = -2 \cdot \mu_N \cdot N_0 \\ c = \mu_N \cdot N_0^2 + \mu_P \cdot (\Delta P - P_0)^2 + \mu_0 \end{gathered} \tag{5.5}$$

The flow becomes:

$$q = q_T = q_1 + q_2 = m(N_1 + N_2) + 2n \tag{5.6}$$

Hence:

$$q_2 = d - mN \tag{5.7}$$

$$N_2 = e - N \tag{5.8}$$

Where:

$$e = \frac{q - 2n}{m} = \frac{q - 2K_P \Delta P^2}{K_q} \qquad\qquad d = q - n = q - K_P \Delta P^2 \tag{5.9}$$

The expression for the total efficiency is therefore:

$$\eta = \frac{1}{q} \cdot [(mN + n) \cdot (aN^2 + bN + c) + (d - mN) \cdot (a \cdot (e - N)^2 + b \cdot (e - N) + c] \tag{5.10}$$

Expanding this expression, the efficiency has a parabola equation:

$$\eta = \frac{1}{q} \cdot [N^2 \cdot (bm + na + ad + 2aem + bm) + N \cdot (nb - 2aed - bd - ame^2 - mbe)] + (nc + cd + ade^2 + bed) \tag{5.11}$$

The extreme of the parabola (vertex) is achieved for:

$$N = -\frac{(nb - 2aed - bd - ame^2 - mbe)}{2(bm + na + ad + 2aem + bm)} \tag{5.12}$$

Now, if N_1 equals N_2, it means that:

$$\frac{q}{2} = q_1 = q_2 = mN + n \qquad \rightarrow \qquad N = \frac{q - 2n}{2m} = \frac{1}{2} \cdot \frac{q - 2n}{m} = \frac{e}{2} \tag{5.13}$$

And

$$d = q - n = me + 2n - n = me - n \tag{5.14}$$

Substituting these expressions in the parabola vertex:

$$\frac{e}{2} = -\frac{(nb - 2ae(me - n) - b(me - n) - ame^2 - mbe)}{2(bm + na + a(me - n) + 2aem + bm)} \tag{5.15}$$

$$\begin{aligned} &-(bme + bme) + (nae - nae) - 3ame^2 \\ &= (-nb + bn) - 3ame^2 - (bme + bme) \end{aligned} \tag{5.16}$$

The expression becomes equal, what means that the vertex of the parabola is achieved for N_1=N_2. □

This provides a necessary condition but not sufficient. For a maximum sufficient condition, the second derivative of the efficiency respect to N must be negative (i.e., the parabola is concave).

The computation of the second derivative is:

$$\begin{aligned} \frac{d^2\eta}{dN^2} &= \frac{1}{q} \cdot 2 \cdot (bm + na + ad + 2aem + bm) \\ &= -\frac{8\mu_N}{q}\left(K_q N_0 + K_P \Delta P^2\right) + 6\mu_N \end{aligned} \tag{5.17}$$

The change of the sign for a given pressure (P) depends on the value of the total flow, q:

$$\frac{d^2\eta}{dN^2} = 0 \qquad \rightarrow \qquad q = \frac{4}{3}\left(K_q N_0 + K_P \Delta P^2\right) \tag{5.18}$$

Then, when:

$$q > \frac{4}{3}\left(K_q N_0 + K_P \Delta P^2\right) \tag{5.19}$$

The extreme value of the parabola is its maximum value, while when the inequality is not true; the extreme value is a minimum.

In the first case, the efficiency is maximum with N_1=N_2 as stated before. However, in the second case it is minimum, but since it is known that the convex parabola only increases away from the vertex, the maximum value is obtained in the edge of the domain, this is, when only one pump is working, and therefore:

$$N = \frac{q - K_P \Delta P^2}{K_q} \tag{5.20}$$

Conclusions of two parallel pumps optimization

The steady-state optimal behavior of two pumps working in parallel is achieved with:

$$\begin{array}{l} \textit{If} \qquad q > \frac{4}{3}\left(K_q N_0 + K_P \Delta P^2\right) \\ \qquad\qquad N_1 = N_2 = \dfrac{\frac{q}{2} - K_P \Delta P^2}{K_q} \\ \textit{else} \\ \qquad\qquad N_1 = \dfrac{q - K_P \Delta P^2}{K_q} \\ \qquad\qquad N_2 = 0 \end{array} \tag{5.21}$$

Where q is the required total flow at the given pressure ΔP. Recalling the conclusions from section 3.1 , Figure 12 and Figure 13 can be used to illustrate this results, where the optimal path for handling to parallel pumps is highlighted:

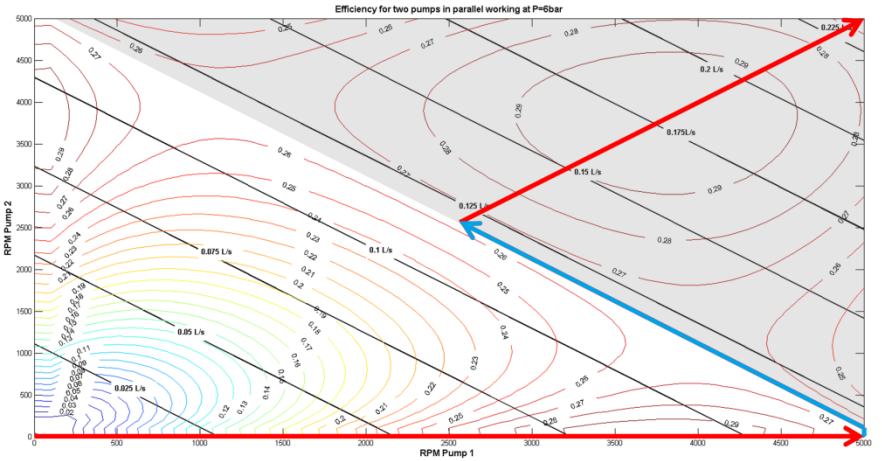

Figure 27: Optimal path for two parallel pumps handling working at a given pressure (6bars). The region where the change is done to two pumps working is shadowed and the arrows show the points where they have to work to supply an increasing demanded flow at the optimal efficiency of the global two-pumps system. The blue/grey arrow means that there is a jump in the regulation of the pumps, when one is started-up. Note that this is valid when both pumps are equivalent.

The results show how to handle two parallel pumps optimally. Once the working point is set i.e. fixed flow and pressure, by handling in this way the two parallel pumps, the efficiency will be maximum. This approach will further be called "optimal pumps handling".

5.2 Pumps endurance

There are different factors that affect the life of an electrical pump. In this section a seeking on what factors and how they affect pumps' life is developed as well as their correlations.

It is not set a specific methodology to account these factors, but for an electrical pump it is its components life's what determines the whole pump endurance. These systems namely are: ball bearings and an electrical motor. The

shortest life's component will indeed determine pump's life. Hence, all system's life should be separately analyzed from different studies and put in common.

- **Ball bearings:** Different factors affecting its life when used in a pump are:
    - Load
    - Rotational speed
    - Cycles
    - Lubrication
    - Temperature

- **Electrical motors:** The most important factor is coil's temperature. If the generated heat is not properly dissipated, the temperature inside the coil will increase, damaging coil and make it easy to suffer corrosion. Therefore, the factors that increase the generated heat and that prevent heat to be dissipated are the ones affecting motor's life:
    - Current, influenced by the rotational acceleration and load
    - Environment temperature

From the control point of view, the factors that can be directly affected are the load and rotational speed. Both of them are directly affected by the RPM's mean, amplitude and frequency. The lower they are, the lower load, rotational speed and consumption, which reduces pump's temperature and lubrication conditions. In addition, a lower flow speed through the filter increases its performance, which means a cleaner fuel and less damage to the pumps.

Since the relation between these factors and pump's life is not clear (as the manufacturer have not provided specific information regarding this issue), a heuristic approach is chosen so that big control actions are punished in a quadratic cost function. The way big control action changes are minimized is by not having big gains for small errors instead, a smooth integral action is more adequate to ensure pump's endurance.

5.3 Tech-Tank level

As the control of the feed-pumps is strictly dependent on the fuel demand, the transfer pumps control has much more freedom. Their responsibility is to provide enough fuel into the Tech-tank so that the fuel pumps can work without any problem, i.e. Tech-tank never empty unless there is no more fuel in the Main-tank.

The actual level of the Tech-tank is not important if the whole system is considered: the energy from the Transfer-pumps into the Tech-tank level will mean less energy consumption for the Feed-pumps. However, these assumptions do not hold as the losses are not constant (actually, they are linear for pipes in laminar flow and quadratic for the filter). Hence, the Tech-tank handling does not depend on its level from the pump energy perspective. It turns that other factors should be considered instead:

- How long the truck lasts in case of double Transfer-pump fault
- How much energy can be accumulated from braking
- How the flow back from XPI affects Tech-tank temperature

The first point arise that the higher the level, the longer it lasts, but it is conflicting with the second point, the lower the level, the more energy can be accumulated. Otherwise, the best practice of holding the level would be running the Transfer-pumps working at its maximum efficiency and at the lower flow velocity so that the pre-filter works better, giving a cleaner fuel and increasing Feed-pumps endurance.

The influence of the Tech-tank level to the different factors is:

- **Temperature influence**: The lower the volume, the bigger the influence from back flow is. This means that, assuming the temperature of the flow back is higher than the fuel inside the Tech-tank, there is an amount of fuel inside the Tech-tank where, still providing the required fuel from the Transfer-pumps and, assuming this flow temperature is lower than the one in the Tech-tank, the temperature can remain constant. Therefore, depending on how fast the temperature wants to be influenced, the Tech-

tank level should be set from the thermal balance of the different flows in and out, in addition to the fuel inside it.

The Tech-tank level limits can be set by different designed switching modes depending on different conditions where the system is working at. A way of setting the switching criteria can be by means of a probabilistic Markov-chain whose different events triggers the jump to a different mode, but this is left for future work. Different possible modes are:

- **Faulty**: The higher the level, the longer the truck can run without having working Transfer-pumps.
- **Energy accumulation**: The lower the level, the more energy can be saved from level accumulation in the Tech-tank by running the Transfer-pumps with "free" electrical energy from braking.
- **Winter/Summer modes**: The ambient temperature is very different at both seasons. In summer the fuel inside the Tech-tank is already at a proper temperature to be used (sometimes too high) and therefore the higher level would influence less the temperature from the fuel coming back from the XPI system. On the other side, in winter the fuel is too cold and it would be better if the flow back makes the fuel temperature increases as soon as possible, this can be achieved by a lower level of the Tech-tank.

6. Controller design

In this chapter, a suitable controller structure considering process dynamics, measured parameters and sensors characteristics is developed. The final goal is to follow the optimal criteria developed in the previous chapter.

6.1 Controller requirements

In this section the requirements for the controller are stated, which includes the controlled variables and the control actions.

The variables of interest are the Tech-tank level, Tech-tank temperature, the output mass flow and the output pressure. However, its relation makes it impossible to control all of them. Think about maintaining the pressure, this would be accomplished for a certain flow velocity, which is obtained for a certain mass flow. The excess of mass flow will be sent back to the Tech-tank at a certain temperature, which in balance with the energy of the flow from the Main-tank will give a certain final temperature to the Tech-tank, independently of the Tech-tank level, which is dependent on the mass balance of these flows i.e., flow back from the XPI and from the Transfer-pumps. However, the regulation of the Tech-tank level may control how fast this final steady temperature is reached; this is discussed in section 0.0

At the end, it turns useful to control the output pressure, whilst the engine gets the needed mass flow, and the Tech-tank level. The set-point for the pressure is given at 6 bars for the study while the set-point of the Tech-tank level is to be determined from the optimization criteria, i.e., keep the temperature as long as possible at a certain value, be more likely to save energy or to provide fuel during

more time when a have fault occurred. In any case, it should be regulated from the controller at that designed set-point.

The chosen control strategy is a state-feedback regulator. Thus, it is easier to handle it as a multivariable system (see the derived model in equation (4.26)). The inputs are the mass flows from the Transfer- and Feed-pumps, the state variables are the Tech-tank level and the mass flow out of the Tech-tank, and the outputs are the Tech-tank level and output pressure.

The controller have to be robust in order to still work under model errors (since every implementation of the system will be different) and the regulation problem means that possible disturbances should be rejected, making integral action needed.

6.2 Controller structure design

In this section the tuning of the controller is discussed. As the strategy is state-feedback, different options can be used, for instance, pole-placement from e.g., Ackerman's formula or optimal quadratic cost function. It turns more useful as the system tries to work optimally from heuristic criteria (see chapter 5.) to use this second option, where the coefficients of the quadratic function become design parameters to be chosen in order to accomplish the control requirements.

In LQ design, the cost function to be optimized is:

$$J = \int [x^T(t)Q_1 + 2x^T(t)Q_{12}u(t) + u^T(t)Q_2u(t)]\,dt \tag{6.1}$$

The quadratic cost criterion is therefore a symmetric matrix Q. The control law that minimizes this criterion is obtained from the Ricatti equation [8], this is:

$$\begin{gathered} L = Q_2^{-1}(SB + Q_{12})^T \\ 0 = Q_1 + A^TS + SA - (SB + Q_{12})Q_2^{-1}(SB + Q_{12})^T \end{gathered} \tag{6.2}$$

Where L is the control gain, computed from S, which is the unique solution to the algebraic Ricatti equation.

For solving the Ricatti equation and obtaining the control law, the *Matlab* command lqr was used, so that the control loop is:

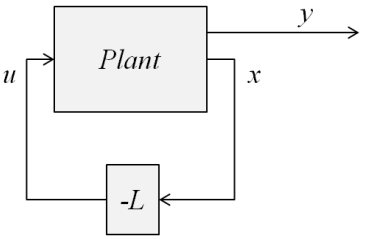

Figure 28: Closed-loop diagram for LQ designed state-feedback. The outputs can be part of the state as well, but they are distinguished for generality.

6.3 Feedback from estimated states

The measurement noise, sensor quantification and time delays affect strongly the performance of the controller. Even though the states can directly been accessed from the measurements, the mentioned problems make it hard to control the output in a fashion of short settle time and low control action. Hence, the approach to improve the controller performance is to use the known information about the system and sensors so that both together can deal to a better estimation of the actual value. Since all the states can be measured, they are not reconstructed, as it would be done otherwise, but estimated. The main problems affecting the controller performance are:

- **Pressure sensor:**
  - Time delay
  - Noise
- **Tank level sensor**
  - Big quantification (12 mm)
  - Big oscillations due to truck movement
  - Noise

The optimal trade-off between system's model and measurements, once the noise power correlation is known, is obtained by a Kalman filter. In the case of the

level this is easy to do as it is linear, but for the pressure it is not that easy. First, the pressure is strongly non-linear, and a non-linear Kalman filter would be needed e.g., Extended Kalman filter or Unscented Kalman filter. This approach would be computational expensive. Hence, the Kalman filter approach is maintained to estimate the tank level, but an Internal Model feedback in a form of Smith predictor is better chosen to compensate for pressure time delay.

Kalman filter estimation

The Kalman filter derivation for Tech-tank level estimation is done here. In order to account for the engine consumption, which can be accessed from an external estimation, it is included in the model, as well as the noise model, which is modelled as random Gaussian noise. The model for the Kalman filter is the one in equation (4.26) including the Main-tank level, process and measurement noise:

$$\begin{bmatrix}\Delta\dot{m}_{TT}\\ \Delta\dot{m}_{MT}\\ \dot{m}_{eng}\end{bmatrix}=\begin{bmatrix}0 & 0 & -1\\ 0 & 0 & 0\\ 0 & 0 & 0\end{bmatrix}\begin{bmatrix}\Delta m_{TT}\\ \Delta m_{MT}\\ \dot{m}_{eng}\end{bmatrix}+\begin{bmatrix}1 & 0\\ -1 & 0\\ 0 & 0\end{bmatrix}\begin{bmatrix}\Delta\dot{m}_{TP}\\ \Delta\dot{m}_{FP}\end{bmatrix}+\boldsymbol{N}\cdot\boldsymbol{w}$$

$$\begin{bmatrix}\Delta m_{TT}\\ \Delta P\end{bmatrix}=\begin{bmatrix}1 & 0 & 0\\ \dfrac{g}{10^5 A_{TT}} & 0 & 0\end{bmatrix}\begin{bmatrix}\Delta m_{TT}\\ \Delta m_{MT}\\ \dot{m}_{eng}\end{bmatrix}+ \tag{6.3}$$

$$\begin{bmatrix}0 & 0\\ 0 & \dfrac{\gamma}{10^5}\left(\dfrac{2\cdot K_{h_{FP}}}{\rho A_{pipe}}\left(\dfrac{\dot{m}_{FP}}{\rho A_{pipe}}+v_{0_{FP}}\right)-\left(k_{p4}+k_{p5}+k_{MF}\right)\right)\Bigg|_{eq}\end{bmatrix}\begin{bmatrix}\Delta\dot{m}_{TP}\\ \Delta\dot{m}_{FP}\end{bmatrix}+\boldsymbol{v}$$

The derivation of the Kalman filter gain is done by minimizing the stationary variance:

$$\boldsymbol{E}(x^T Q_1 x+2x^T Q_{12}x+u^T Q_2 u) \tag{6.4}$$

Being Q the quadratic cost of the LQG regulator.The stationary variance is minimized when *L* is computed as (6.2) and *K* solving the Ricatti equation, whose unique solution is *P* [8]:

$$\begin{aligned} Kest &= (PC^T + NR_{12})R_2^{-1} \\ 0 &= NR_1N^T + AP + PA^T - (PC^T + NR_{12})R_2^{-1}(PC^T + NR_{12})^T \end{aligned} \tag{6.5}$$

The observer turns to another dynamic system in state-space form, with the estimated states as an output and the measured signals and control actions as inputs, which makes it very suitable for easy implementation:

$$\dot{\hat{x}} = (A - Kest \cdot C) \cdot \hat{x} + (B - Kest \cdot D) \cdot u + Kest \cdot y \tag{6.6}$$

The controller structure thus becomes:

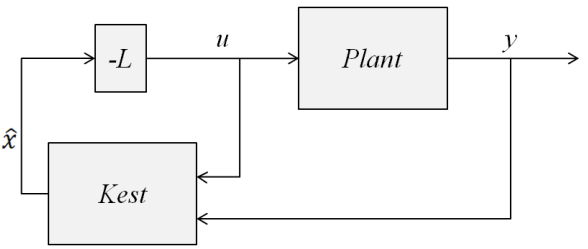

Figure 29: Closed-loop for LQG controller where the state-feedback is done from states estimated by a Kalman filter (*Kest*) in order to compute the control action, *u*, with the control gain, *L*

Internal Model for delayed feedback

As mentioned, the output pressure measurement is delayed and a simple way to reduce the response time is by means of using an Internal Model Compensation in the form of a Smith Predictor.

The main idea behind it is to eliminate the time delay from the measurement by only feedback the model output, which is corrected by comparing a delayed model output with the output signal. The modelled signal can be obtained from the Kalman filter estimator if it is design so that it relies more on the model i.e., high measurement noise. The structure of the feedback for this subsystem is shown in Figure 30. Note that the system's internal time delay is stated specifically in the drawing as well. The internal output is distinguished from the real output *y*, by the

notation *y'*. This internal output cannot be accessed from the measurements, and therefore the need of the internal model.

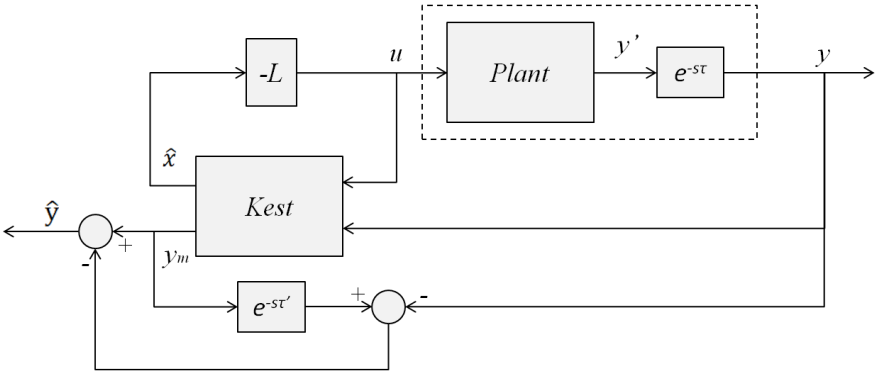

Figure 30: Closed-loop structure diagram for LQG control and IMC from Smith Predictue delay feedback correction. Only the measured states can be corrected. For this project, it is the case for all the states. Note that system's delay τ can be different from the modelled time delay τ', which affects the control performance in different ways depending on it is overstimated or understimated.

6.4 Disturbance rejection

The model has to be extended with the integral of the error in order to provide integral action from the state-feedback. The state can be extended as [9]:

$$\begin{aligned} \begin{bmatrix} \dot{x} \\ \dot{e} \end{bmatrix} &= \begin{bmatrix} A & 0 \\ C & I \end{bmatrix} \begin{bmatrix} x \\ e \end{bmatrix} + \begin{bmatrix} B \\ 0 \end{bmatrix} \cdot u \\ y &= \begin{bmatrix} C & 0 \end{bmatrix} \begin{bmatrix} x \\ e \end{bmatrix} + D \cdot u \end{aligned} \tag{6.7}$$

The designed controller with the augmented state providing integral action makes the system loop look as follows:

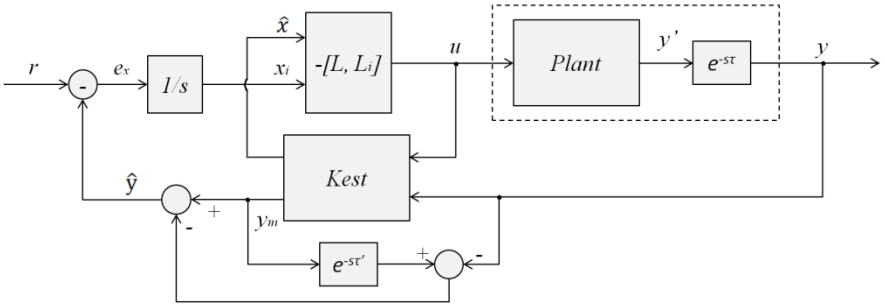

Figure 31: Closed-loop for LQG controller with delay compensation from IMC of Smith-Predictor form and reference tracking by augmented state integral action.

Antiwindup and bumpless transfer

When using integral control with limited output control actions, the windup problem should be avoided. The solution is related as well to bumpless transfer when a manual input is included. Next figure illustrates this problem [9]:

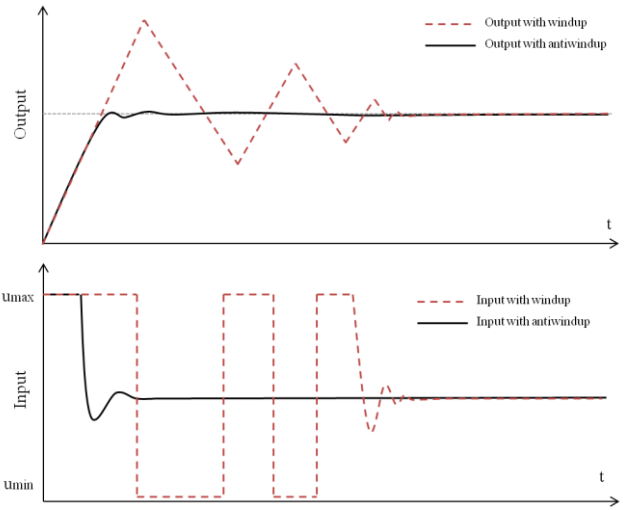

Figure 32: Effects to the control action and system output when limited control action is not accounted, provoking the windup effect in comparison to the output when it is compensated.

The bumpless transfer problem relies on the same one as the windup: the controller thinks the output is due to its action output, but it is not. In the case of the windup, it is because the control action is actually limited, while in the manual mode because it is not the controller action what is sent to the plant. In both cases, the solution to the problem is telling the controller which is the actual input (control action) to the system, which can be estimated with a saturation model in the case of limited control action. This information is provided to the controller by backwards compensation [9]:

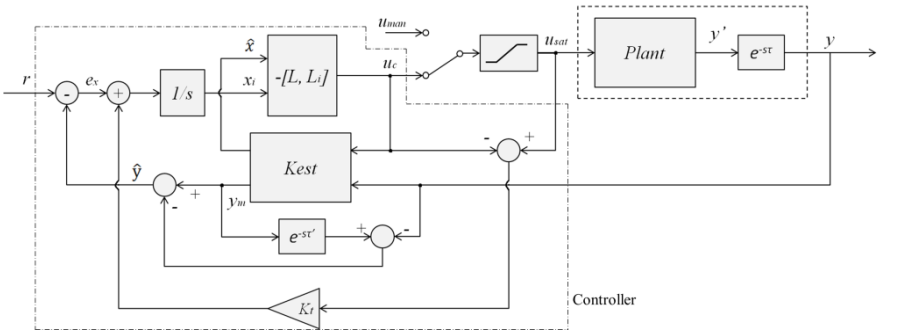

Figure 33: Closed-loop diagram for LQG controller with delay compensation from IMC of Smith-Predictor form and reference tracking by augmented state integral action and antiwindup and bumpless transfer mode from backwards compensation where the saturated control action is estimated from a matematical model of the actuator. The controller is envolved by a dashed line.

The gain of the backward compensation K_t should be chosen so that the reset time of the integral action is properly obtained.

6.5 Controller tuning

LQG costs

The quadratic cost matrix are chosen as:

$$\boldsymbol{Q} = \begin{bmatrix} Q_1 & Q_{12} \\ Q_{12}^T & Q_2 \end{bmatrix} = \begin{bmatrix} \begin{bmatrix} I_{3x3} & \mathbf{0_{3x2}} \\ \mathbf{0_{2x3}} & \begin{bmatrix} 0.01 & 0 \\ 0 & 0.001 \end{bmatrix} \end{bmatrix} & \mathbf{0_{2x5}} \\ \mathbf{0_{2x5}} & \begin{bmatrix} 0.1 & 0 \\ 0 & 0.5 \end{bmatrix} \end{bmatrix} \tag{6.8}$$

$$\boldsymbol{N} = \begin{bmatrix} Q_n & N_n \\ N_n^T & R_n \end{bmatrix} = \begin{bmatrix} \begin{bmatrix} \begin{bmatrix} 0.1 & 0 & 0 \\ 0 & 0.1 & 0 \\ 0 & 0 & 1 \end{bmatrix} & \mathbf{0_{3x2}} \\ \mathbf{0_{2x3}} & \mathbf{0_{2x2}} \end{bmatrix} & \mathbf{0_{2x5}} \\ \mathbf{0_{2x5}} & \begin{bmatrix} 1 & 0 \\ 0 & 1 \end{bmatrix} \end{bmatrix} \tag{6.9}$$

An important fact in the design of the cost functions is that it is not important the norm of the matrix, but the relative weights between the states and control actions (for the LQR) and between the model error and the measurement noise (for the Kalman filter). In addition, this relation is affected as well by the magnitude of the signal itself. Compare for instance the pressure output in bars (~6 bars) against the control action in RPM's (~2000). These different scales should be considered for a good understanding of the weighting selection.

The chosen values affects how the system behaves and since the relation between controller requirements and weightings is not straight-forward, the explanation of why the values for the LQR regulator is as follows:

- $\mathbf{Q_1}$ matrix is punishing the different states. It is chosen simply as a diagonal matrix where the state itself is punished. The first diagonal terms correspond to the Tanks levels and the engine demand. The two lasts terms are the punishment to the integral errors. For the states the cost is chosen to 1, this is, the controller will try to keep them as close as possible to the steady value. For the integral actions, the first term corresponds to the Tech-tank level whilst the second one is the output pressure integral error. Note that even though its value is much smaller than the one for the others, the states keep integrating, and therefore a smaller value would avoid big overshoots, saturations and big control actions. Note again the difference in magnitude of the different states. After some trying, these values showed a good trade-off between fast response, error avoidance and small control actions.
- $\mathbf{Q_2}$ matrix is in charge of punishing the control actions. Again, note the relation between the weightings and value of the signal. It is chosen as a diagonal

matrix too. The first diagonal entrance corresponds to the Transfer-pumps mass flow, and it is less punished than the one for the Feed-pumps as the reference tracking for the pressure can generate big control actions. The chosen value is a good trade-off, again, between error rejection, fast response and small control action.

- $\mathbf{Q_{12}}$ punishes the cross states, and it is left in zero because of the states' correlation is not very big and it does not help an easy controller tuning.

The same thinking is used for the Kalman filter quadratic costs. In this case, however, the interpretation is more related to how much the observer should trust the model against the measurements, depending on how the random Gaussian noise is modelled. The noise is modelled as:

$$\begin{aligned} \boldsymbol{N} \cdot \boldsymbol{w} &= \begin{bmatrix} 0.5 \\ 0.5 \\ 1 \end{bmatrix} \cdot \boldsymbol{w} \\ \boldsymbol{v} = H \cdot \boldsymbol{w} &= \begin{bmatrix} 0.1 \\ 0.001 \end{bmatrix} \cdot \boldsymbol{w} \end{aligned} \tag{6.10}$$

And the cost functions are chosen as follows:

- $\mathbf{Q_n}$ is the noise power correlation, $\mathbf{E}\{\mathbf{w}\mathbf{w}^T\}$. It is chosen as 0.1 for the Tech- and Main-tank levels as the system should better trust the model than the measurements, due to sensor's big quantifications, this is, the level signal does not change continuously but in big steps (12mm level changes). The third entrance punishes the correlation of the engine mass flow demand, and it is set to 1 due to the fact that the pressure model error is higher than the error for the level estimation.
- $\mathbf{R_n}$ is the noise power correlation, $\mathbf{E}\{\mathbf{v}\mathbf{v}^T\}$ and it is set to 1 for the Tech-tank level measurement, as it should trust more the model in accordance with what was explained before. Tthe pressure it is set to 1as it should better trust the model, even though the measurement noise is low.
- $\mathbf{N_n}$ is the cross noise power correlation, $\mathbf{E}\{\mathbf{w}\mathbf{v}^T\}$ and it is left as zero as its correlation is neglected and that will not help a good design to the controller

The regulator is designed by means of the *Matlab* commands lqi and kalman, whose combinations gives the LQG regulator with integral action. They

solve the Ricatti equations and obtain the gains as in equations (6.2) and (6.5) respectively. The cost functions are stated as the parameters needed to use those commands. This is:

```
K  = lqi(SYS,Q1,Q2,Q12);
```

This command builds up the extended system to include the integral action, so SYS is simply the system model and Q1, Q2, Q12 the mentioned matrix. The function returns the controller gain, so that the controller still has the block diagram in Figure 33:

$$u = -K \cdot z = -[L \quad L_i] \cdot \begin{bmatrix} \hat{x} \\ x_i \end{bmatrix} \tag{6.11}$$

For the kalman command, the system should be extended with the noise model, hence it becomes:

```
SYSn = (A,[B G],C,[D H]);
```

It returns the state-space system Kest that outputs the state vector estimation and the output estimation as well. Its syntax is:

```
Kest = kalman(SYSn,QN,RN,NN);
```

Delay estimation for Smith-Predictor

As explained, the measurement time delay plays an important role in the output pressure regulation as it changes very fast and much faster than the rest of the controlled variables e.g., Tech-tank level. Therefore, a good compensation relies as well on the time delay estimation. However, this time delay depends not only on the sensor delay, but in its signal process, handled by the ECU, which utilization and computational time can affect this time delay. Figure 34 shows the response time of the used pressure sensor against a step response. The response time can be considered instantaneous compared with the delay provoked by the ECU.

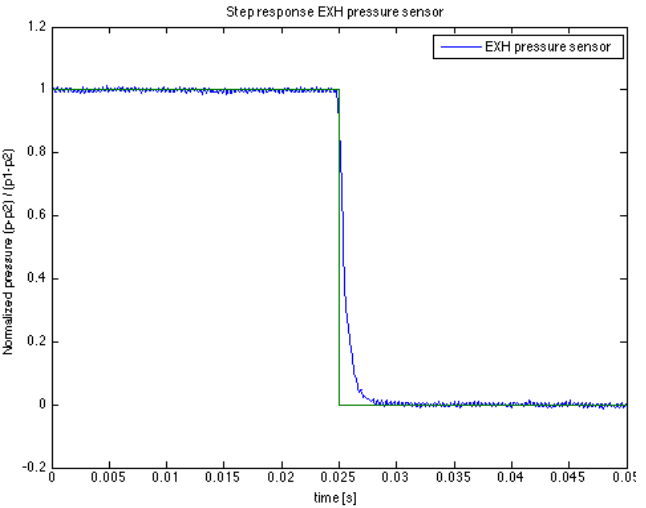

Figure 34: Step response of the used pressure sensor. The response time can be considered instantaneous compared with the system's setling times where it is used.

An underestimation of the time delay increases the response time, but it does not make the output unstable. However, if the integral action is too big, it can generate big overshoots. On the other hand, if the time delay is too much overestimated, it can arise to an unstable system; even if the plant is stable itself. Because of these considerations, the time delay will be underestimated by a factor of 0.8, which is a good balance and a robust.

From previous tests, the time delay is estimated at least to be around 300ms, and therefore the Smith-Predictor will compensate with a time delay rounded to 250ms.

Optimal handling of the actuators

The whole control structure has so far been developed for the mass flow as the controlled variable. However, the way of obtaining that mass flow is by running the pumps at a certain amount of RPM's. As the pumps are in parallel, their handling is optimal from the results in section 5.1 . Considering this result, the calibration of the pumps flows (see section 3.2) and a constant density of the

fuel, the mass flow is simply proportional to the RPM's. Combining both results, the optimal handling of two pumps providing the giving mass flow have the following structure:

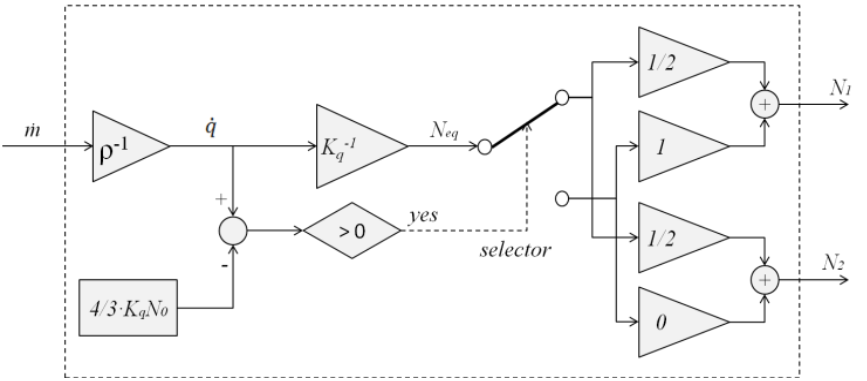

Figure 35: Optimal selector for handling two equal parallel pumps known their volumetric gain K_q and constant fuel density from the endurance optimization discussion (see 5.2) it is better to run always the same pump and use the other one when required, because the endurance reduction is not linear with the amount of start and stop of the pump.

The figure shows how a switch between running one pump or two pumps is done at an appropiate mass-flow demand (chosen from results in section 5.2 The RPM's to provide that mass flow are then calculated depending on how many pumps are runing. The transition is done with a switch, making it too sudden. A smooth transition will be better, as discussed in the results. This can be done, for exapple, by having a first order filter in the output or by going from [1,0] to [0.5, 0.5] little by little. However, this is left as future work.

6.6 Controller overview

The whole regulator structure, combining the structures of the controller shown in Figure 33 and the optimal actuator handling shown in Figure 35, and including the manual commanded signals, is shown in Figure 36:

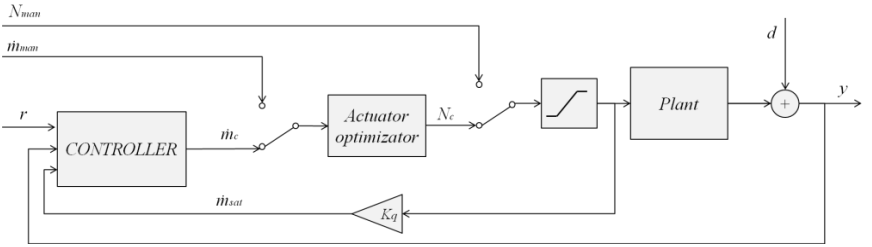

Figure 36: Overview of the whole controller structure, including the regulation controller from Figure 33, the optimal actuator handler from Figure 35 and the selectors for manual input of the mass flow and pumps RPM's. The setpoint reference can also be chosen from a manual source or from a reference generator, discussed in section 6.7 . There is a disturbance, named *d*, included at the output. Note that the signals are vector magnitudes. The commanded mass flow after saturation is computed from the pumps mass-flow/RPM's relation because of the fact that the regulator uses this variable.

The model, substituting the values from the modeling experiments in section 3.1 is:

$$\begin{bmatrix} \Delta\dot{m}_{TT} \\ \Delta\dot{m}_{MT} \\ \ddot{m}_{eng} \end{bmatrix} = \begin{bmatrix} 0 & 0 & -1 \\ 0 & 0 & 0 \\ 0 & 0 & 0 \end{bmatrix} \begin{bmatrix} \Delta m_{TT} \\ \Delta m_{MT} \\ \dot{m}_{eng} \end{bmatrix} + \begin{bmatrix} 1 & 0 \\ -1 & 0 \\ 0 & 0 \end{bmatrix} \begin{bmatrix} \Delta\dot{m}_{TP} \\ \Delta\dot{m}_{FP} \end{bmatrix} + \begin{bmatrix} 0.5 \\ 0.5 \\ 1 \end{bmatrix} \cdot \boldsymbol{w}$$
$$\begin{bmatrix} \Delta m_{TT} \\ \Delta P \end{bmatrix} = \begin{bmatrix} 1 & 0 & 0 \\ 0.0025 & 0 & 0 \end{bmatrix} \begin{bmatrix} \Delta m_{TT} \\ \Delta m_{MT} \\ \dot{m}_{eng} \end{bmatrix} + \begin{bmatrix} 0 & 0 \\ 0 & 5.316 \end{bmatrix} \begin{bmatrix} \Delta\dot{m}_{TP} \\ \Delta\dot{m}_{FP} \end{bmatrix} + \begin{bmatrix} 0.1 \\ 0.001 \end{bmatrix} \cdot \boldsymbol{w} \quad (6.12)$$

At the working point:

$$\dot{m}_{TT_{eq}} = 0\ Kg/s \quad (6.13)$$
$$\dot{m}_{MT_{eq}} = 0\ Kg/s \quad (6.14)$$
$$P_{3_{eq}} = 6\ bar \quad (6.15)$$
$$\dot{m}_{FP_{eq}} = 0.0855\ Kg/s \quad (6.16)$$
$$\dot{m}_{TP_{eq}} = 0.02\ Kg/s \quad (6.17)$$
$$\dot{m}_{eng_{eq}} = 0.02\ Kg/s \quad (6.18)$$

With these particular values, the designed LQG controller is:

$$\begin{bmatrix} \Delta\hat{P} \\ \Delta\hat{\dot{m}}_{TT} \\ \Delta\hat{\dot{m}}_{MT} \\ \Delta\hat{\dot{m}}_{eng} \end{bmatrix} = \begin{bmatrix} -0.01 & 0 & 0 & 0 \\ 0 & -0.05 & 0 & 0 \\ 0 & 0 & -0.05 & 0 \\ 0 & 0 & 0 & 0 \end{bmatrix} \begin{bmatrix} \Delta\hat{P} \\ \Delta\hat{\dot{m}}_{TT} \\ \Delta\hat{\dot{m}}_{MT} \\ \Delta\hat{\dot{m}}_{eng} \end{bmatrix} + \begin{bmatrix} 0.01 & 0 & 0 & 0 & 0 & 0 \\ 0 & 0.05 & 0 & -1 & 1 & 0 \\ 0 & 0 & 0.05 & 0 & -1 & 0 \\ 0 & 0 & 0 & 0 & 0 & 0 \end{bmatrix} \begin{bmatrix} \Delta P \\ \Delta m_{TT} \\ \Delta m_{MT} \\ \dot{m}_{eng} \\ \Delta\dot{m}_{TP} \\ \Delta\dot{m}_{FP} \end{bmatrix}$$

$$\begin{bmatrix} \Delta\hat{P} \\ \Delta\hat{\dot{m}}_{TT} \\ \Delta\hat{\dot{m}}_{MT} \\ \Delta\hat{\dot{m}}_{eng} \end{bmatrix}_{out} = \begin{bmatrix} -0.01 & 0 & 0 & 0 \\ 0 & 1 & 0 & 0 \\ 0 & 0 & 1 & 0 \\ 0 & 0 & 0 & 0 \end{bmatrix} \begin{bmatrix} \Delta\hat{P} \\ \Delta\hat{\dot{m}}_{TT} \\ \Delta\hat{\dot{m}}_{MT} \\ \Delta\hat{\dot{m}}_{eng} \end{bmatrix} + \begin{bmatrix} 0.01 & 0.0025 & 0 & 0 & 0 & 5.316 \\ 0 & 0 & 0 & 0 & 0 & 0 \\ 0 & 0 & 0 & 0 & 0 & 0 \\ 0 & 0 & 0 & 1 & 0 & 0 \end{bmatrix} \begin{bmatrix} \Delta P \\ \Delta m_{TT} \\ \Delta m_{MT} \\ \dot{m}_{eng} \\ \Delta\dot{m}_{TP} \\ \Delta\dot{m}_{FP} \end{bmatrix} \tag{6.19}$$

$$\begin{bmatrix} \Delta\dot{m}_{TP} \\ \Delta\dot{m}_{FP} \end{bmatrix} = -\left[\begin{bmatrix} 10.0036 & 0 & -1 \\ -0.1954 & 0 & 0 \end{bmatrix} \begin{bmatrix} -0.9904 & -0.0146 \\ 0.0195 & -0.0143 \end{bmatrix}\right] \begin{bmatrix} \Delta P(k) \\ \Delta\hat{\dot{m}}_{TT} \\ \Delta\hat{\dot{m}}_{eng} \\ \hat{e}_{m_{TT}} \\ \hat{e}_{P} \end{bmatrix} \tag{6.20}$$

Robustness analysis

The robustness of the controller is based on the frequency response of the sensitivity and complementary sensitivity functions, defined as:

$$S = G_{d\to y} = \frac{1}{1 + G(s)C(s)} \tag{6.21}$$

$$T = G_{r\to y} = \frac{G(s)C(s)}{1 + G(s)C(s)} \tag{6.22}$$

Where *G(s)* is the plant transfer function and *C(s)* is the controller transfer function in Laplace domain. Their relation becomes the identity matrix [8]:

$$T + S = I \tag{6.23}$$

The sensitivity function relates the influence of an output disturbance to the output of the closed-loop system. In the ideal case, the gain of the system should be zero, which means that a disturbance of the system does not affect its output. Of course, this is not possible for all frequencies, as system's robustness will decrease substantially. There is, therefore, a trade-off between disturbance rejection and controller robustness. In this controller design it is a high requirement the system to be strongly robust, as big differences can be encountered between the different realizations, i.e., each truck is different. The tool to analyze this is the complementary sensitivity function, which relates the commanded signal to the output signal. In the ideal case, its gain should be unitary for all frequencies. As both functions are related by (6.23), the parameter to be designed is the frequency at both Bode plots crosses. These two functions are shown for the multivariable system in Figure 37.

In Figure 37 , the mentioned above can be observed. The reference tracking for both signals is very good, even though until low frequencies, (~0.1Hz for the Tech-tank level and ~1Hz for the output pressure). This means that the system is very sensitive to high frequencies inputs, but fortunately, the signals spectrum is composed by low frequencies, so still the controller fulfills the requirements as it perfectly follows the reference for the regulation problem.

If the same analysis is done for the cross-coupling signals i.e., from pressure reference to Tech-tank level output and from Tech-tank level reference to output pressure, the resulting plots are shown in Figure 38. In this case, the requirements are that the signals affects as less as possible each other i.e., low gain at every frequency. This is shown to be easily achieved.

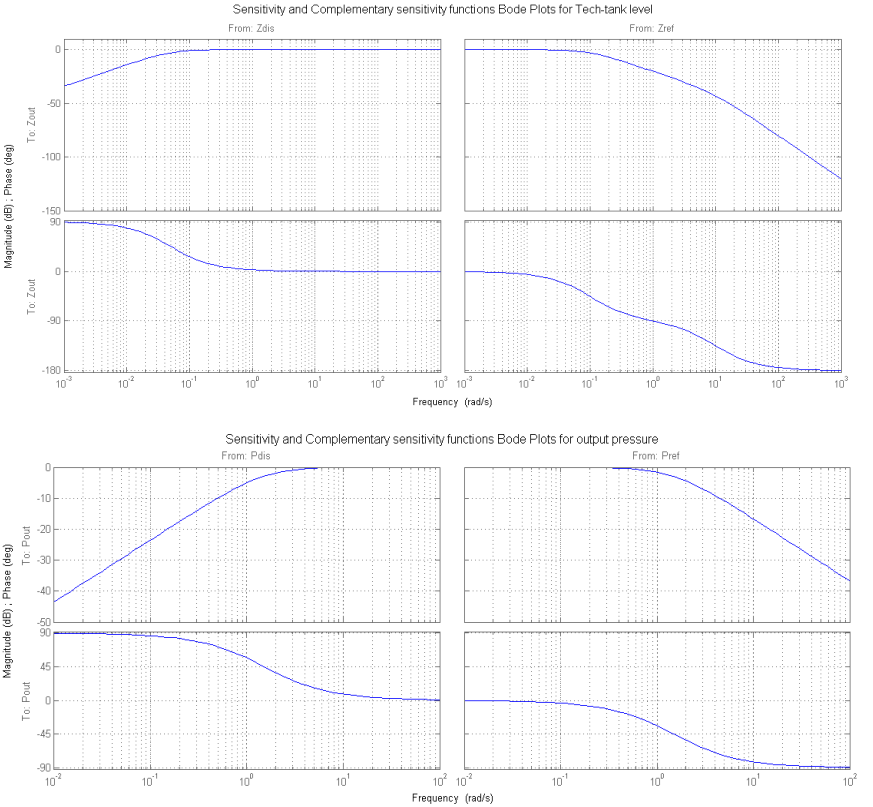

Figure 37: Sensitivity (left) and Complementary sensitivity (right) fucntions Bode plots for the two main variables, Tech-tank level (up) and output pressure (down), of the closed-loop system with the designed regulation in (6.19) and (6.20).

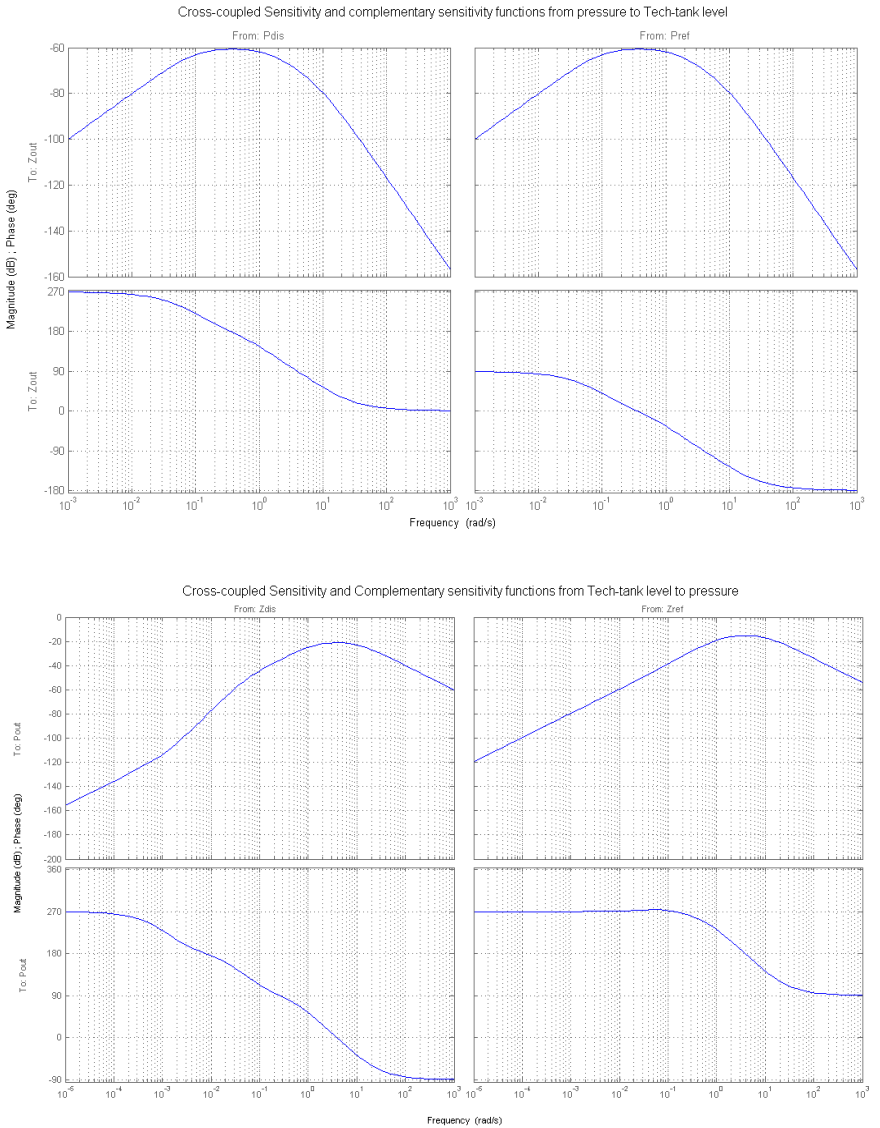

Figure 38: Cross-coupled sensitivity and complementary senstivity functions for the designed controller in (6.19) and (6.20) betwen the pressure and Tech-tank level (up) and Tech-tank level and pressure (down).

Control signals analysis

Another important analysis of the controller is how the reference signals and disturbances affect the control action sent to the actuators. They are wanted to be as small as possible, which means a longer life of the actuators as discussed in section 5.2 Hence, the transfer function from the reference and output disturbance to the control action can be analyzed from the frequency response point of view, as done before, which completes what is known as " the gang of four":

$$G_{d\to u} = G_{r\to u} = \frac{C(s)}{1 + G(s)C(s)} \tag{6.24}$$

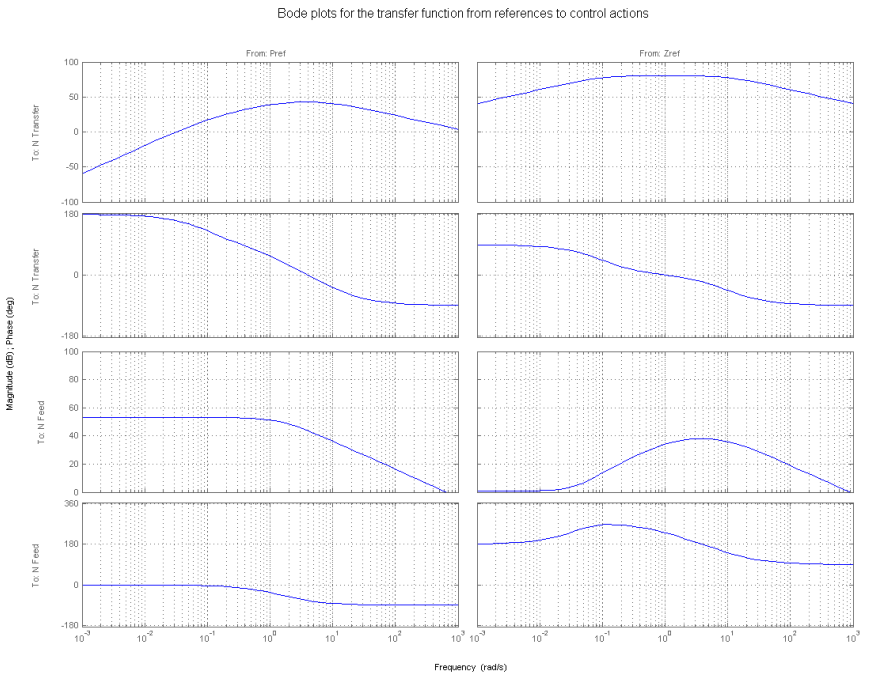

Figure 39: Bode plots for the transfer functions between the Tech-tank level reference (right) and the pressure reference (left) to the control actions (pumps RPM's).

As can be observed in Figure 39, the gain is not big in any case i.e., no resonance peaks, so the saturations of the controller actions will be limited by the magnitude of the commanded signal. Worth to note the gain between the pressure reference and the Transfer-pumps RPM's (upper left plot in Figure 39) tends to zero for low frequencies. In other words, there is no relation between changes in the output pressure reference and the Transfer-pumps RPM's. However, between the Tech-tank level reference and Feed-pumps RPM's (lower right plot in Figure 39) it is directly related as the gain is close to be unitary.

6.7 Tech-tank level reference generator

As explained in section 5.3 the final temperature of the fuel inside the Tech-tank cannot be controlled if the pressure is regulated, however, it is possible to modify its transient behavior by modifying the level of the fuel inside the tank by letting more or less fuel into from the Main-tank. This idea is illustrated in next figure:

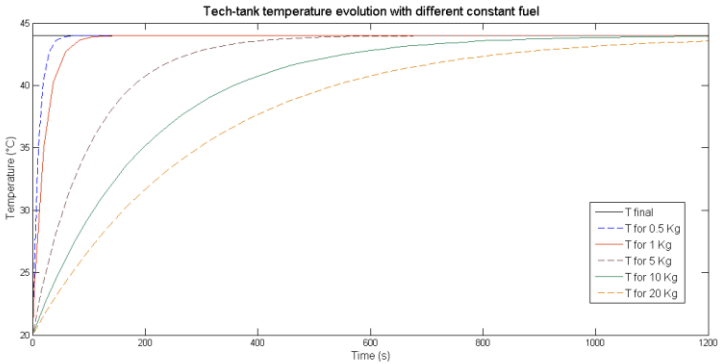

Figure 40: Temperature evolution over time for different constant fuel mass inside the Tech-tank for an engine consumption of 0.02Kg/s and 0.01Kg/s flow back from XPI at 60°C and 20°C fuel inside the Main-tank temperature.

In the figure above, the transient of the Tech-tank temperature is shown where the amount of fuel remains constant i.e., same amount of fuel in and out, but at different temperatures. The flow back from the XPI is 0.01Kg/s at 60°C whilst the fuel inside the Main-tank is at 20°C. The flow into the Tech-tank, which should equal the engine demand, is 0.02Kg/s. If the constant amount of fuel is set

to different values, the time to reach the final temperature from the energy balance, (2.20), is longer and longer as there is more fuel at the Main-tank. With a specific level, the final temperature can be reached sooner or later, depending on what is more interesting.

But the question now is: how should the level be set in order to control that settling time? The answer becomes a new control problem. This controller should handle the level so that the reference temperature is reached as soon as possible, and if it is not possible, keep as close as possible to it and as long as possible. The designed controller structure is:

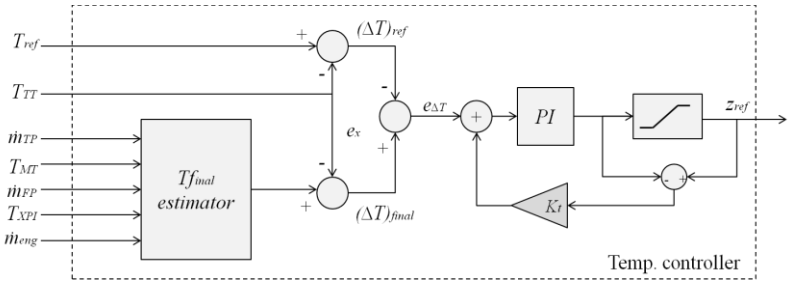

Figure 41: Temperature controller by generating the Tech-tank level reference. It is based on the estimation of the final temperature and includes a PI regulator with antiwindup and saturation according to the Tech-tank minimum and maximum level.

The regulator is based on the temperature difference that should exist between the reference temperature and the final temperature. Hence, an estimator computing the final temperature in equilibrium is needed. It uses the flows into and out the Tech-tank and the temperature at they are. Then, the error to the controller is the difference between the wanted difference and the actual temperature difference. The controller is a PI regulator that sets the appropriated Tech-tank level in order to maintain the wanted temperature difference. A saturation module is included to avoid overflows of the Tech-tank, which is set to the selected limits. Antiwindup action is included as well to not keep increasing the integral term. Worth to note that the error will never be zero, unless the reference temperature and the final one are equals. Hence, the antiwindup is very necessary to not overflow the integral term variable. The designed PI controller, in parallel form, has the coefficients: $K = 0.01$, $Ki = 0.1$, $Kt = 10$.

7. Controller implementation

In this chapter, the implementation of the controller developed previously is discussed.

7.1 Sampling time

The selection of the sampling time for the system depends on different criteria as stated in [9]:

- Response to reference signals
- Influence of disturbances
- Computational load of the computer
- Digital filtering of the signals

In order to avoid aliasing, the sampling frequency should be, at least, twice the natural frequency of the system, as the sampling theorem (Shannon-Nyquist) states. But to account for the previously mentioned factors, it is a common practice to have it of one order of magnitude higher. A basic selection rule is to choose it as [9]:

$$\omega h_\tau = 0.1 \; to \; 0.6 \tag{7.1}$$

This frequency, from the robustness analysis, is 0.1Hz, and therefore h_τ would be enough with 1s. However, if systems' delay are accounted, it is better to be selected as 50ms and still not requiring too much computational power.

7.2 Controller discretization

In this section, the controller is discretized with the designed sample time h_τ *=50ms* so that it can be implemented in a digital system.

First, as the Kalman filter is a state-space system realization, it can be discretized as [9]:

$$x(kh_\tau + h_\tau) = \Phi x(kh_\tau) + \Gamma u(kh_\tau) \tag{7.2}$$

$$\Phi = e^{Ah_\tau} \tag{7.3}$$

$$\Gamma = \int_0^{h_\tau} e^{As} ds B \tag{7.4}$$

For the state-feedback gain, it is a bit more complex and to simplify its discretization from continuous time, it can be computed as [9]:

$$\tilde{L} = L\left(I + (A - BL)\frac{h_\tau}{2}\right) \tag{7.5}$$

Assuming a second order error. Applying these formulas to the controller in (6.19) and (6.20) gives the digital regulator for h_τ*=50ms*:

$$\begin{bmatrix} \Delta\hat{P}(k+1) \\ \Delta\hat{m}_{TT}(k+1) \\ \Delta\hat{m}_{MT}(k+1) \\ \Delta\hat{m}_{eng}(k+1) \end{bmatrix} = \begin{bmatrix} 0.9995 & 0 & 0 & 0 \\ 0 & 0.9975 & 0 & 0 \\ 0 & 0 & 0.9975 & 0 \\ 0 & 0 & 0 & 1 \end{bmatrix} \begin{bmatrix} \Delta\hat{P}(k) \\ \Delta\hat{m}_{TT}(k) \\ \Delta\hat{m}_{MT}(k) \\ \Delta\hat{m}_{eng}(k) \end{bmatrix} +$$

$$\begin{bmatrix} 0.499 & 0 & 0 & 0 & 0 & 0 \\ 0 & 2.497 & 0 & -49.94 & 49.94 & 0 \\ 0 & 0 & 2.497 & 0 & -49.94 & 0 \\ 0 & 0 & 0 & 0 & 0 & 0 \end{bmatrix} \cdot 10^{-3} \cdot \begin{bmatrix} \Delta P(k) \\ \Delta m_{TT}(k) \\ \Delta m_{MT}(k) \\ \dot{m}_{eng}(k) \\ \Delta\dot{m}_{TP}(k) \\ \Delta\dot{m}_{FP}(k) \end{bmatrix} \tag{7.6}$$

$$\begin{bmatrix} \Delta\hat{P}(k) \\ \Delta\hat{m}_{TT}(k) \\ \Delta\hat{m}_{MT}(k) \\ \Delta\hat{m}_{eng}(k) \end{bmatrix}_{out} = \begin{bmatrix} -0.01 & 0 & 0 & 0 \\ 0 & 1 & 0 & 0 \\ 0 & 0 & 1 & 0 \\ 0 & 0 & 0 & 0 \end{bmatrix} \begin{bmatrix} \Delta\hat{P}(k) \\ \Delta\hat{m}_{TT}(k) \\ \Delta\hat{m}_{MT}(k) \\ \Delta\hat{m}_{eng}(k) \end{bmatrix}$$

$$+\begin{bmatrix} 0.01 & 0.0025 & 0 & 0 & 0 & 5.316 \\ 0 & 0 & 0 & 0 & 0 & 0 \\ 0 & 0 & 0 & 0 & 0 & 0 \\ 0 & 0 & 0 & 1 & 0 & 0 \end{bmatrix} \begin{bmatrix} \Delta P(k) \\ \Delta m_{TT}(k) \\ \Delta m_{MT}(k) \\ \dot{m}_{eng}(k) \\ \Delta \dot{m}_{TP}(k) \\ \Delta \dot{m}_{FP}(k) \end{bmatrix}$$

$$\begin{bmatrix} \Delta \dot{m}_{TP}(k) \\ \Delta \dot{m}_{FP}(k) \end{bmatrix} = -\begin{bmatrix} 7.477 & 0 & -1 & -0.7675 & -0.0113 \\ -0.146 & 0 & 0 & 0.015 & -0.0147 \end{bmatrix} \begin{bmatrix} \Delta P(k) \\ \Delta \widehat{m}_{TT}(k) \\ \Delta \widehat{m}_{eng}(k) \\ \hat{e}_{m_{TT}}(k) \\ \hat{e}_P(k) \end{bmatrix} \tag{7.7}$$

The same can be done for the integrators and PI's. In this case, it is simpler to use Tustin's approximation of their transfer functions [9]:

$$\boldsymbol{s}' = \frac{2}{h_\tau} \cdot \frac{\boldsymbol{z}-1}{\boldsymbol{z}+1} \tag{7.8}$$

Giving:

$$I(\boldsymbol{z}) = 0.025\,\frac{\boldsymbol{z}+1}{\boldsymbol{z}-1} e(\boldsymbol{z}) \tag{7.9}$$

$$PI_{temp}(\boldsymbol{z}) = 0.01 \cdot e_{\Delta T}(\boldsymbol{z}) + 0.0025 \frac{\boldsymbol{z}+1}{\boldsymbol{z}-1} e_{\Delta T}(\boldsymbol{z}) \tag{7.10}$$

Note that as the system is linearized, the equilibrium points should be extracted from the inputs (measurement signals) and added to the outputs (control actions).

7.3 Time delays in discrete time

The continuous-time delays are infinite as all the differentially small past values have to be stored. However, in discrete time it can be handled easily as they become finite, because the control action remains constant between sample instants [9]. The system, composed by the delayed reading of the output, can therefore be expressed (see chapter 3 of [9] for more information) as:

$$\begin{bmatrix} x(k+1) \\ x(k+2) \\ \vdots \\ x\big(k+(d_\tau-1)\big) \\ x(k+d_\tau) \end{bmatrix} = \begin{bmatrix} 0 & 0 & \cdots & 0 & 0 \\ 1 & 0 & \cdots & 0 & 0 \\ \vdots & \vdots & \ddots & \vdots & \vdots \\ 0 & 0 & \cdots & 0 & 0 \\ 0 & 0 & \cdots & 1 & 0 \end{bmatrix} \begin{bmatrix} x(k) \\ x(k+1) \\ \vdots \\ x\big(k+(d_\tau-2)\big) \\ x\big(k+(d_\tau-1)\big) \end{bmatrix} + \begin{bmatrix} 1 \\ 0 \\ \vdots \\ 0 \\ 0 \end{bmatrix} u(k)$$
$$y(k) = \begin{bmatrix} 0 & 0 & \cdots & 0 & 1 \end{bmatrix} \begin{bmatrix} x(k) \\ x(k+1) \\ \vdots \\ x\big(k+(d_\tau-2)\big) \\ x\big(k+(d_\tau-1)\big) \end{bmatrix} \tag{7.11}$$

In other words, a discrete time-delay is a set of variables saving the past information as many samples as the whole time-delay is covered. The content of the variables is shifting forward every sample. It can be expressed by the *z* transform as:

$$y(\boldsymbol{z}) = \boldsymbol{z}^{-d_\tau} \cdot u(\boldsymbol{z}) \tag{7.12}$$

In the expressions, d_τ is an integer equal to the amount of sample time to cover the time delay, τ (assuming $\tau > h_\tau$):

$$d_\tau = \left\lceil \frac{\tau}{h_\tau} \right\rceil \tag{7.13}$$

For the system considered, $d_\tau = 5$. Using the ceiling operation includes a rounding error that is negligible if it is compared with the delay estimation error.

7.4 Real-time considerations

When implementing a discrete controller, the way it is programmed affects the expected behavior. Some of these factors are the computational delay, the numerical rounding inside the machine and how the scheduling of the concurrency of the threads is handled.

Therefore, special attention should be put on the implementation of the algorithm. In order to avoid concurrency problems, the actions should be encapsulated in a way all of them are fully completed, or stopped at an allowed point. This is dependent on the code used and how the threads are handled in the machine.

Respect to the rounding effects on the computations, it should be considered in the controlled design as a quantification factor. In addition, the selected representation of the numbers limits the number range, so possible overflows have to be accounted for.

Another problem with respect to the digital calculations is how float numbers are handled inside the machine. Float operations can make the computational time too large, and a way to reduce this computation time is by means of using fixed-point representation with a suitable word length. This can reduce the computational time considerably.

It is convenient to reduce the computational delay between reading the inputs and outputting the control actions as much as possible. The way of doing this is to compute only the necessary operations as soon as possible in the code i.e., read the inputs and compute the control actions from the state feedback; and to the updating of all the rest of variables is left for later e.g., computation of observed states, error integrators, etc.

8. Results

In this section, the results of the controller are presented, both from simulation and testing in the rig. It is subdivided into output pressure, Tech-tank level and temperature. Step response experiments are shown for all three, whilst disturbance rejection is only shown in the case of the pressure and its influence on the influence on the Tech-tank level.

8.1 Pressure control

This subsection consists of the output pressure performance against step reference tracking and disturbance rejection. The influence on the Tech-tank level is also commented.

Figure 42 shows the output pressure predicted by simulation when the controller in (6.19) and (6.20) is used. The same is presented in Figure 43 for the system in the rig when the discretized controller of (7.6) and (7.7) is used. In both results the system starts in steady-state, at 6 bars output pressure. The valve simulating different engine consumptions is left at the same position; therefore the mass-flow provided by the feed-pump varies in order to follow the pressure reference. The response behavior is obtained for steps of ± 1bar.

The results are very close to each other, but some differences can be seen. First, the time delay of the rig is much less than the one in the real system (as the one used in simulations). This makes the pressure reaches the final value faster than the simulation (about 1s settling time in the rig). The simulated response is over-damped whilst the real one is a bit under-damped, but it follows the step response even better.

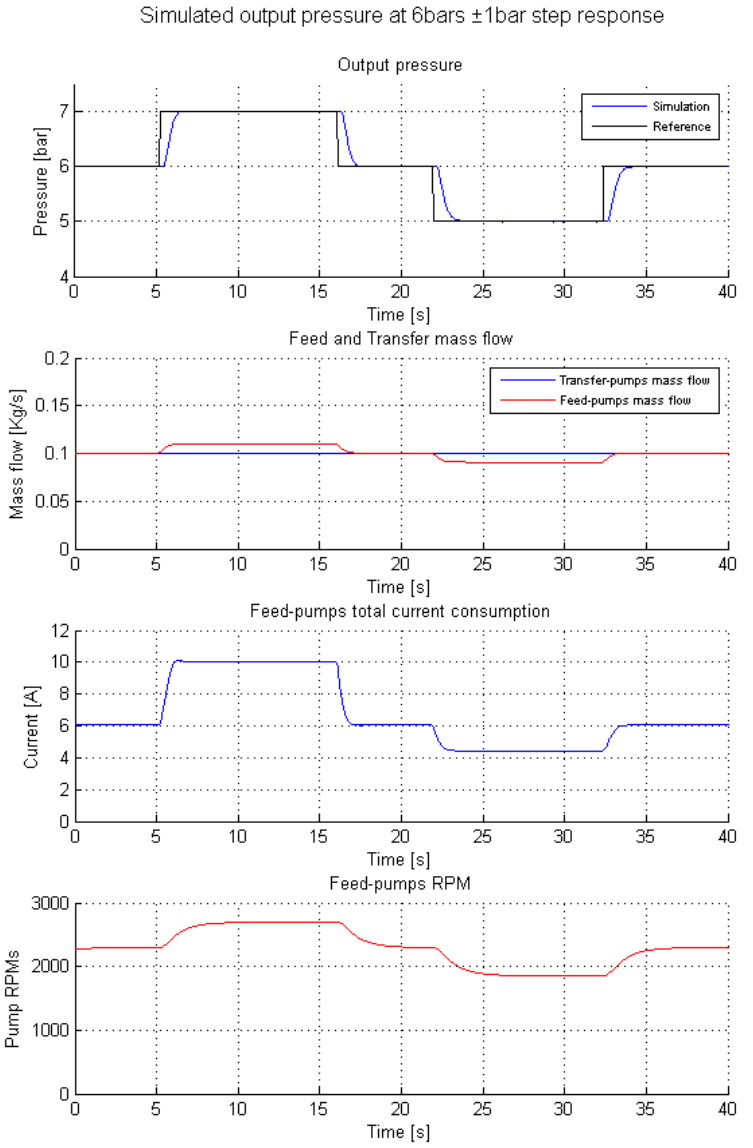

Figure 42: Output pressure reference tracking for positive and negative steps of one bar, at the equilibrium point of 6 bars, predicted by simulation. The output mass-flow and total current consumption are included with the Feed-pumps RPM's.

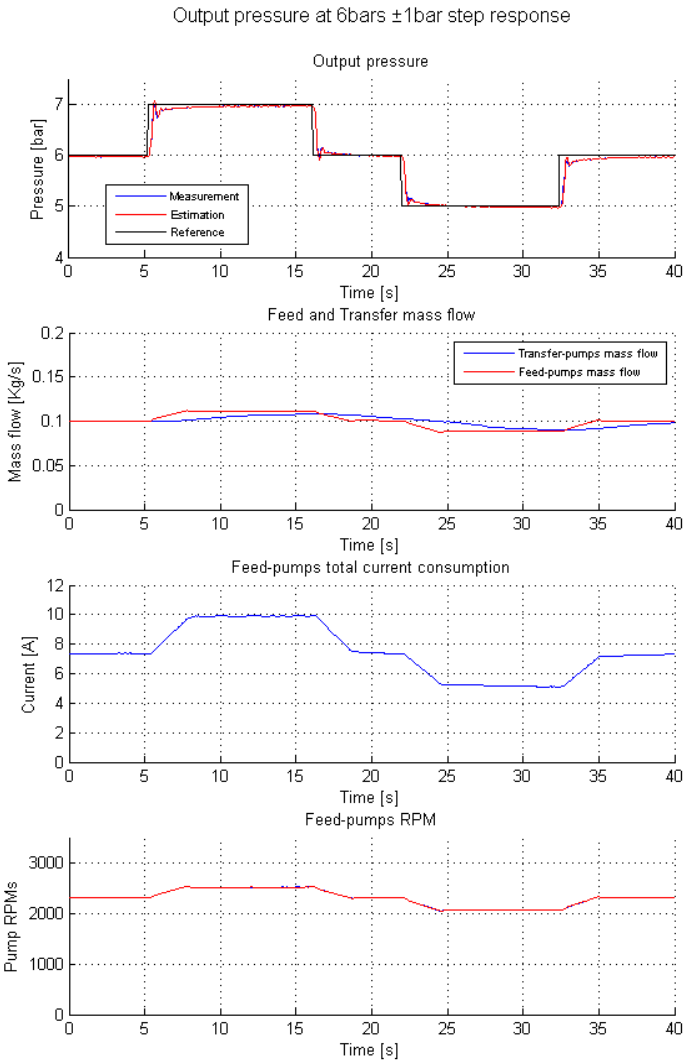

Figure 43: Output pressure reference tracking for positive and negative steps of one bar, at the equilibrium point of 6 bars, in the rig. The output mass-flow and total current consumption are included with the Feed-pumps RPM's.

Regarding the mass out of the Tech-tank, it is similar in both simulation and rig, for the feed mass-flow, but it is not the case for the transfer mass-flow. The reason is that the transfer-pumps tries to keep the Tech-tank level in both cases, but for the system in the rig, the feed mass-flow is sent back to the main-tank, but in the simulations it is assumed to be partly consumed by the engine (at a rate of 0.02 Kg/s).

Looking at the current consumption, it can be seen that it is slightly higher for the real system. This is because of the different estimations used for the simulated system. Despite of this, it can be conclude that the simulation environment is good enough to work with for controller design, as it represents the real system accurately enough.

The configuration used so far is without the optimal pump handling explained in section 6.5 the results obtained by running the same previous experiments in the real system are shown in Figure 44. It can be seen how the same amount of mass flow is obtained by running the Feed-pumps at different RPM's whilst tracking the reference output pressure.

The first difference is in the settling time it takes for the pressure to reach the reference. In the real system, the pumps do not behave as ideally as expected. The main problem is the start-ups. The internal controller tries to reach the commanded RPM by means of internal current feed-back. This arise big transients (it takes up to 5s) and can even make the output pressure unstable because of big start-ups and stops due to too big demand of current. This is shown in Figure 45.

Hence, the optimal handling of two parallel pumps must be modified in order to allow smooth start-up of the pump that helps the main one. Currently, the minimum value is set to 1300 RPM i.e., the pumps are never stop. What this provokes is that the current consumption is not really reduced with the optimal handling as the standby pump consumes around 0.3A, which is around the improvement with the optimal handling.

Another consequence of this internal regulator problem is that the tracking takes longer due to the start-up time. Note how the steps, where the pump's RPM are different, takes longer than the ones when both pumps run at time (from 6 bars to 7 bars), which is similar as the one obtained without the optimal handling.

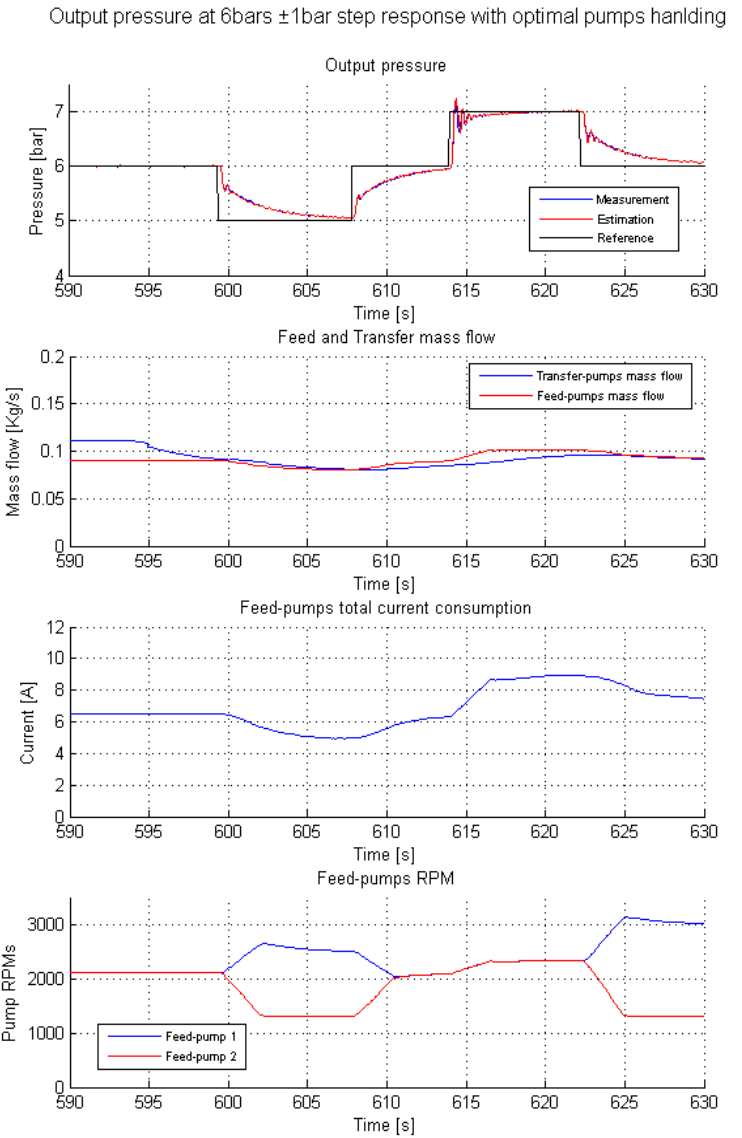

Figure 44: Output pressure reference tracking for positive and negative steps of one bar, at the equilibrium point of 6 bars, in the rig with optimal pumps handling. The output mass-flow and total current consumption is included with the Feed-pumps RPM's.

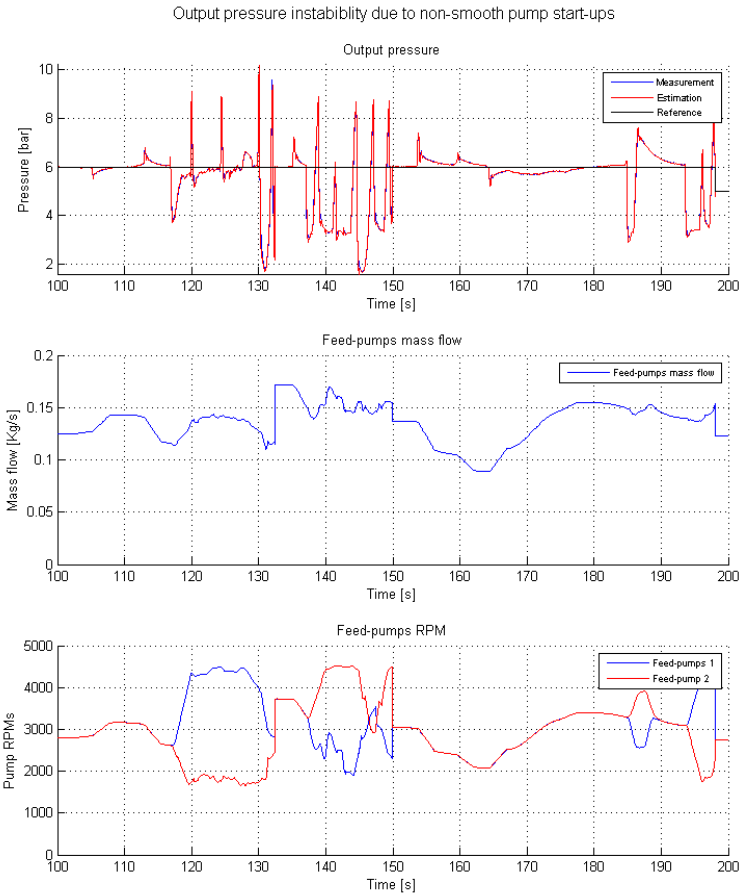

Figure 45: Pressure output when the pump start-up is not handle smooth. It shows how the pressure gives a very high value and the control action tries to overcome that transient, giving a big change on the control action and resulting in an unstable behavior.

Figure 46, Figure 47 and Figure 48 show the output pressure tracking with steps of ± 1.5 bars, in simulation, in the rig, and with optimal handling. In this case, the steady-state pressure is set to 4 bars as at 6 bars the maximum would reach 7.5 bars, deriving too much current consumption for the pumps, which makes them to overload and turn off by the internal control system. Then they will

try to restart again, provoking the same overload and making the system unstable, never reaching the commanded output pressure.

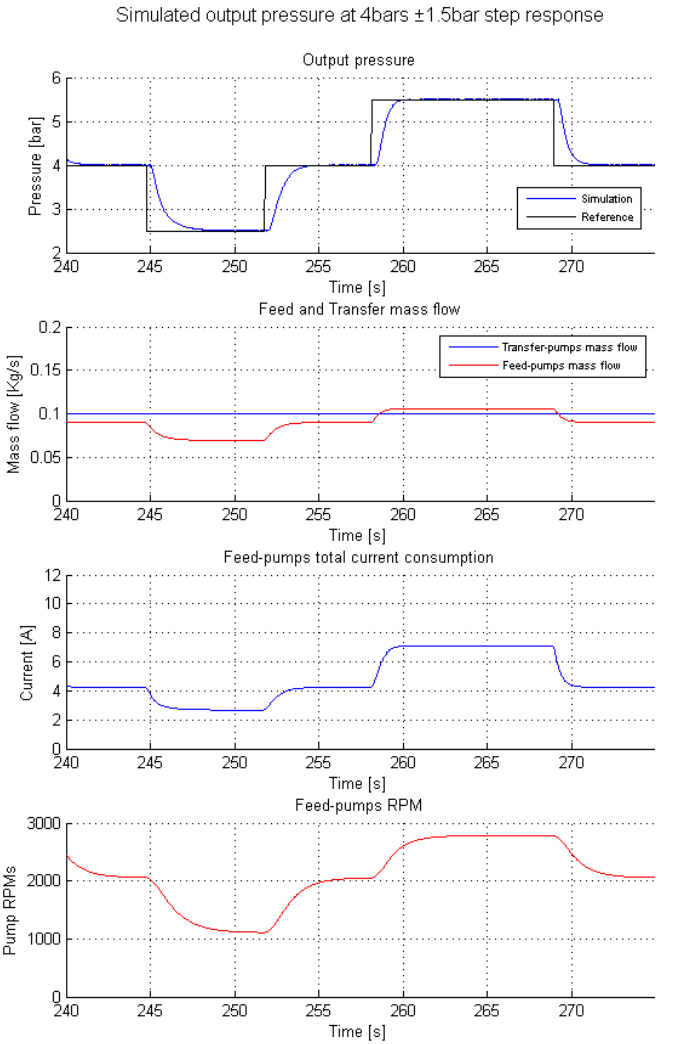

Figure 46: Output pressure reference tracking for ±1.5bar steps, at the equilibrium point of 4 bars, predicted by simulation. The output mass-flow and total current consumption is included with the Feed-pumps RPM's.

The results are very similar to the previous ones for steps of ±1bar. The real system reaches the commanded pressure faster than what the simulation predicts due to the difference in the estimated time delay. However, for these experiments the transient is closer to simulation i.e. same damping.

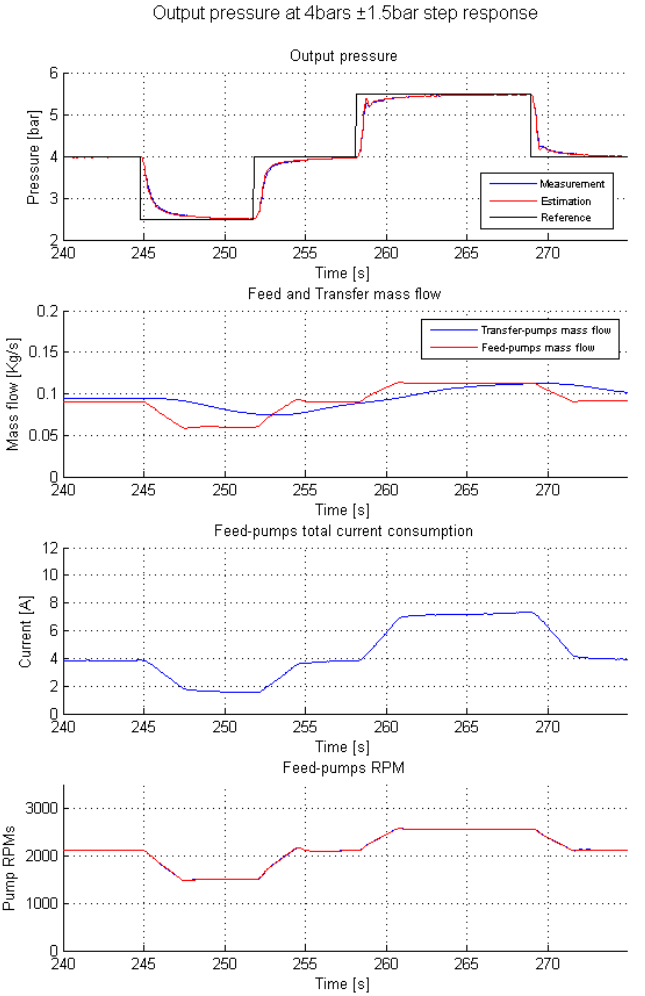

Figure 47: Output pressure reference tracking for ±1.5 bar steps, at the equilibrium point of 4 bars, in the rig. The output mass-flow and total current consumption is included with the Feed-pumps RPM's.

The comments regarding the results for the optimal parallel pump handling is still valid, despite of the different set point and steps amplitude, this can be seen in Figure 48.

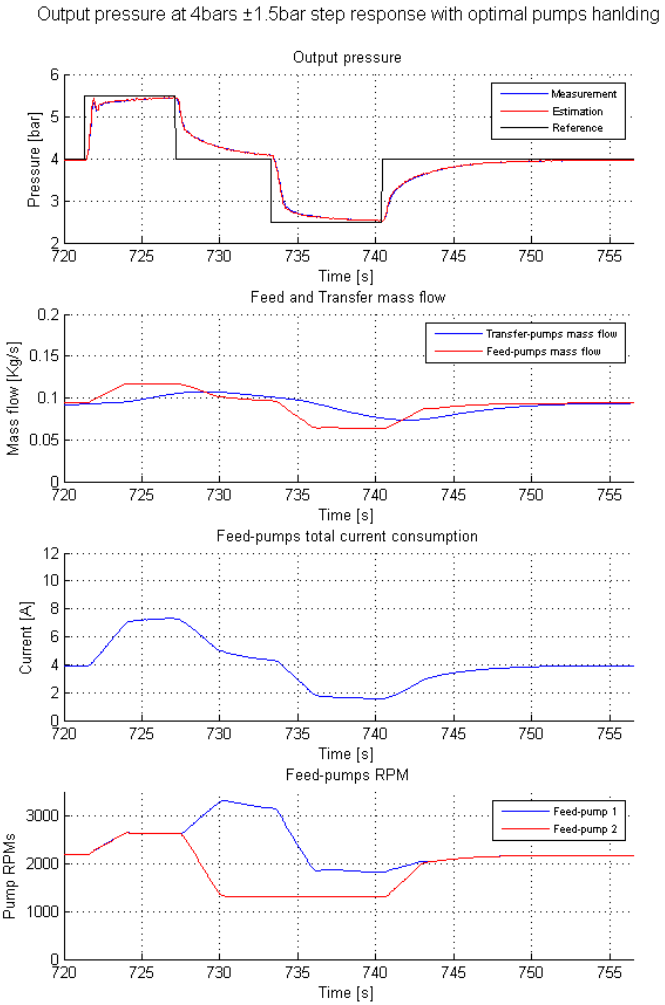

Figure 48: Output pressure reference tracking for ±1.5 bar steps, at the equilibrium point of 4 bars, , in the rig with optimal pumps handling. The output mass-flow and total current consumption is included with the Feed-pumps RPM's.

Once the reference tracking results have been presented, the most important aspect of the system is the disturbance rejection. This comes from the different engine fuel demand at the different RPM's of the engine. In the rig, it is simulated by changing the ball-valve at the output pipe of the feed-pumps. This modifies the relation between velocity and pressure and thus, for maintaining the same pressure, the pumps have to run at different speed, as it would happen in the real system. Simulation results are not presented here as it is hard to get values closer to the experimental ones and therefore there is not possible to make the comparisons.

An important limitation in the performance is how the rig is built. This is, the demanded mass-flow from the engine is not prior known, and therefore no feed-forward can be used to anticipate big pressure drops when the engine demand changes. In the real system, the mass-flow consumption is estimated from the engine RPM's and load, and this signal can be used as input to the state-feedback, behaving as a feed-forward when it is properly designed i.e., by punishing the corresponding state change in the state-feedback gain. As a consequence, the pressure drops are bigger than they would be when this is considered in the real system.

Figure 49 and Figure 50 shows the disturbance rejection performance when the engine mass-flow demand is not prior known. It is however included in the plot as an estimation that equals the steady feed mass-flow.

In the first case (Figure 49) both pumps share the total required mass-flow. The transients are properly over-damped i.e., no overshoots are seen, even for big changes in the engine mass-flow demand. However, the pressure drops are quite big and it takes some time (around 2s) until they are overcome because of the mentioned above. This settling time is higher when the optimal handling is used (Figure 50) due to the same considerations as for the reference tracking.

Some points are highlighted for comparison, where the mass-flow consumed by the engine is similar. The first points in both figures are selected to show a mass-flow demand around 0.07Kg/s. If the current is extrapolated from the first case to match the mass-flow of the second, it should be 6.122A, whilst it actually is 6.178A. This follows the previous conclusions: the standby current consumption

is as big as the improvement. In the second case, it is shown that when both pumps run at a time, the working point is the same, and so it is the current consumption.

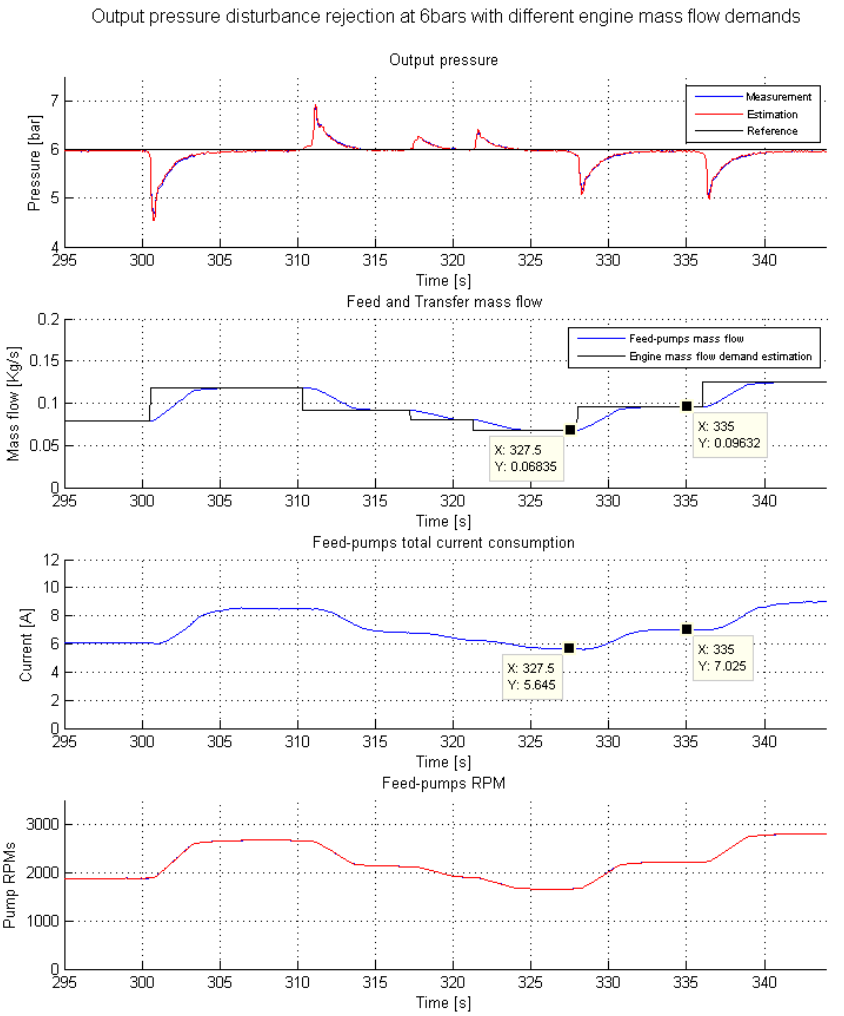

Figure 49: Output pressure disturbance rejection at 6bars set-point. Different engine mass-flows demands are simulated by changing the output ball-valve position. The total current consumption and RPM's of the Feed-pumps are included. The engine demand mass-flow is estimated as the Feed-pumps steady mass-flow.

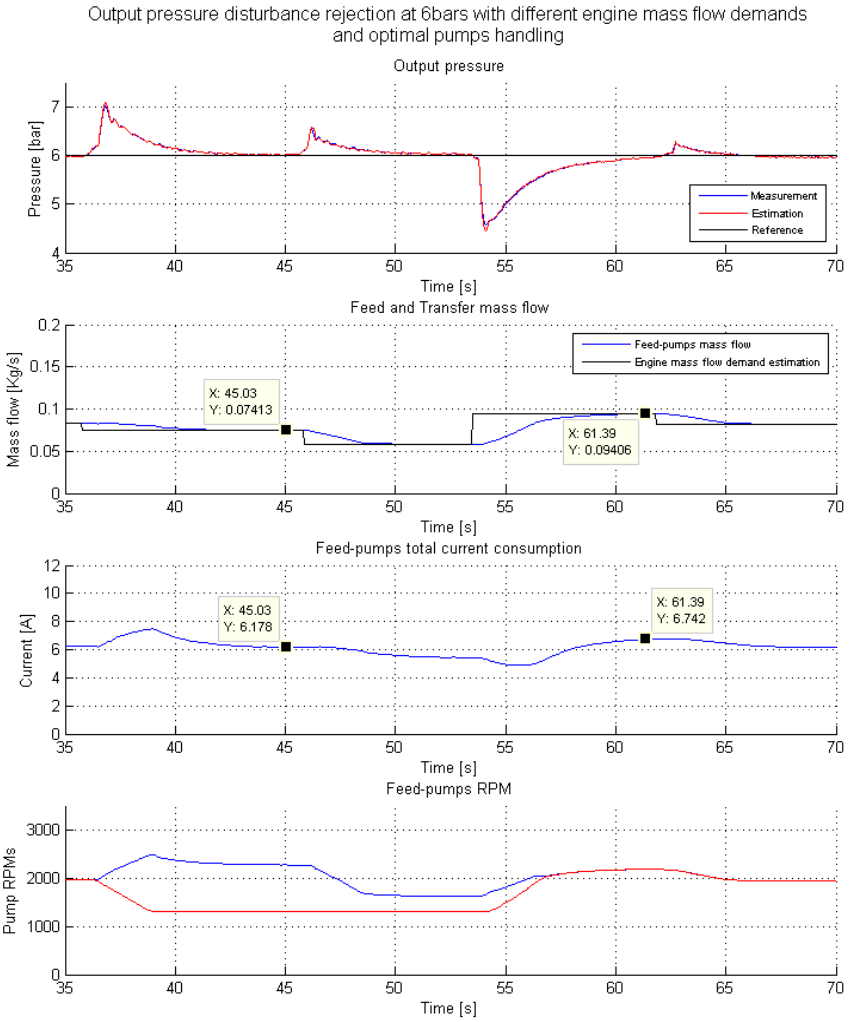

Figure 50: Output pressure disturbance rejection at 6 bars set-point with optimal pumps handling. Different engine mass-flows demands are simulated by changing the output ball-valve position. The total current consumption and RPM's of the Feed-pumps are included. The engine demand mass-flow is estimated as the Feed-pumps steady mass-flow.

As a conclusion, the controller works fine even without knowing the engine mass-flow demand, and its performance can be improved when it is considered.

The settling time is doubled from the results without the optimal handler i.e., around 4s.

Finally, as the system is multivariable, the coupling between output pressure and Tech-tank level are shown in Figure 51 and Figure 52. In the first case, the changes in the pressure are caused by the reference set point, whilst in the second case the output pressure are caused by different demanded mass-flows from the engine. In both cases, the Tech-tank level is presented next to the pressure to see its changes because of the system's coupling.

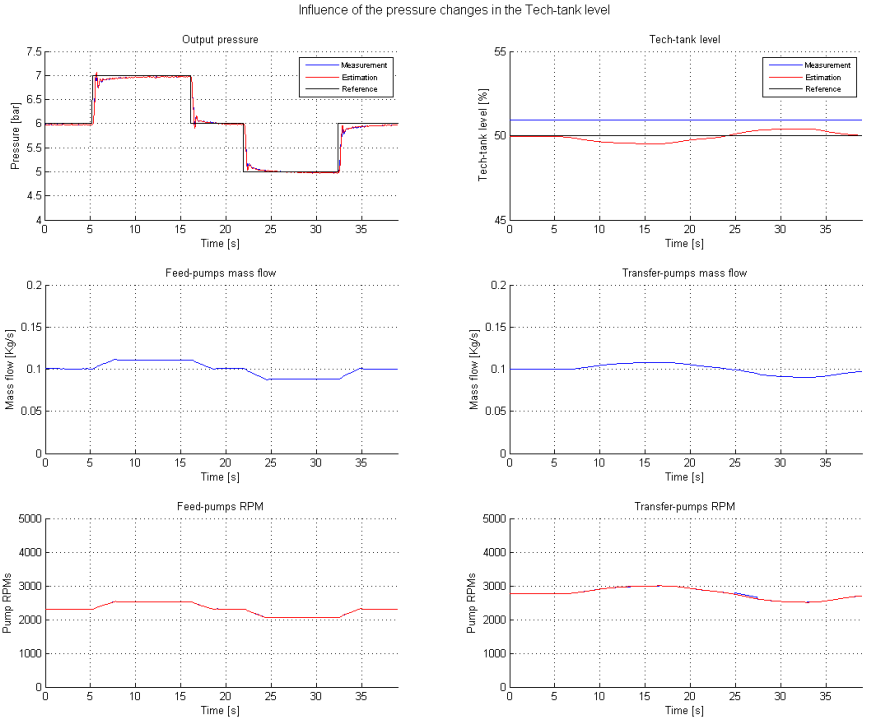

Figure 51: Output pressure reference tracking and Tech-tank level. The commanded Feed-pumps and Transfer-pumps at the shown RPM's providing the feed and transfer mass-flows are included.

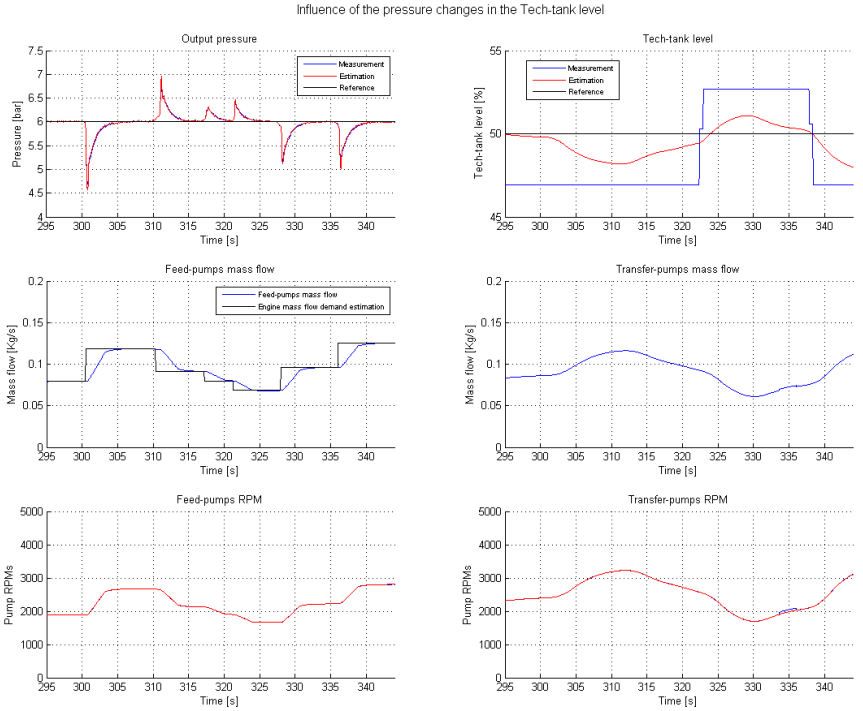

Figure 52: Output pressure disturbance rejection and Tech-tank level. The commanded Feed-pumps and Transfer-pumps at the shown RPM's providing the feed and transfer mass-flows are included.

As shown, the Tech-tank level remains almost constant for both cases as the Transfer-pumps reacts against the different mass-flow that the Feed-pumps output. It is achieve by supply the same mass-flow with the Transfer-pumps: note the similar shape of the transfer mass-flow in both cases. The influence of the changes in the Feed-pumps mass-flow is bigger as these changes are, making the reaction of the Transfer-pumps longer to overcome the transient.

8.2 Level control

In this subsection the Tech-tank level performance is shown from steps reference tracking. For the Tech-tank level, there are not load disturbances in the normal behavior, as it can happen when, for instance, the sensor gets stuck.

At first point, the estimation of the tank's levels is presented in Figure 53 and **Figure 54** when the Tech-tank level is following steps of ±10% over the 50% steady level. The first figures are the results in simulation whilst the in the second it is shown the results from experiments.

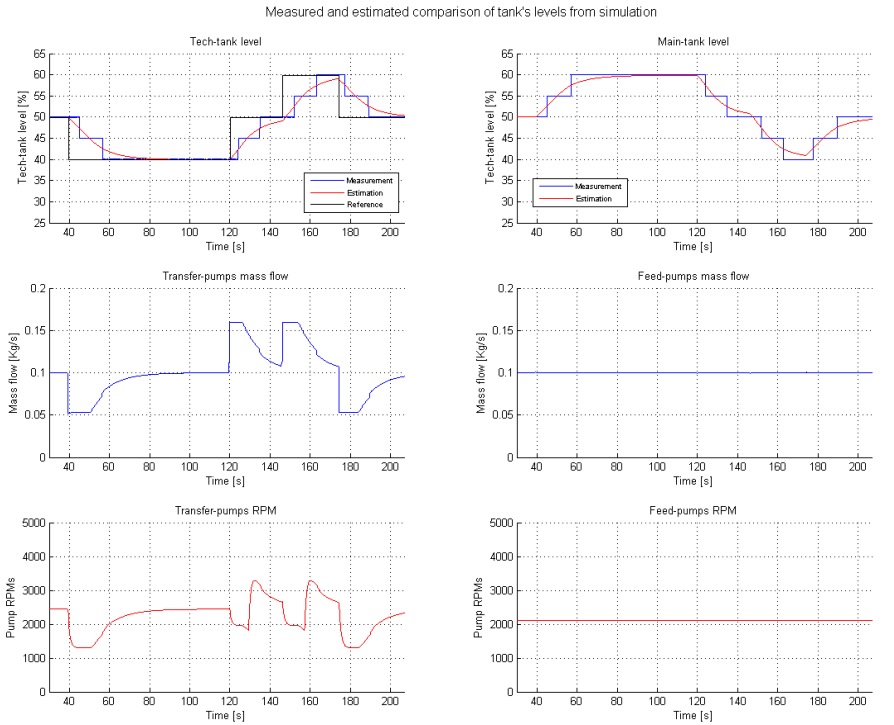

Figure 53: Tech-tank (left) and Main-tank (right) level measurement in simulation with the estimation overlaid. The Tech-tank level is set at 50% and ±10% seteps are input. The mass flow into the tanks is presented below each tank level as well as the pump's RPM's the pupms work at.

It can be shown how the levels estimations follows the measured values, that are quantized, and it provides a continuous signal used for the controllers, which improves considerably its performance as no big drops from the measurement provokes big drops in the control signals. These results validate the observer design by means of a Kalman filter.

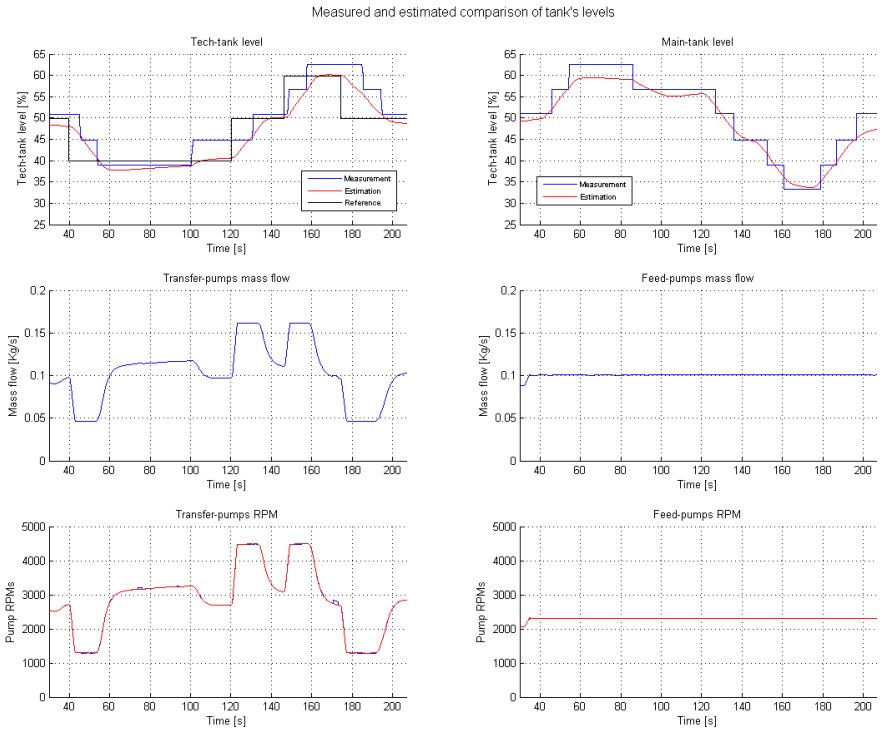

Figure 54: Tech-tank (left) and Main-tank (right) level measurement in the rig with the estimation overlaid. The Tech-tank level is set at 50% and ±10% seteps are input. The mass into the tanks is presented below each tank level as well as the pump's RPM's the pupms work at.

Once the tanks' level are accepted to be properly estimated, the Main-tank level is left (as it is not controlled) and only the Tech-tank level behavior will be following presented. First, the reference tracking with ±10% level steps at a steady level of 50% is presented in Figure 55 and Figure 56.

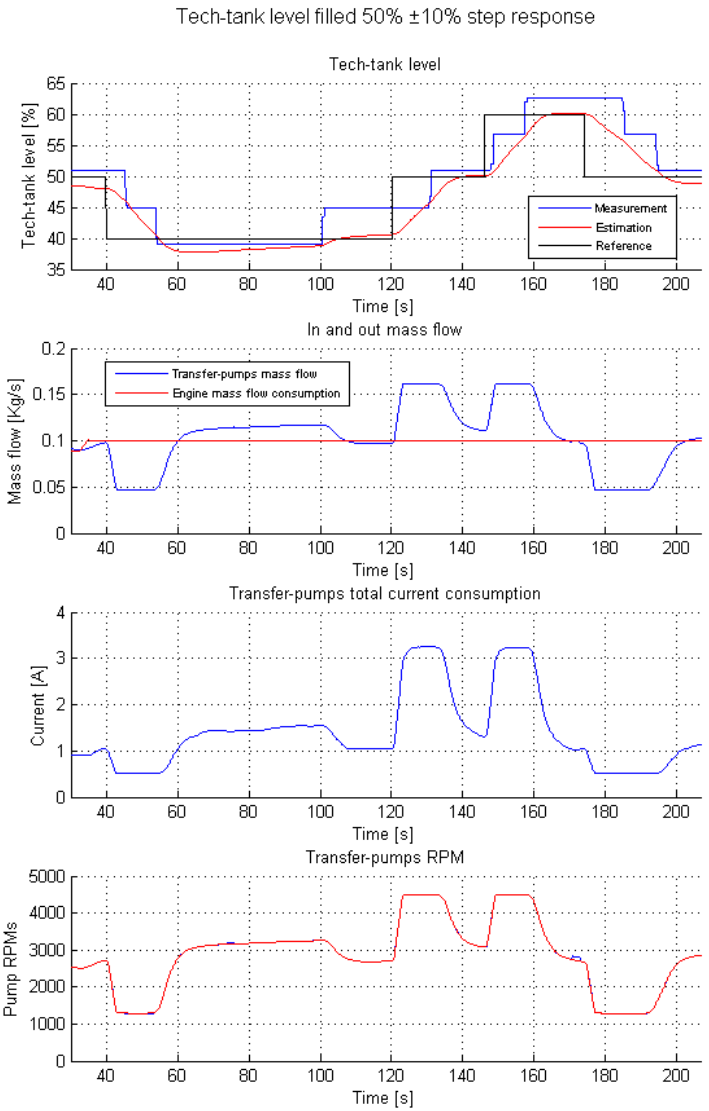

Figure 55: Tech-tank level measurement with the estimation overlaid. The Tech-tank level is set at 50% and ±10% steps are input to show the reference tracking performance. The mass flows into and out of the tank are presented below each tank level as well as the pump's RPM's the pumps work at and the total current consumption.

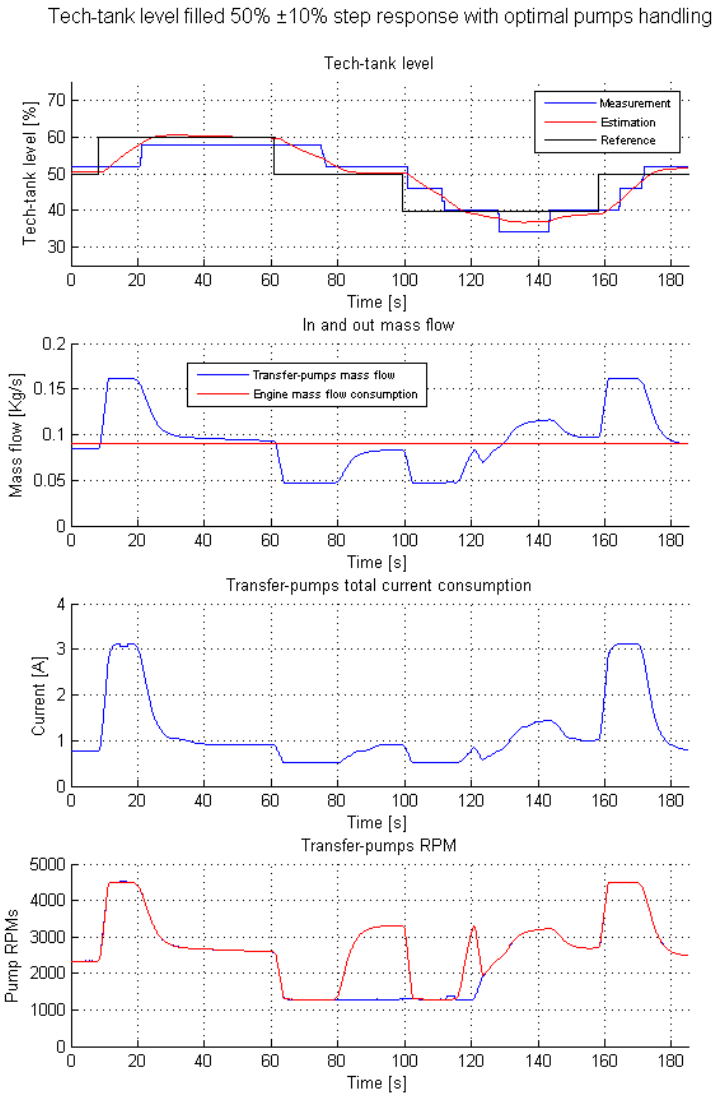

Figure 56: Tech-tank level measurement with the estimation overlaid. The Tech-tank level is set at 50% and ±10% steps are input to show the reference tracking performance with optimal pumps handling. The mass flows into and out of the tank are presented below each tank level as well as the pump's RPM's the pumps work at and the total current consumption.

The first plots show the reference tracking performance of the Tech-tank level when no optimal handling of the Transfer-pumps is used, whilst the second uses it. Both cases have almost the same performance regarding the reference tracking: the reference is easily reached when the step is positive i.e., the Transfer-pumps are completely deciding its level. However, when the step is negative, the Transfer-pumps cannot do anything but being turned off (actually, they are left in the standby position of 1300RPM to avoid the previously commented start-up's transients). Hence, for negative steps the set point settling time depends on the engine demand i.e., Feed-pumps mass-flow setting out fuel from the Tech-tank. This makes that a small error still remains as the integral action is not very big since the Tech-tank level error is not very important compared to the pressure set point.

Again, the same considerations regarding the current consumptions can be done here: the standby current consumption is as big as the improvement with the optimal handling and no difference can be seen in these experiments.

The Tech-tank level can be considered linear as it behaves in the same way for higher input steps.

8.3 Temperature control

In this subsection, the temperature performance with the controller designed in section 6.7 is presented. Due to the rig's limitations, it could not be shown with experimental data (there is no heater for simulating the engine mass-flow back to the Tech-tank at high temperature). Therefore, the results are presented from the simulation environment.

Figure 57 shows how the Tech-tank temperature reference is achieved. The temperature controller sets the Tech-tank level providing an equilibrium that keeps the temperature at the reference point. That temperature is reached as fast as possible and then kept as long as possible. Note that the Tech-tank level controller should work properly in order to follow the reference, but as it has been designed for set-point tracking, there is a ramp error as it only includes one integrator, but this does not limit the temperature set-point tracking. The Tech-tank level keeps

increasing to maintain the in and out energy flows that keeps the temperature at the desired value.

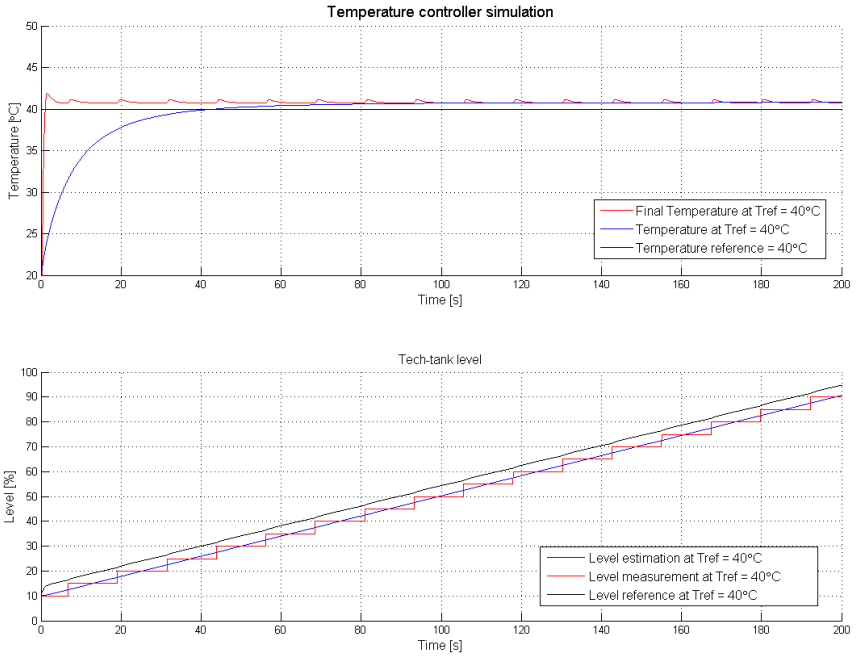

Figure 57: Tech-tank temperature reference tracking at 40°C. The commanded Tech-tank level is presented as the control action for the temperature controller.

The temperature value will always be between the Main-tank fuel temperature and the temperature of the mass-flow back from the engine. Therefore, the demanded temperature can only be maintained while the Tech-tank is not saturated (at high or low limits), then the final equilibrium temperature will necessarily be the final Tech-tank temperature value for the energy flows in and out the Tech-tank that maintains the engine demand at the required pressure, and the flow back from the engine.

The effects of the Tech-tank saturation in the temperature are shown in Figure 58. It can be seen how, if the limitation of the pumps allow it (see the behavior for 20°C reference), the commanded temperature is reached in a short

time, until the Tech-tank saturates and the same final temperature is reached, but in a much longer settling time. When closer to the final temperature the commanded temperature is, the longer it takes to the Tech-tank to saturate (see the behavior for 50°C).

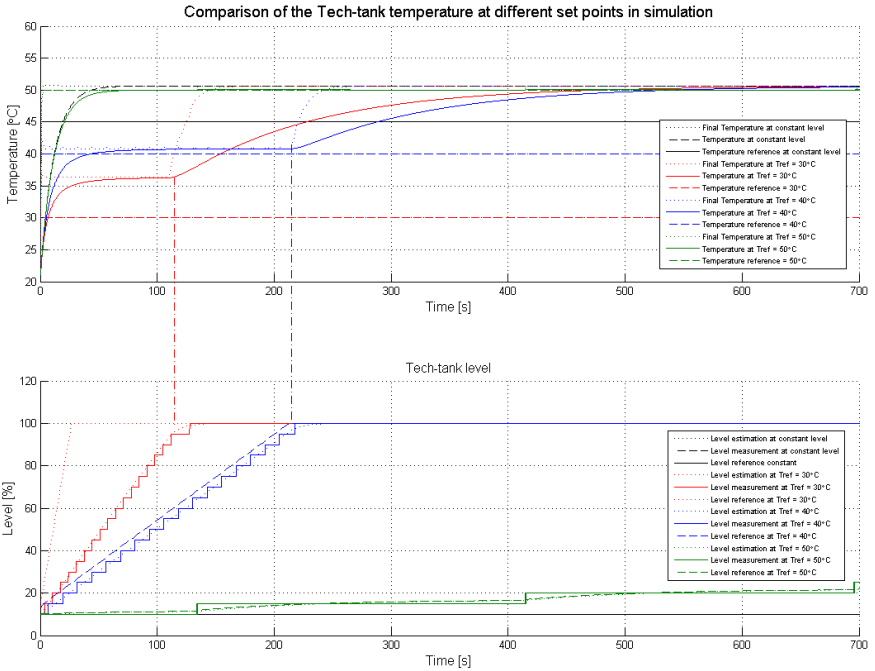

Figure 58: Temperature trakcing at different set points. The Tech-tank level is shown and the simulations are performed until the final temperature is reached for all diferent cases after saturation. The instant when the saturation occurs is marked with a line matching the start of the new temperature transient.

As a conclusion, the final temperature cannot be controlled, but the transient behavior can be modified with the temperature controller, as shown in the figures above.

9. Discussion and conclusions

In this chapter, the discussion of the thesis and the conclusions of the results are commented. The results are divided in different sections, concerning the modeling, optimization and control.

9.1 Discussions

The thesis has shown how a hydraulic system can be modeled in many different ways depending on the assumptions taken regarding the fluid model. The integral expressions are applied for the study of every component in the rig. Regarding these questions, the required modeling have been decided to be a quasi-one dimensional flow of a Newtonian incompressible flow, which allows to treat the limitations properly.

The different components have been detailed modeled by fitting the theoretical equations to the experimental data. The theoretical formulation allows predicting how the system will behave in order to design proper experiments to create the models used for control and diagnosis. Some of the models had to be adapted in order to include deviations of the theoretical models, as some assumptions do not hold for every single component, specially the filters.

The models could seem too accurate for a control design, but the point is to fully understand which variables affect the actuators performance and how, in order to design and dimension the actuators in the best way.

The thesis have not focused on the pumps selection, as they were given for the system in the rig as well as the previous information from some truck tests were using them. Therefore, the control will consider them as the final actuators. However, their study is still valid if they are decided to be changed e.g., different power, different efficiency curves, etc. Nonetheless, depending on the final controller set-point, the same analysis can give a better choice of the pumps.

Tech-tank level handling turned to be not as easy as thought in the beginning, due to it can be managed in many different ways. The heuristic optimization approach show good performance accordingly to the endurance and low energy consumptions criterions. More information about long-term behavior of the pumps should be required for a better results, but the selected approach will still be used.

With these statements, the controller structure has been discussed to be a LQG regulator modified so that other problems were overcome. These problems were mainly the estimation of the tank's levels, the non-linearity in the pressure measurements and its delay. This structure deals very well with handling the multivariable regulation problem, whilst it is easy to modify in case the system changes. The linear structure allows an easy discretization depending on the selected sampling time. This structure makes it easy to implement in a few code lines, minimizing the computational power requirements.

The results show a good performance in terms of reference tracking and disturbance rejection. Results from the rig shows that the disturbance rejection is still taking too long settling time, but it is designed so if the engine mass-flow is accounted, it will be substantially reduced.

9.2 Conclusions

Modeling

The detailed derivation of the fluid mechanics equations would not be necessary if only the controller design is needed. However, it turned very useful to understand all the possible sources of error and differences between the theory predictions and the experimental results. Furthermore, it is essential for implementing a good

simulation environment where fluid transients want to be accounted. In that sense, the results are out of the scope of the regulation goals, as was shown after investigating the experimental behavior.

It is important to note that every system is different and not better accuracy would mean better results in the control performance, as much more different factors affects it. Instead, the overall behavior have to be represented by the model used for the controller design, how the variables are related and how they behave. The linear approximation of the non-linear equations shown to be adequate as the system would work at a given set-point. This simplifies the controller derivation, tuning and implementation with the required performance fulfilled.

Important conclusions for modeling are the order of the dynamic equations of the different components, and the order of the independent variables. If the order of the derivatives or the polynomials cannot be linearized within the error tolerance in the working range, a linear model would not be enough.

From the experiments, it is explain how hard it is to model the heat transfer coefficients and it is better to leave its influence as a disturbance in the Tech-tank temperature.

Optimization

An important conclusion from the optimization is that it is never easy to establish a completely true criterion for everything. Experience plays an important role in telling what is important and what is not. In that sense, optimization of quadratic functions is very well developed. By quadratic cost criterion, an heuristic problem can be design to match what experience tells. This approach is suitable to assure the endurance of the pumps.

Regarding the optimization of the pumps, the most important conclusion is that their efficiency is too low for the working point (maximum efficiency around 30% when positive displacement pumps can reach up to 90%). How to select them is a conclusion from this optimization problem. In addition, handling two pumps in parallel optimally have been solved with correct results. However, asymmetry in the pumps characteristics have not been studied, which would modify this conclusions.

Controller

The experimental results of the designed controller shows a very good behavior regarding reference tracking (settling time around 1.5s for two pumps working at a time, and 5s when one is standby) and it validates the structure chosen for its design. It handles the multivariable problem easily and the variables are slightly influenced by each other. Results from the experiments in the rig shows that the behavior is not that good for disturbance rejection (settling time around 2s with two pumps working at a time, and around 4s when one is standby), and hence it confirms the importance of including the mass-flow demand from the engine, which would show a lower effect on the pressure output drop. The Smith-predictor showed a good improvement in the results regarding that issue.

The estimation of the system's states was precise and it is shown how important it is for a good controller performance when having big quantification sensors. Furthermore, this approach can overcome as well future problems that are not seen from the rig experiments. For instance, when the truck is moving, the level would oscillate due to big accelerations in the truck or if the tank is tilted.

From the experimental results, the most important conclusion for the controller is how the optimal handling of the two parallel pumps is implemented. During its design in simulation, the internal controller of the pumps was not accounted and it was shown how sudden start-ups, while providing big pressure i.e., a big current is demanded, are not properly handled by the internal controller of the pumps. Therefore, the controller should consider that and smooth transitions would better be included. In addition, the minimization of the current consumption can only be achieved if one of the pumps is fully turned off, and not having it in standby, which can only be achieved if the smooth transition is implemented.

10. Recommendations and future work

From the conclusions of the thesis, an important point to be considered in the implementation of the system is the pumps selection. They should be selected so that the maximum efficiency is achieved at the working point, they should be powerful enough to handle the maximum pressure peaks and to move the demanded mass-flow. Information about their endurance would better be provided from the manufacturer as well more information about the internal regulator.

Future work will first be the implementation of the designed controller in a truck, and to include the information of the mass-flow demand from the engine. Based on the results of the real testing, the controller may be slightly modified to achieve the demanded performance.

About the controller itself, some extra features can be added, for instance, as every truck is different and therefore the pumps will not be exactly the same, adaptation can thus be included to improve the performance of the controller: estimate at which RPM's the pumps should switch from running one pump to two. An option to estimate the optimal working point of one pump is to use an extremum seeking controller during a tuning period (e.g., when the truck is stop) and to use the final value to compute the switching value for the RPM's. It can also be performed online if one of the pumps is idle.

Another improvement would be in the estimation of the tanks levels: the level sensors will give wrong measurements when the truck is tilted, but the information of the on-truck accelerometer can be used to estimate the total fuel inside the tank from the sensor.

Extra considerations can be taken into the level limits of the Tech-tank. For instance, the level limits can be determined by the probability of fault, which can be determined by different states in a Markov chain. These boundaries in the level would have to be included in the temperature controller in order to not reach them.

Extra modes of the controller have to be included for diagnosis purposes. The designed structure allows to input manual references and control actions. In a diagnostic mode, the diagnostic algorithm will run the controller and it would provide the signals to compare and decide if a fault have occur and where.

11. Bibliography

[1] I. M. C. D. R. D. Pijush K. Kundu, Fluid Mechanics, Fifth Edition, U.S.A.: Academic Press, 2012.

[2] N. Portland, *Pump characteristics presentation,* Nichols Portland, 2011.

[3] "Control Volume," [Online]. Available: http://www.fluidsbarrierscns.com/content/6/1/12/figure/F1. [Accessed 6 February 2014].

[4] S. Batterton, "Water Hammer: An Analysis of Plumbing Systems," Virginia Polytechnic, Blacksburg Virginia, 2006.

[5] F. M. White, Fluid Mechanics, 5th ed., McGraw Hill, 2003.

[6] A. G. Hansen, Fluid Mechanics, Wiley, 1967.

[7] R. L. G. Z. W. a. J. K. V. Street, Elementary Fluid Mechanics, 7th ed., Wiley, 1996.

[8] H. D. Pasinato, "Fundamentos de Mecanica de Fluidos," Universidad Tecnologica Nacional, Plaza Huincul, 2008.

[9] V. L. E. Benjamin Wylie, Fluid transients, McGraw-Hill, 1978.

[10] "Roughness Values—Darcy-Weisbach (Colebrook-White) Equation," [Online]. Available: http://docs.bentley.com/en/HMFlowMaster/FlowMasterHelp-09-5.html. [Accessed 10 March 2014].

[11] "Waterhammer and the method of characteristics," [Online]. Available: http://www.gwefr.co.uk/moc.pdf. [Accessed 10 March 2014].

[12] S. Pump, "Screw Pump," [Online]. Available: http://en.wikipedia.org/wiki/Screw_pump. [Accessed 27 January 2014].

[13] "Bombas Hidraulicas - Universidad Politecnica Salesiana," [Online]. Available: http://dspace.ups.edu.ec/bitstream/123456789/1045/6/3.CAPITULO%20I.pdf. [Accessed 28 January 2014].

[14] T. G. a. L. Ljung, Control Theory. Multivariable and Nonlinear Methods., Linköpink: Taylor&Francis Group, 2000.

[15] "Wikipedia - Numerical methods for ordinary differential equations," [Online]. Available: http://en.wikipedia.org/wiki/Numerical_methods_for_ordinary_differential_equations. [Accessed 9 April 2014].

[16] Y. A. Çengel, "Transient heat conduction," in *Heat and Mass Transfer (3th Edition)*, University of Nevada-Reno, McGraw-Hill, pp. 217 - 285.

[17] K. J. Å. K.-E. Å. Björn Wittenmark, Computer Control: An Overview, Department of Automatic Control, Lund University, Sweden: IFAC Professional Brief, 2012.

[18] J. Dvaorkin, "Kozeny-Carman equation revisted," Standford University, Standford, 2009.

[19] H.Federer, "The Gauss-Green theorem," in *Trans- Amer. Math. Soc.*, 1945, pp. 44-76.

[20] T. W. Peter von Böckh, Heat Transfer: Basics and Practice, Springer, 2011.

[21] P. P. Carreras, Algebra Lineal: Notas de clase, Valencia: Servicio de Publicaciones UPV, 1999.

[22] E. Larson, Multivariable calculus - 9th Edition, Brooks/Cole, 2010.

[23] K. P.Menard, Dynamic Mechanical analysis: a practical introduction, Second Edition, CRC Press, 2008.

Appendix A: Derivation of fluid mechanics equations

In this appendix, the derivation of the fluid mechanics equations is developed.

Reynolds's transport theorem

As a general expression, the changes of any extensive property of a continuum medium can be explained by the Reynolds' transport theorem [3]. This is an integral formulation, which can be turned to the differential form formulation if needed.

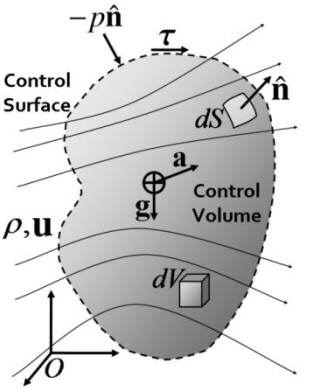

Figure 59: Flow control volume concept. The stream lines crosses the control surface, represented in dashed line and expressed differentially by vector *dS*, normal to its surface. The stream introducies a property change in and out the control volume, expressed by its differencial unit *dV*. Forces are applied to the surface, decompossed in its normal components *p* and tangencial, τ. The total property is expressed as its value per mass unit, *u*,

and its mass is expressed per volume unit, this is, its density ρ. As an inertial system, its movement is expressed at its mass centroid, where the gravity acceleration g and any other acceleration, a (such as one due to increasing velocity) are applied. The origin of coordinates serves as the vectorial system's reference, O. (source: [10]).

In the Lagrangian formulation, each particle is studied individually, while in the Euler formulation, it is the whole volume that is considered.

The Reynolds' transport theorem expression for a fixed control volume is [3]:

$$\frac{d\vec{H}}{dt} = \iiint_{C.\forall.} \frac{\partial}{\partial t} \rho \vec{h} d\forall + \iint_{C.S.} \rho \vec{h} \overrightarrow{V_{CS}} d\vec{S} \tag{A.1}$$

Explained in words, the total change in a property $\vec{H}$ can be seen as its change over time within the control volume $C.\forall.$ plus the change of property through the control surface $C.S.$ that crosses the boundary at velocity $\overrightarrow{V_{CS}}$ respect to the control boundary surface. $\vec{h}$ is the property per mass unit and ρ is the volumetric density.

The expression can be applied to any extensive property [11] of the system so that different expressions are derived in integral form.

Mass conservation

The mass conservation principle, as known as *continuity equation*, is developed so that it accounts for the water hammer phenomenon. Hence, as develop in [12], next assumptions are considered:

- Continuity of the flow.
- Pipe wall expansion and compressibility of the fluid.

Based on [11] and [13], the continuity equation is develop for a moving and deforming control volume as is the pipe under the previous assumptions. The property to account is the fluid mass. From the previous formulation (A.1):

$H = m$ total fluid mass, and obviously $h = \frac{H}{m} = \frac{m}{m} = 1$ (mass per mass unit). Then, applying Reynolds' theorem, results:

$$0 = \iiint_{C.\forall.} \frac{\partial}{\partial t}\rho d\forall + \iint_{C.S.} \rho V_r cos\,(\theta) dS \qquad (A.2)$$

Where V_r is the relative velocity of the flow to the control surface and θ is the angle between the fluid velocity and a vector normal to the surface.

Writing it in the differential form [11] for a constant section conduct:

$$0 = \frac{D\rho}{Dt} + \rho V_r = S \cdot \frac{\partial \rho}{\partial t} dl + \rho \cdot \frac{\partial \forall}{\partial t} + S \cdot \frac{\partial(\rho v)}{\partial x} dl \qquad (A.3)$$

Where dl is a differential length of the conduct and $\delta\forall$ represents the increase in the conduct volume due to its expansion. V is the fluid velocity and S the cross-sectional area. The capital 'D' indicates the material derivative [3].

From [14], the conduct expansion can be calculated as:

$$\delta\forall = S \cdot dl \cdot \frac{(1-\nu^2)\cdot d}{E \cdot e} \cdot \delta p \qquad (A.4)$$

With ν the Poisson's ratio, E Young's modulus, d conduct's inner diameter, e conducts thickness and δp the pressure increment.

Substituting (A.4) in (A.3), eliminating the common factors and dividing by ρ:

$$\begin{aligned} 0 &= S \cdot \frac{\partial \rho}{\partial t} dl + \rho \cdot \frac{S \cdot dl \cdot \frac{(1-\nu^2)\cdot d}{E \cdot e} \cdot \delta p}{\partial t} + S \cdot \frac{\partial(\rho v)}{\partial x} dl \\ 0 &= \frac{\partial \rho}{\partial t} dl + \rho \cdot \frac{(1-\nu^2)\cdot d}{E \cdot e} \cdot \frac{dp}{dt} + \frac{\partial(\rho v)}{\partial x} \\ 0 &= \frac{1}{\rho}\frac{\partial \rho}{\partial t} + \frac{(1-\nu^2)\cdot d}{E \cdot e} \cdot \frac{dp}{dt} + \frac{v}{\rho} \cdot \frac{\partial \rho}{\partial x} + \frac{\partial v}{\partial x} \end{aligned} \qquad (A.5)$$

The partial derivatives of ρ can be arranged together so that it equals the total derivative:

$$\begin{aligned} 0 &= \frac{1}{\rho}\left(\frac{\partial \rho}{\partial t} + v \cdot \frac{\partial \rho}{\partial x}\right) + \frac{(1-\nu^2)\cdot d}{E \cdot e} \cdot \frac{dp}{dt} + \frac{\partial v}{\partial x} \\ 0 &= \frac{1}{\rho}\left(\frac{\partial \rho}{\partial t} + \frac{\partial \rho}{\partial x} \cdot \frac{dx}{dt}\right) + \frac{(1-\nu^2)\cdot d}{E \cdot e} \cdot \frac{dp}{dt} + \frac{\partial v}{\partial x} \\ 0 &= \frac{1}{\rho} \cdot \frac{d\rho}{dt} + \frac{(1-\nu^2)\cdot d}{E \cdot e} \cdot \frac{dp}{dt} + \frac{\partial v}{\partial x} \end{aligned} \quad (A.6)$$

From the definition of Bulk modulus, *K* [3]:

$$K = -\frac{dp}{d\forall/\forall} = \rho \frac{dp}{d\rho} \quad \rightarrow \quad d\rho = \frac{\rho}{K} \cdot dp \quad (A.7)$$

$$0 = \frac{1}{K} \cdot \frac{dp}{dt} + \frac{(1-\nu^2)\cdot d}{E \cdot e} \cdot \frac{dp}{dt} + \frac{\partial v}{\partial x} \quad (A.8)$$

Rearranging the equation:

$$0 = \left(\frac{1}{K} + \frac{(1-\nu^2)\cdot d}{E \cdot e}\right) \cdot \frac{dp}{dt} + \frac{\partial v}{\partial x} \quad (A.9)$$

Taking partial derivatives instead of total:

$$0 = \left(\frac{1}{K} + \frac{(1-\nu^2)\cdot d}{E \cdot e}\right) \cdot \left(\frac{\partial p}{\partial t} + \frac{\partial p}{\partial x} \cdot v\right) + \frac{\partial v}{\partial x} \quad (A.10)$$

Since $\frac{\partial \mathrm{p}}{\partial \mathrm{t}} \gg \frac{\partial \mathrm{p}}{\partial \mathrm{x}} \cdot \mathrm{v}$ for an incompressible fluid [13], the term $\frac{\partial \mathrm{p}}{\partial \mathrm{x}} \cdot \mathrm{v}$ can be neglected:

$$0 = \left(\frac{1}{K} + \frac{(1-\nu^2)\cdot d}{E \cdot e}\right) \cdot \frac{\partial p}{\partial t} + \frac{\partial v}{\partial x} \quad (A.11)$$

From the definition of sound velocity in a fluid [3]

$$c = \sqrt{\frac{1}{\rho\left(\frac{1}{K} + \frac{(1-\nu^2)\cdot d}{E\cdot e}\right)}} \tag{A.12}$$

The final differential equation in partial derivatives for the fluid continuity is:

$$0 = \frac{\partial p}{\partial t} + \rho c^2 \frac{\partial v}{\partial x} \tag{A.13}$$

Linear momentum conservation

In this case, the property that is studied is the linear momentum. Then, $H = M_L = mV$ therefore$h = \frac{mV}{m} = v$. The equation has been developed by following [12] and [15].

From Newton's second law:

$$\sum \vec{F} = m\frac{d\vec{V}}{dt} = \frac{d(\overrightarrow{mV})}{dt} = \frac{d\overrightarrow{M_L}}{dt} \tag{A.14}$$

The external momentum can be separated in:

$$\frac{d\overrightarrow{M_L}}{dt} = \sum \vec{F} = -\iint_{C.S.} (p+\tau)d\vec{S} - \iiint_{C.\forall.} \rho\vec{g}d\forall + \sum \overrightarrow{F_{ext}} \tag{A.15}$$

This is, the shear force τ, in the surface due to viscosity, the pressure force p in the surface and the gravity force in the volume, plus any other external force, such as one that is moving the control volume (think about a rocket moving).

By applying Reynolds' theorem to this property and stating that no external forces are applied:

$$-\iint_{C.S.}(p+\tau)d\vec{S}-\iiint_{C.\forall.}\rho\vec{g}d\forall=\iiint_{C.\forall.}\frac{\partial}{\partial t}(\rho\vec{v})d\forall+\iint_{C.S.}\vec{v}\left(\rho\overrightarrow{v_{rs}}\cdot d\vec{S}\right) \tag{A.16}$$

Where v_{rs} is the flow velocity relative to the control surface.

From the divergence theorem [16]:

$$\iint_{C.S.}\vec{v}\left(\rho\overrightarrow{v_{rs}}\cdot d\vec{S}\right)=\iiint_{C.\forall.}\nabla(\rho\vec{v}\vec{v})d\forall \tag{A.17}$$

The expression is rearranged as:

$$0=\iiint_{C.\forall.}\left(\frac{\partial}{\partial t}(\rho\vec{v})+\nabla(\rho\vec{v}\vec{v})+\rho\vec{g}\right)d\forall+\iint_{C.S.}(p+\tau)dS \tag{A.18}$$

For a differential slice with constant properties of area S:

$$0=\left(\frac{Dv}{Dt}+g\frac{\partial x}{\partial z}\right)\rho Sdl+\frac{\partial p}{\partial x}SdL+\tau Sdl \tag{A.19}$$

From the material derivative:

$$\frac{Dv}{Dt}=\frac{\partial v}{\partial t}+v\cdot\nabla v=\frac{\partial v}{\partial t}+v\frac{\partial v}{\partial x} \tag{A.20}$$

And dividing the by *ρSdl*

$$0=\left(\frac{\partial v}{\partial t}+v\frac{\partial v}{\partial x}+g\frac{\partial z}{\partial x}\right)+\frac{1}{\rho}\frac{\partial p}{\partial x}+\frac{1}{\rho}\tau \tag{A.21}$$

Now, from the Darcy-Weisbach equation for a circular conduit of diameter *D*, the shear force stress can be estimated from this empirical equation. Even the flow is studied under transient conditions, the shear stress can be approximated as the velocity were steady [17].

$$\tau=\nu\frac{\partial^2 v}{\partial x^2}\Leftrightarrow f\frac{\rho v^2}{2D} \tag{A.22}$$

The momentum conservation equation becomes as follows. The modulus in the velocity is taken to account for its sign.

$$0 = \frac{\partial v}{\partial t} + v\frac{\partial v}{\partial x} + \frac{1}{\rho}\frac{\partial p}{\partial x} + g\frac{\partial z}{\partial x} + \frac{fv|v|}{2D} \tag{A.23}$$

Energy equation

Now, the property to be used in the Reynolds' transport theorem is the energy of the fluid: $H = E$ and therefore$h = \frac{E}{m} = e$.

However, the balance depends on which forms of energy are considered. Different properties of the fluid are wanted to be account: velocity, pressure and temperature. The evaluation of those properties should be evaluated for an incompressible flow of a viscous fluid under transient conditions, this is, and its elasticity should be considered as well. Hence, the different forms of energy, with its expressions, are (case letters mean specific values, i.e., per mass unit):

- ***Potential energy***: this form of energy accounts for the position of the flow:

$$de_p = g \cdot dz \tag{A.24}$$

- ***Kinematic energy***: the velocity of the flow is considered:

$$de_k = \frac{1}{2}dv^2 \tag{A.25}$$

- ***Internal energy***: this accounts for all the energy inside the fluid, i.e., electrical, magnetic, chemical... Here, only the thermal energy is considered. For a isochoric process where the volume is considered constant, the internal energy can be computed as:

$$du = C_v dT + \frac{1}{\rho}dp \tag{A.26}$$

Where C_v is the heat capacity at constant volume.

- ***Friction losses***: due to the viscosity of the fluid, the friction generates heat that makes the fluid lose its energy. For a circular conduit, from the Darcy-Weisbach equation (2.1):

$$\dot{W}_{losses} = \dot{m} \cdot f \frac{L}{D} \frac{v^2}{2} \tag{A.27}$$

Where *f* is the Darcy friction factor [3].

Hence, the total flow energy becomes:

$$de_{int} = C_v dT + \frac{1}{\rho} dp + \frac{1}{2} dv^2 + g \cdot dz \tag{A.28}$$

And the external energies, with units in fluid height:

$$\dot{E}_{ext} = \dot{Q}_H + \dot{W} + \dot{W}_{losses} \tag{A.29}$$

Applying Reynolds' transport theorem, the conservation of energy within the control volume is satisfied:

$$\begin{aligned} \dot{Q}_H + \dot{W} + \dot{W}_{losses} = & \iiint_{C.\forall.} \frac{\partial}{\partial t} \left[C_v T + \frac{1}{2} v^2 \right] \rho d\forall \\ & + \iint_{C.S.} \left[C_v T + \frac{1}{\rho} p + \frac{1}{2} v^2 + gz \right] \rho v d\vec{S} \end{aligned} \tag{A.30}$$

Note that the velocity respect to the surface control is equal to the flow velocity, because all the systems considered will remain fixed to the reference system. In addition, within the control volume there is no pressure energy because it is homogeneous in it, so it is only considered in the surface boundaries (this is, the flow only generates work on the system's boundary, where it has to push material in and out the system). From the same criteria, the potential energy is constant with time, this is, the system does not move.

As with the previous equations, it is interesting to get the equation in differential form by using the divergence theorem:

$$\begin{aligned}\dot{Q}_H + \dot{W} + \dot{W}_{losses} &= \iiint_{C.\forall.} \frac{\partial}{\partial t}\left[C_v T + \frac{1}{2}v^2\right]\rho d\forall \\ &+ \iiint_{C.\forall.} \nabla\left[C_v T + \frac{1}{\rho}p + \frac{1}{2}v^2 + gz\right]\rho v d\forall \\ \dot{Q}_H + \dot{W} + \dot{W}_{losses} &= \iiint_{C.\forall.} \left[\frac{\partial}{\partial t}\left(C_v T + \frac{1}{2}v^2\right)\rho \right. \\ &\left. + \nabla\left(C_v T + \frac{1}{\rho}p + \frac{1}{2}v^2 + gz\right)\right]\rho v d\forall \\ \dot{Q}_H + \dot{W} + \dot{W}_{losses} &= \iiint_{C.\forall.} \left[\left(\frac{\partial}{\partial t}\rho C_v T + \nabla\rho v C_v T\right) + \left(\frac{\partial}{\partial t}\rho\frac{1}{2}v^2 + \nabla\rho\frac{1}{2}v^3\right.\right. \\ &\left.\left. + \nabla v p + g\rho\frac{vz}{\partial x}\right] d\forall\end{aligned} \tag{A.31}$$

The PDE equation becomes, for a circular conduit with losses:

$$\begin{aligned}\frac{\dot{q}_H}{\rho} + \frac{\dot{w}}{\rho} + \frac{f}{2D}\frac{v^2}{\rho} &= \frac{D}{Dt}\left(C_v T + \frac{1}{2}v^2\right) + \frac{1}{\rho}\frac{\partial(vp)}{\partial x} + g\frac{\partial(vz)}{\partial x} \\ 0 &= C_v\left(\frac{\partial T}{\partial t} + v\frac{\partial T}{\partial x}\right) + v\left(\frac{\partial v}{\partial t} + v\frac{\partial v}{\partial x}\right) + \frac{v}{\rho}\frac{\partial p}{\partial x} + gv\frac{\partial z}{\partial x} \\ &- \frac{1}{\rho}\left(\dot{q} + \dot{w} + f\frac{v|v|}{2D}\right)\end{aligned} \tag{A.32}$$

Note that the external heat q and work w are divided by rho in order to have the same dimension as the other terms, so that they can be expressed in Jules per second per mass unit.

Appendix B: *Simulink*® hydraulics library implementation

In this appendix, the Simulink® library implementation is detailed explained. First, the numerical methods that are used for solving the ODE are explained as well as how the PDE system is solved. Then, the equations discretization and implementation of each component is depicted. Finally, the data structure used for the system coherence is explained.

Numerical solution to ODE's

To simulate the system, the PDE and ODE must be solved so the value of the parameter is obtained at each time instant. The system is highly non-linear (note the modulus in the friction term, limitations in the tank volumes…) and therefore no analytical solution can be easily obtained. Instead of that, numerical solutions are required.

Method of characteristics

First of all, the PDE system should be solved in order to reduce it to a set of ODE. The procedure typically used in fluid dynamics is the method of characteristics [18].

Recalling the continuity equation (2.6) and momentum conservation (2.7), they can be linearly combined by means of using the Lagrange multiplier [19], λ:

$$0 = \left(\frac{\partial p}{\partial t} + \rho c^2 \frac{\partial v}{\partial x}\right) + \lambda \cdot \left(\frac{\partial v}{\partial t} + v\frac{\partial v}{\partial x} + \frac{1}{\rho}\frac{\partial p}{\partial x} + g\frac{\partial z}{\partial x} + \frac{f}{2D}v|v|\right) \tag{B.1}$$

The convective acceleration term is neglected against other terms, since the flow velocity is much smaller than the sound wave celerity, hence$v\frac{\partial \mathrm{v}}{\partial \mathrm{x}} \approx 0$. Setting together terms for the same variables:

$$0 = \left(\lambda\frac{\partial v}{\partial t} + \rho c^2 \frac{\partial v}{\partial x}\right) + \left(\frac{\partial p}{\partial t} + \lambda\frac{1}{\rho}\frac{\partial p}{\partial x}\right) + \lambda g\frac{\partial z}{\partial x} + \lambda\frac{f}{2D}v|v| \tag{B.2}$$

The Lagrange multiplier should be selected so that the material derivative is obtained and therefore a set of ODE is reached. This is:

$$\lambda\frac{Dv}{Dt} = \lambda\frac{\partial v}{\partial t} + \lambda\frac{dx}{dt}\frac{\partial v}{\partial x} = \lambda\frac{\partial v}{\partial t} + \rho c^2\frac{\partial v}{\partial x} \tag{B.3}$$

$$\frac{Dp}{Dt} = \frac{\partial p}{\partial t} + \frac{dx}{dt}\frac{\partial p}{\partial x} = \frac{\partial p}{\partial t} + \lambda\frac{1}{\rho}\frac{\partial p}{\partial x} \tag{B.4}$$

Making equal the term in both equations, it must be verified that:

$$\lambda\frac{dx}{dt} = \rho c^2 \tag{B.5}$$

$$\frac{dx}{dt} = \lambda\frac{1}{\rho} \tag{B.6}$$

The solution that verifies (B.5) and (B.6) at the same time is therefore:

$$\lambda\left(\lambda\frac{1}{\rho}\right) = \rho c^2$$

$$\lambda^2 = \rho^2 c^2$$

$$\lambda = \pm\rho c \tag{B.7}$$

And therefore, substituting in (B.2) and from (B.6), the characteristic curves become:

C+
$$\begin{cases} \dfrac{dx}{dt} = +c \\ \dfrac{dv}{dt} + \dfrac{1}{\rho c} \cdot \dfrac{dp}{dt} + g\dfrac{dz}{dx} + \dfrac{f}{2D} v|v| = 0 \end{cases} \tag{B.8}$$

C-
$$\begin{cases} \dfrac{dx}{dt} = -c \\ \dfrac{dv}{dt} - \dfrac{1}{\rho c} \cdot \dfrac{dp}{dt} + g\dfrac{dz}{dx} + \dfrac{f}{2D} v|v| = 0 \end{cases} \tag{B.9}$$

If the piezometric height is instead used, the geometric height and pressure terms can set together and the expression is further simplified:

$$\begin{gathered} H = \rho g \cdot p + z \\ \frac{dp}{dt} = \rho g \cdot \frac{dH}{dt} - \rho g \cdot \frac{dz}{dt}\frac{dx}{dt} \\ \frac{dp}{dt} = \rho g \cdot \frac{dH}{dt} \mp \rho g \cdot c \cdot \frac{dz}{dt} \end{gathered} \tag{B.10}$$

Using this expression in the characteristics equations and substituting properly $\frac{dx}{dt}$ with +c or –c:

C+
$$\begin{cases} \dfrac{dx}{dt} = +c \\ \dfrac{dv}{dt} + \dfrac{g}{c} \cdot \dfrac{dH}{dt} + \dfrac{f}{2D} v|v| = 0 \end{cases} \tag{B.11}$$

C-
$$\begin{cases} \dfrac{dx}{dt} = -c \\ \dfrac{dv}{dt} - \dfrac{g}{c} \cdot \dfrac{dH}{dt} + \dfrac{f}{2D} v|v| = 0 \end{cases} \tag{B.12}$$

At this point, all the equations have turned into ODE that can be solved by using numerical methods.

Numerical method for solving the ODE's

The goal is to implement the solution to the equations in a computer. There are multiple reasons: the equations have no analytical solution, the system becomes very complex and many operations should be done, the computer implementation

provides high flexibility and modifications can be done easily. However, a numerical method should be selected and implemented by means of difference equations.

The nature of the equations determines the goodness of the results for the algorithm used. Complex algorithms can be used for a better performance, but they would take more time of implementation and computation afterwards. Some much extended methods are the fourth order Runge-Kutta or the Predictor-Corrector algorithms [20]. These methods provide a better numerical performance in terms of stability, error and converge, and are improved for stiff systems. Despite of these considerations, the chosen method is the forward's Euler first order approximation, which is the simplest one and therefore numerical problems arise when big discontinuities are due to be simulated. However, results show that this implementation is good enough for obtaining meaningful results (see Appendix C for some examples).

The forward's Euler approximation consists in the finite difference equation:

$$f'(t) \approx \frac{f(t + \Delta t) - f(t)}{\Delta t} \tag{B.13}$$

And therefore, the function's value at the current instant is:

$$f(t + \Delta t) \approx f(t) + \Delta t \cdot f'(t) \tag{B.14}$$

This method is applied to the previous equations used in each component.

Implementation of system's components

The *Simulink*® library consist in different components shown in next figure:

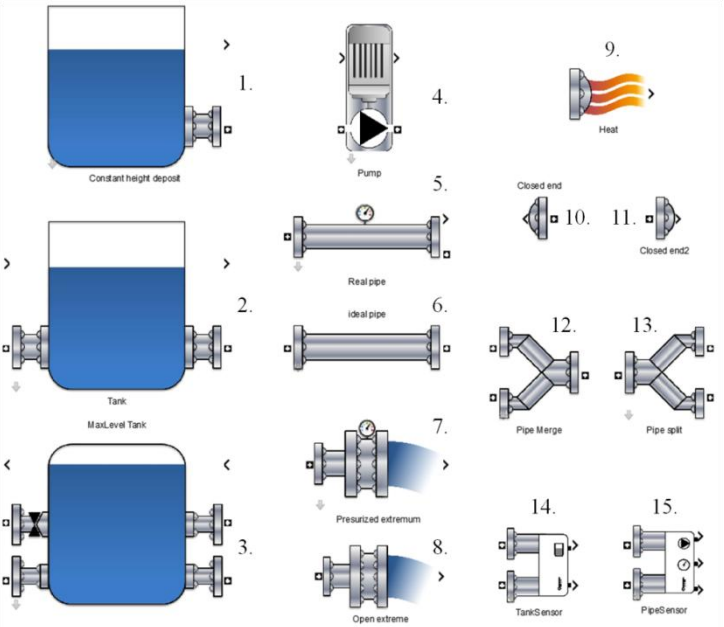

Figure 60: Simulink library components. Main components and boundary conditions are implemented for each different component: Main tank with constant level (1), Variable level tank with one input and output (2), two inputs and two outputs with maximum level tank (3); volumetric pump (4), real pipes (5), ideal pipes (6), pressurized output (7), open air extremum (8), heat source (9), closed extremums (10 and 11), pipe merge (12) and pipe split (13), tank sensor for level and temperature (14) and pipe sensor for flow, pressure and temperature (15).

Ideal pipe

Figure 61: Ideal pipe simulink icon. It can be connected to the different components that share the same type of connectors.

In this case, 'ideal' refers that there is no transient effect on the flow behavior: changes in one extremum of the pipe are seen from the other extremum instantaneously. The pipe is a source of pressure loss due to flow friction. The

piezometric head loss is computed according to the velocity within the pipe, computed with the Darcy-Weisbach formula (2.1). The friction factor is computed with the Swamee-Jain equation (2.2) for turbulent flow and interpolated in the transient area with the friction factor for laminar flow (2.4). Therefore, no numerical approximation is done directly in this block. However, its proper simulation can be affected by numerical issues coming from the blocks where it is connected.

Conservation of mass is applied in cases where pipes with different diameter are connected (2.5):

$$\begin{aligned} 0 &= \dot{m}_{in} - \dot{m}_{out} \\ 0 &= \rho \frac{{D_{in}}^2}{\pi} v_{in} - \rho \frac{{D_{out}}^2}{\pi} v_{out} \\ v_{out} &= \frac{{D_{in}}^2}{{D_{out}}^2} v_{in} \end{aligned} \tag{B.15}$$

Real pipe

This implementation looks for simulate flow transients by the water-hammer effect. With Euler's forward approximation (B.14) applied to the characteristics equations (B.11) and (B.12), the discretized characteristics equations are:

C+
$$\begin{cases} x_P = x_S + c \cdot \Delta t \\ \dfrac{v_P - v_S}{\Delta t} + \dfrac{g}{c} \cdot \dfrac{H_P - H_S}{\Delta t} + \dfrac{f}{2D} v_S |v_S| = 0 \end{cases} \tag{B.16}$$

C-
$$\begin{cases} x_P = x_R - c \cdot \Delta t \\ \dfrac{v_P - v_R}{\Delta t} - \dfrac{g}{c} \cdot \dfrac{H_P - H_R}{\Delta t} + \dfrac{f}{2D} v_R |v_R| = 0 \end{cases} \tag{B.17}$$

This is better understood with the next diagram:

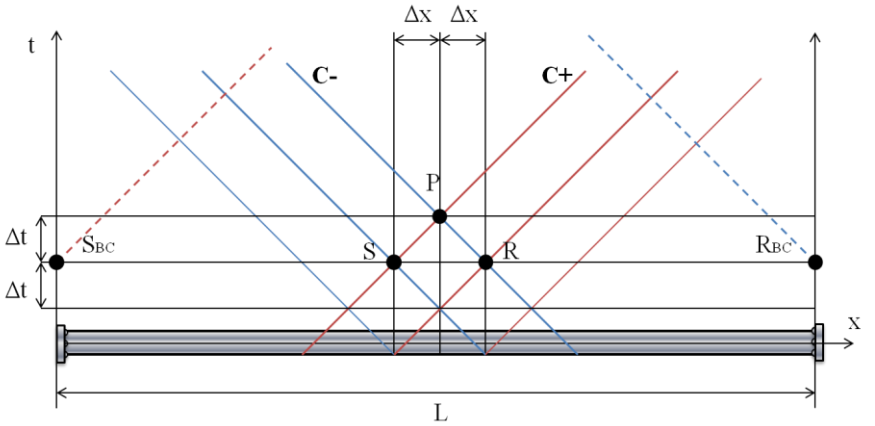

Figure 62: Discretized method of characteristics diagram. The value of piezometric head (*H*) and flow velocity (*v*) at the next time instant is obtained by solving the system of equations C+ from the discrete point R and C- comming from S. This is repeated for every discrete point all along the pipe. At the extremums, the boundary conditions are applied and therefore the C+ equation from the left (S_{BC}) and C- from the right (R_{BR}) are fully known and propagated along the pipe and time.

The time and length discretization is related so that the characteristics equations are valid. In this case, no Mach velocities are reached, and hence the flow velocity is neglected against the celerity. The resulting grid becomes symmetric. In addition, the discretization step is fixed, so that it is regular as well. More complex grids can be built with better numerical behavior such as with no constant steps or interpolation, however for this study the simplest case is enough.

Sound speeds in fluids can be around 800m/s [3] for big pressure drops. Hence, the time discretization is selected in trade-off between computation time and accuracy. The time step was selected to be 500μs which showed good results and not too big computation time. As an example, for a 10m long pipe and flow celerity of 800m/s, 25 iterations are needed to solve the equation in the whole pipe.

The pipe update is done with iteration from the previous values, at each position i, the next value at time P is computed as:

$$H_{P_i} = \frac{1}{2}\left[(V_{i-1} + V_{i+1}) + \frac{g}{c}(H_{i-1} - H_{i+1}) - \frac{f\Delta t}{2D}(v_{i-1}|v_{i-1}| + v_{i+1}|v_{i+1}|)\right] \quad \text{(B.18)}$$

$$V_{P_i} = \frac{1}{2}\left[\frac{c}{g}(V_{i-1} - V_{i+1}) + (H_{i-1} + H_{i+1}) - \frac{c}{g}\frac{f\Delta t}{2D}(v_{i-1}|v_{i-1}| - v_{i+1}|v_{i+1}|)\right] \quad \text{(B.19)}$$

These equations are only valid for inner points, this is, for $2 \leq i \leq N$. The extremum points are computed depending on the boundary conditions.

This method makes that everything have to work with the same time step, and hence *Simulink*® is configured to work in a fix-step solver with the same sample time.

Some numerical issues are produced because of big values not cancelled properly. In order to avoid that, every new step in the grid is filtered with a recurrent exponential filter with a time constant to be selected. This avoids the simulation go out of bounds for a sudden changes in the boundary conditions of the pipes.

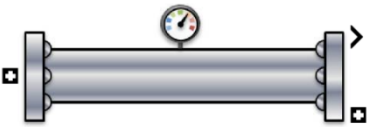

Figure 63: Real pipe Simulink icon. It can be connected to the different components that share the same type of connectors. An extra output sends out the value of piezometric head, velocity and temperature of a selected position within the pipe.

This block uses a *Matlab*® *function* to compute, for each sample time, the head and flow velocity along the pipe from equations (B.18) and (B.19). In the case it is connected to another pipe with different diameter, the piezometric head in the connection should be the same as the mass conservation holds.

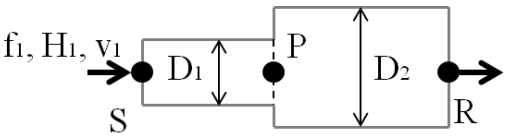

Figure 64: Boundary conditions setting for a connection between pipes with different diameter.

The conditions that should hold are:

$$H_{P,1} = H_{P,2} = H_P \tag{B.20}$$
$$Q_{P,1} = Q_{P,2} = Q_P \tag{B.21}$$

The characteristics equations and conservation of mass gives:

$$v_{P,1} = \frac{{D_1}^2}{{D_2}^2} v_{P,2} \tag{B.22}$$

C_1+
$$\left(v_{P,1} - v_{S,1}\right) + \frac{g}{c} \cdot \left(H_P - H_{S,1}\right) + \frac{f_1 \Delta t}{2D_1} v_{S,1} \left|v_{S,1}\right| = 0 \tag{B.23}$$

C_2-
$$\left(v_{P,2} - v_{R,2}\right) - \frac{g}{c} \cdot \left(H_P - H_{R,2}\right) + \frac{f_2}{2D_2} v_{R,2} \left|v_{R,2}\right| = 0 \tag{B.24}$$

The solutions to this system of equations are:

$$S_1 = -v_{S,1} - \frac{g}{c} H_{S,1} + \frac{f_1 \Delta t}{2D_1} v_{S,1} \left|v_{S,1}\right| \tag{B.25}$$
$$S_2 = -v_{R,2} + \frac{g}{c} H_{R,2} + \frac{f_2}{2D_2} v_{R,2} \left|v_{R,2}\right| \tag{B.26}$$
$$v_{P,1} = \frac{-{D_2}^2}{\left({D_1}^2 + {D_2}^2\right)} (S_1 + S_2) \tag{B.27}$$
$$v_{P,2} = \frac{-{D_1}^2}{\left({D_1}^2 + {D_2}^2\right)} (S_1 + S_2) \tag{B.28}$$
$$H_P = \frac{c}{g} \left(\frac{S_2 D_2^2 - S_1 D_1^2}{{D_1}^2 + {D_2}^2} \right) \tag{B.29}$$

Pipe branches. Split and merge

These blocks work as the previous ones for the pipes. However, the method of characteristics here becomes a 3x3 system that has to be solved. The characteristic equations are computed depending on the boundary conditions and then the system is solved to generate the outputs.

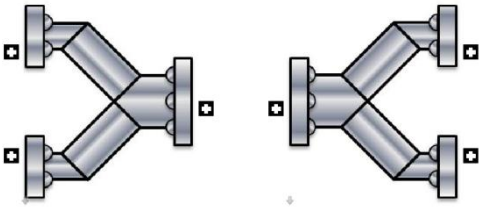

Figure 65: Pipe merge (left) and split (right) Simulink icons. It can be connected to the different components that share the same type of connectors.

The computation is similar to the previous one for a different diameters pipes connection. However, there are more equations to be satisfied:

$$v_{P,1}D_1^2 = v_{P,2}D_2^2 + v_{P,3}D_3^2 \tag{B.30}$$

C_1+
$$\left(v_{P,1} - v_{S,1}\right) + \frac{g}{c}\cdot\left(H_P - H_{S,1}\right) + \frac{f_1\Delta t}{2D_1}v_{S,1}\left|v_{S,1}\right| = 0 \tag{B.31}$$

C_2-
$$\left(v_{P,2} - v_{R,2}\right) - \frac{g}{c}\cdot\left(H_P - H_{R,2}\right) + \frac{f_2}{2D_2}v_{R,2}\left|v_{R,2}\right| = 0 \tag{B.32}$$

C_3-
$$\left(v_{P,3} - v_{R,3}\right) - \frac{g}{c}\cdot\left(H_P - H_{R,3}\right) + \frac{f_2}{2D_2}v_{R,3}\left|v_{R,3}\right| = 0 \tag{B.33}$$

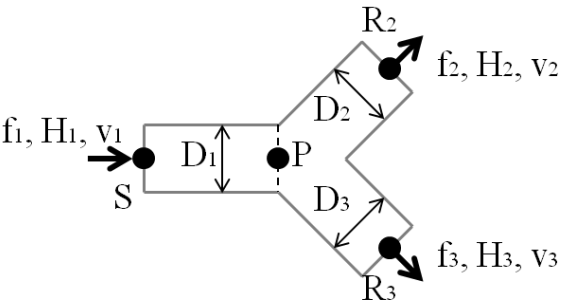

Figure 66: Boundary conditions setting for a pipe split

Calling:

$$B_1 = -v_{S,1} - \frac{g}{c} H_{S,1} + \frac{f_1 \Delta t}{2D_1} v_{S,1} |v_{S,1}| \tag{B.34}$$

$$B_2 = -\left(-v_{R,2} + \frac{g}{c} H_{R,2} + \frac{f_2}{2D_2} v_{R,2} |v_{R,2}|\right) \tag{B.35}$$

$$B_3 = -\left(-v_{R,3} + \frac{g}{c} H_{R,3} + \frac{f_2}{2D_2} v_{R,3} |v_{R,3}|\right) \tag{B.36}$$

The solution can be expressed in matrix form:

$$\begin{bmatrix} D_1^2 & -D_2^2 & -D_3^2 & 0 \\ 1 & 0 & 0 & \frac{c}{g} \\ 0 & 1 & 0 & -\frac{c}{g} \\ 0 & 0 & 1 & -\frac{c}{g} \end{bmatrix} \begin{bmatrix} V_{P,1} \\ V_{P,2} \\ V_{P,3} \\ H \end{bmatrix} = \begin{bmatrix} 0 \\ B_1 \\ B_2 \\ B_3 \end{bmatrix} \tag{B.37}$$

For the pipe merging, the equations are the same, but instead of using two C- equations, it is two C+, that allows setting a problem as (B.37).

Closed input and output

Figure 67: Closed input (left) and output (right) Simulink icons

These components are used when an input or output is closed, so no flow gets in or out the component where they are attached. It is modeled as a valve where the velocity is forced to be zero. Hence, that boundary condition is used in the C+ or C- characteristic equation; depending at which extremum of the pipe they are connected.

Open extreme

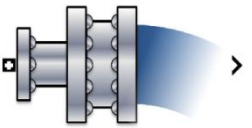

Figure 68: Open extreme Simulink icon.

The component reproduces the boundary condition for an open extreme. It is modeled as a constant height source that is set to zero, so the flow velocity is computed depending on the upwards conditions. Hence, that boundary condition is used in the C+ or C- characteristic equation; depending at which extremum of the pipe they are connected.

It includes an output that can be connected to a scope for plotting the parameters at that extremum of the pipe.

Pressurized extreme

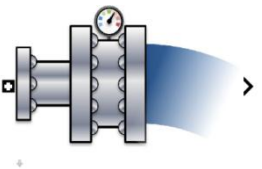

Figure 69: Pressurized extreme output Simulink icon.

The component reproduces the boundary condition for a pressurized open extreme. It is modeled as a constant height source that is set to the pressure plus the height position (piezometric head), so the flow velocity is computed depending on the upwards conditions. Hence, that boundary condition is used in the C+ or C- characteristic equation; depending at which extremum of the pipe they are connected.

The pressure and the fluid density are the required parameters as well as the output height position, since the piezometric height is computed from the pressure with the fluid density by:

$$H = \rho g \cdot p + z \tag{B.38}$$

It includes an output that can be connected to a scope for plotting the parameters at that extremum of the pipe.

Pump

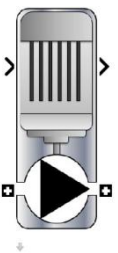

Figure 70: Pump Simulink icon. It can be connected to different components and it includes one input for a heat source and an output for plotting data in case of using a scope.

This block models a pump. It is done by means of setting the input and output boundary condition to a constant velocity. Hence, that boundary condition is used in the C+ or C- characteristic equation; depending at which extremum of the pipe they are connected. The velocity of the flow is set by the RPM input and from the pressure difference and the RPM the pump efficiency is output. The relation between RPM, pressure and efficiency is accomplished from the experimental data obtained from the pipes (see section 3.1 Modeling of the pumps for more information). The efficiency is set to zero if there is no fluid at the entrance, since it is still working but no flow is moved.

The pumps are assumed to generate heat flow into the fluid stream. The computation of the temperature is done with Euler's approximation (B.14) to the equation (2.22):

$$T_{t+\Delta t} = T_t + \frac{\dot{Q}_f}{\rho \cdot q \cdot C_v} \cdot \Delta t \tag{B.39}$$

Constant height tank

This component models a big tank so that its height level does not varies with flow output. It uses the specific boundary constraint in its output in order to do that. Hence, that boundary condition is used in the C+ or C- characteristic equation; depending at which extremum of the pipe they are connected. The temperature is considered constant. It includes an output showing the tank output height and velocity.

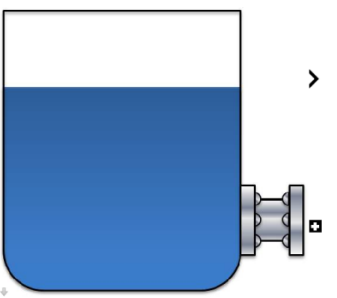

Figure 71: Constant height tank Simulink icon

Variable level tanks

These blocks model the tank as the previous one. However, its level is computed at each time from the flow balance of every input and output. When empty, its height is set to zero.

The level is updated from Euler's approximation (B.14) to the mass conservation (2.17) and level continuity equations (2.18):

$$z_{t+\Delta t} = z_t + \frac{\pi}{4A}\left(D_{in}^2 \cdot v_{in} - D_{out}^2 \cdot v_{out}\right) \tag{B.40}$$

The temperature is computed from equation (2.20):

$$T_{t+\Delta t} = T_t + \frac{1}{\rho \cdot z \cdot A \cdot C_v}\left[\rho\frac{\pi}{4}\left(\dot{v}_{in}D_{in}^2 C_v\left(T_t - T_{t_{in}}\right) - \dot{v}_{out}D_{out}^2 C_v\left(T_t - T_{t_{out}}\right)\right) + \dot{Q}_H\right] \cdot \Delta t \tag{B.41}$$

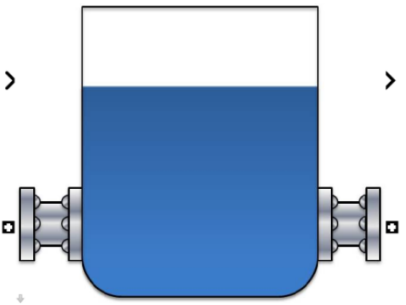

Figure 72: One input and one output variable level tank Simulink icon

This tank is used to simulate the main-tank.

For the tank with limited maximum level, there are used the same equations but for two inputs and two output, so that those extra terms are added. However, one of its outputs is closed until it reaches its maximum level, when it opens letting flow out of it.

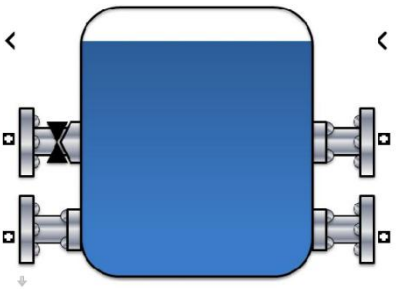

Figure 73: Two inputs and two outputs variable level tank with maximum level Simulink icon

This tank is used for simulating the tech-tank.

Constant source of heat

This block is only a constant representing the heat sent to the component where it is connected.

Figure 74: Constant heat source Simulink icon.

Sensors

The sensors can be connected between the other components in order to access de shared data. There are two types:

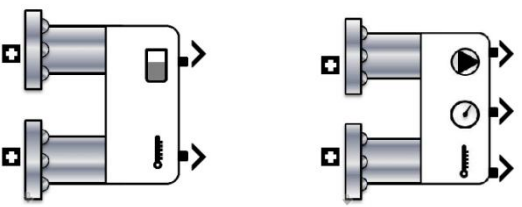

Figure 75: Tank sensor (left) and pipe sensor (right) Simulink icons

The outputs for the tank sensor are:

- Tank level. This output quantizes the actual tank level as the actual sensor does. It includes some noise as well. Both parameters can be adjusted.
- Temperature in Celsius.

The outputs for the pipe sensor are:

- Flow. It is computed from the flow velocity and pipe diameter. It includes some noise that can be adjusted.
- Pressure. It is computed from (B.38) and it includes some noise that can be adjusted.
- Temperature in Celsius.

Simulink® structure

For including the boundary conditions of the different elements, a criterion is used to inform the connected component what is attached to it. A three element column vector is used:

$$\begin{bmatrix} H_{BC} \\ V_{BC} \\ T_{BC} \\ BC \end{bmatrix}$$

BC refers to the boundary condition. Its different values could be:

- ***-1*** For a tank, where the height is known but not the output velocity, which depends on the other extreme boundary conditions
- ***-2*** For a pump or valve, where the flow velocity is known and the head is the required for getting that flow velocity depending on the boundary conditions.
- ***D*** For a pipe with a diameter of value D (m)
- ***-D*** To inform the pumps that the tank is empty. This was chosen like that due to the pipe inertia and numerical issues made tanks not seen never empty.

With these criteria, all the components are interconnected and the equations can be balanced.

Since the system is discrete, simultaneous conditions cannot be verified and hence algebraic loops should be avoided. To do that, outputs are delayed in one sample time.

Discussion

Despite of its flexibility, the simulation environment still has some problems for certain topologies that may arise undesirable results, such as when many different components are connected in line, which deals with unexpected behaviors due to the sum of the output time delays that might make the whole system unstable. In addition, for very big sudden changes, these time delays provokes numerical issues due to bad cancellation that makes big pressure drops and oscillations, and even make unstable the system. This is why it should be carefully used.

Appendix C: *Simulink*® hydraulics library examples

The different components behavior is shown in the following examples by the simulation of different system topologies. In all the examples the used parameters are for water as the fluid and steel for the pipes, which does not mean a loss of generality (Values from [3], [21], [22]):

```
rho = 1000;          %Water density at P=1atm (kg/m^3)
mu = 1.788e-3;       %Water dynamic viscosity (N*s/m^2)
K = 1.60e9;          %Steel pipe Bulk's modulus (Pa)
E = 200e9;           %Steel pipe Young's modulus (Pa)
e = 0.0008;          %Pipe thickness (m)
epsilon = 0.045e-3; %Pipe roughness height (m)
```

Example 1: Sudden opening of a constant height tank

This example shows the comparison of the flow transient when a sudden opening of a constant height tank is done through an ideal pipe and a real pipe to an open extreme. The *Simulink*® model is:

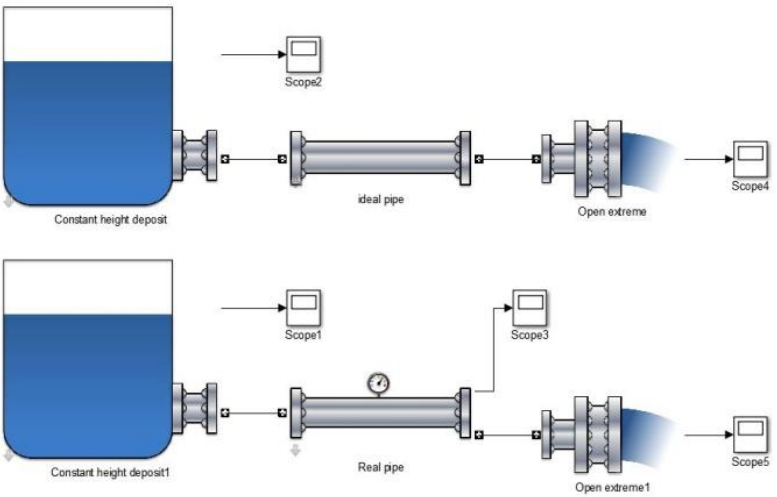

Figure 76: Simulink diagram for Example 1. The system is a tank connected to an open extremum by an ideal pipe (upper system) and by a real pipe (lower system).

The flow velocity of both systems is:

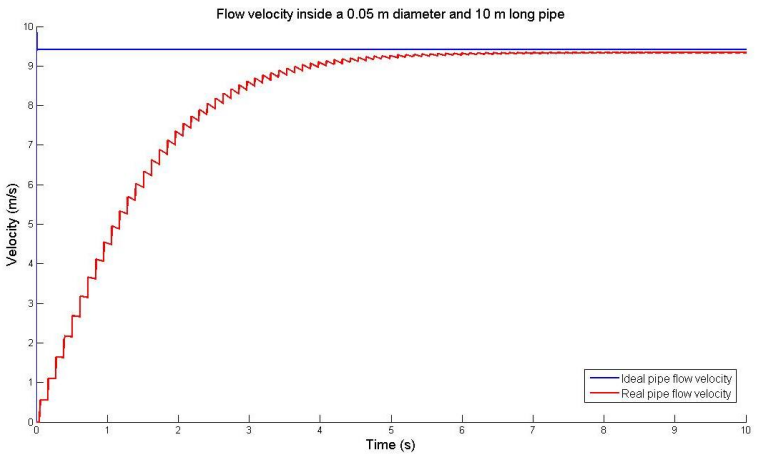

Figure 77: Flow velocity in a real pipe (red) and an ideal pipe (blue)

As shown, for the ideal pipe the steady velocity is reached in one instant, while for the real pipe it takes some time until it reaches the steady state. The sharpen edges of its evolution is due to the shock wave from the water hammer effect along the pipe, that makes the velocity oscillates as the shock wave is going back and forth the pipe, until it is finally reduced due to friction losses.

If the velocity and piezometric head is measured at the middle of the real pipe, this effect can be better shown:

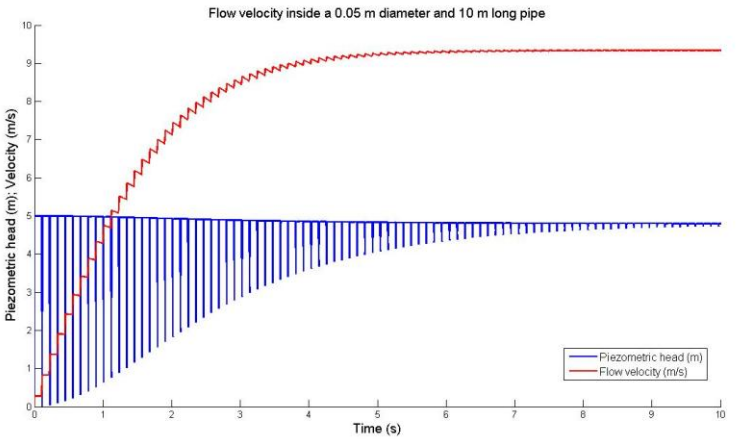

Figure 78: Flow velocity (red) and pressure height (blue) in a real pipe. Note how the pressure pulses makes the velocity to have a sawy shape.

Example 2: Sudden connection of two variable height tanks

In this example, as in the previous one, the different transient behavior of a real pipe and an ideal one is shown. In this case however, the pipes are connecting two variable height tanks. The initial height of the first tank is 5m while the final tank is 0m. Hence, the final height should be 2.5m since both tanks have the same cross section area. The *Simulink*® model is:

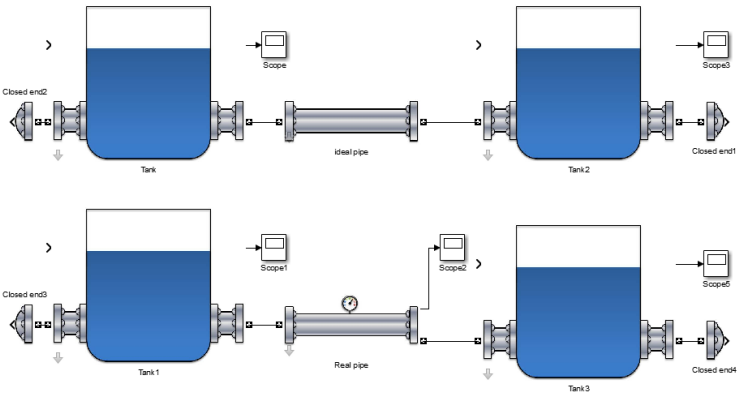

Figure 79: Simulink diagram for Example 2. The system is a tank connected to another tank by an ideal pipe (upper system) and by a real pipe (lower system).

The comparison between both systems is down by showing the flow velocity and level evolution of the first tank:

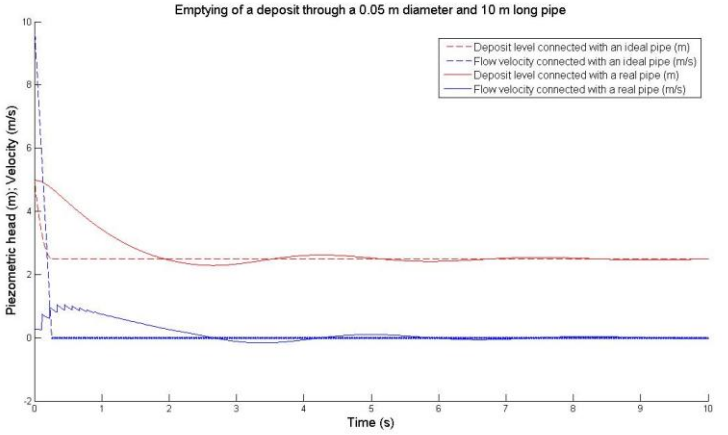

Figure 80: Flow velocity and level while emptying a tank with a real pipe (solid) and an ideal pipe (dashed). It can be seen the big difference in the transient behaviors.

The level evolution of the final tank connected to the main one from an ideal pipe and a real pipe is:

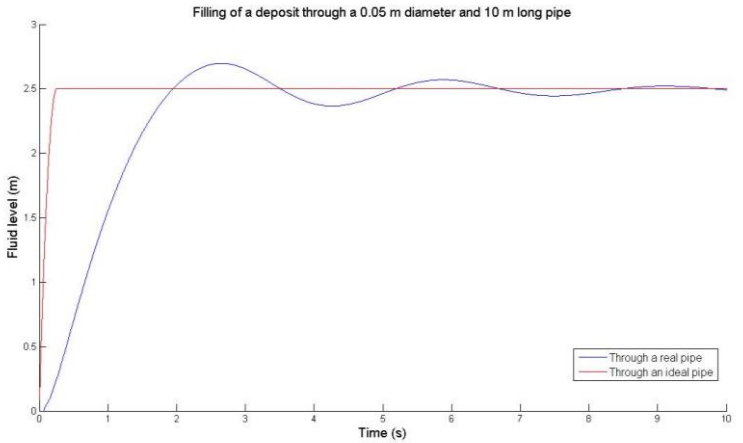

Figure 81: Level while filling a tank from an ideal pipe (red) and a real pipe (blue). Again, the transient behaviour is very different: step response in the ideal case v.s. second order system for the real pipe.

The piezometric height and flow velocity evolution inside the real pipe is:

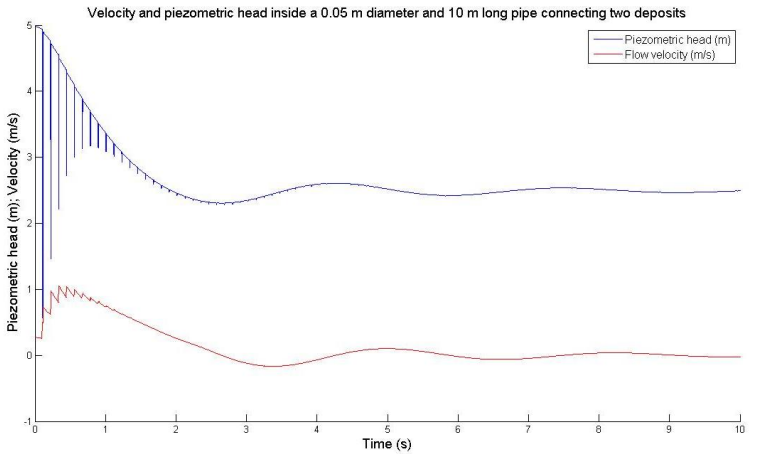

Figure 82: Pressure height (blue) and flow velocity (red) inside a pipe connecting two variable level tanks.

This example shows how the height difference of the deposits is not seen immediately from each other in the case of real pipe connection. While the transient when emptying a deposit is very fast if it is done with an ideal pipe, it is not the case for a real pipe. This is because of the different levels are seen from each other with a delayed equal to the time the pressure wave travels along the pipe. That transient generates pressure peaks inside the pipe, as shown in the last figure.

About the velocity oscillations in the first tank for the case of ideal pipe connection, it is due to the simulation requires a time delay that does not allow a proper cancelation, generating that ringing.

Example 3: Connection of three tanks

In this example, the behavior of the pipe branching with different diameters is shown. To do that, three tanks with initial different levels but same cross section area are interconnected and its level evolution is shown. Only real pipes are used now that the different behavior is understood in the previous examples.

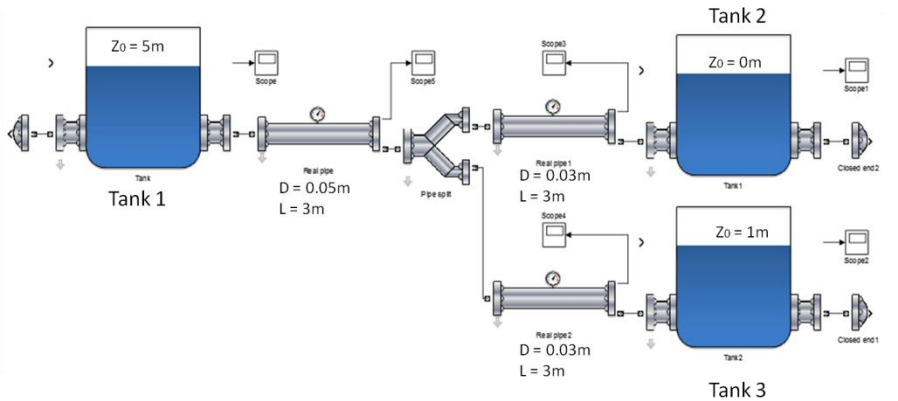

Figure 83: Simulink diagram for Example 3. One tank is connected to another two tanks by ideal pipes and a pipe split. Parameters are included in the image.

The level evolution of the three tanks is shown in the next plot:

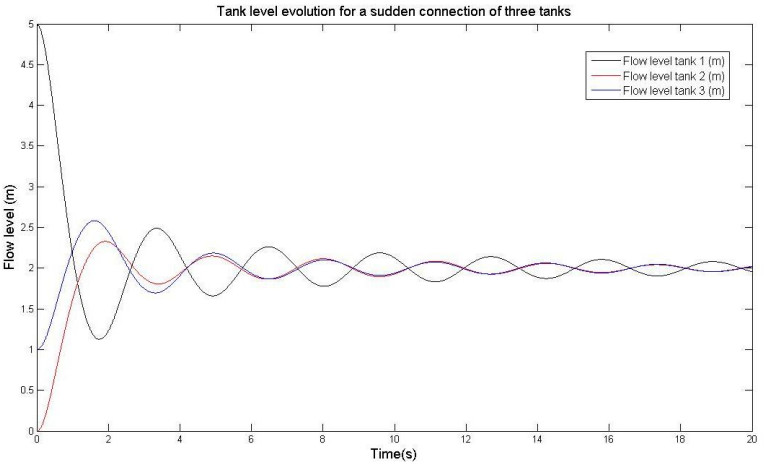

Figure 84: Level evolution of three interconnected tanks. The evolution is a second order system for all three tanks and the final value is when all three have the same level.

The flow velocity out of the first tank and into the second and third tank is:

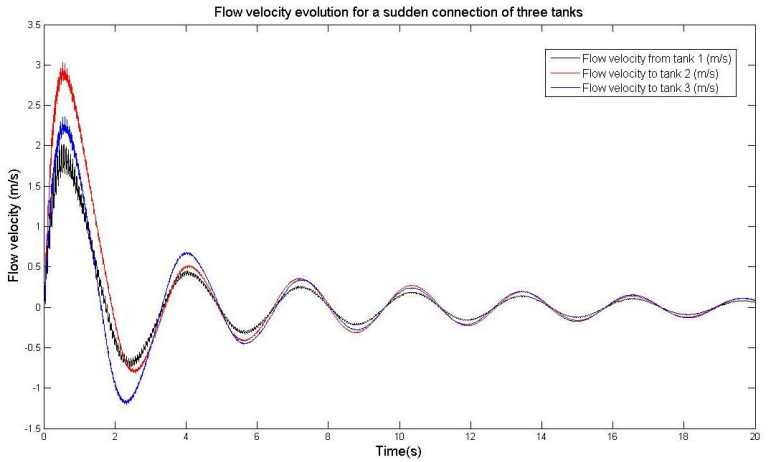

Figure 85: Velocity out and into three interconnected tanks.

And the piezometric height and flow velocity inside the pipe from the first tank are:

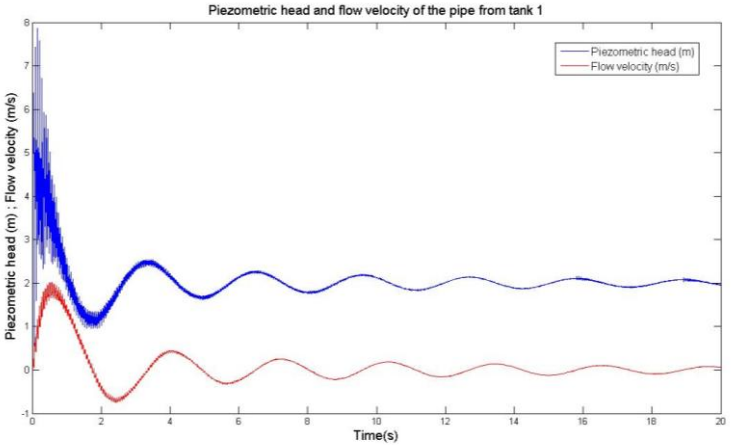

Figure 86: Pressure height and flow velocity inside the pipe out of the first tank

The transient results are similar to the ones from the previous example with a real pipe. In this case, the difference is how the equilibria are reached for the three tanks: since all three have the same cross section area, the total initial and final levels should be the same, as it happens. The pressure transients are noisier due to the new dynamics included from the extra tank.

Example 4: Transfer from one tank to another with a pump

The behavior of the volumetric pumps is shown in this example. The system consists in two tanks with initial levels and same cross section area connected with a transfer pump and real pipes.

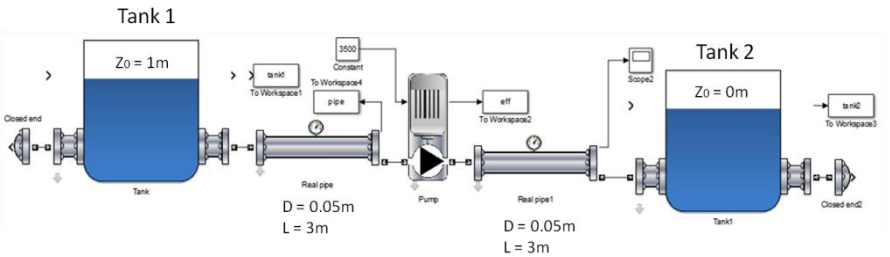

Figure 87: Simulink diagram for Example 4. Fuel in one tank is transfered to another tank by a pump that uses real pipes.

The evolution of the first tank level and its output flow velocity is shown in the next figure:

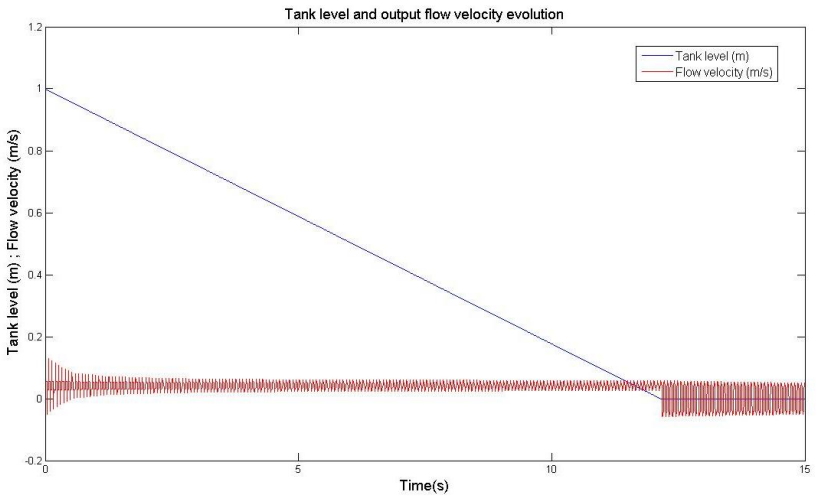

Figure 88: First tank level and output flow velocity while emptying

Of course, the level of the second tank is the opposite of this first tank:

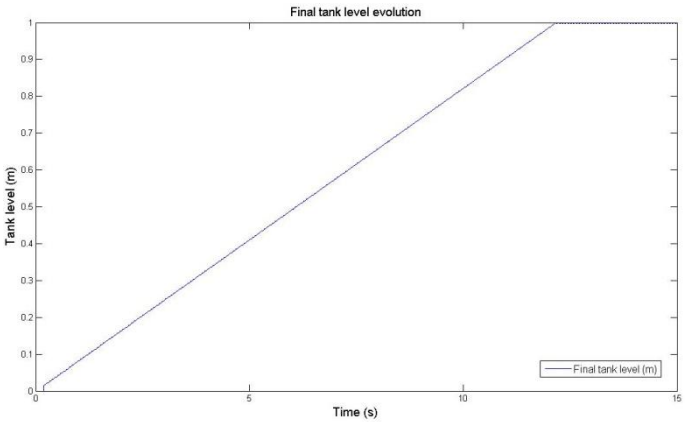

Figure 89: Second tank level while filling

The transient behavior of the piezometric head and flow velocity inside the pipe from the first tank is:

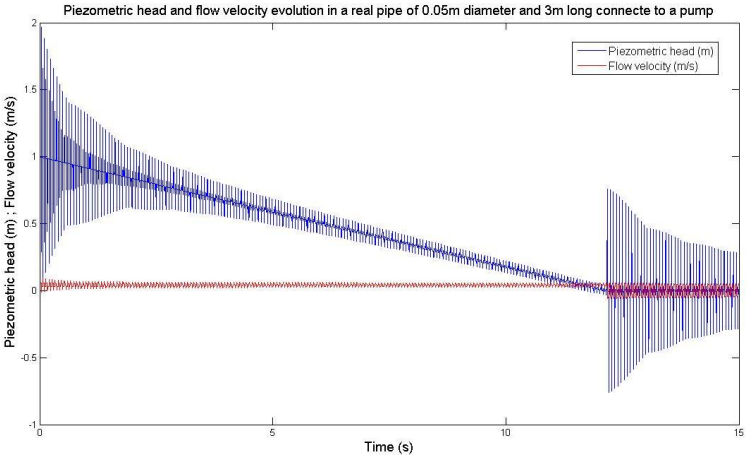

Figure 90: Pressure height and flow velocity inside the pipe from the emptying tank

In this case, the oscillations goes back and forth around the tank level until it is empty, when the output velocity becomes zero (since there is no more fluid to

move) that generates a new pressure peak and transient with a zero mean velocity and pressure.

The efficiency of the pump is:

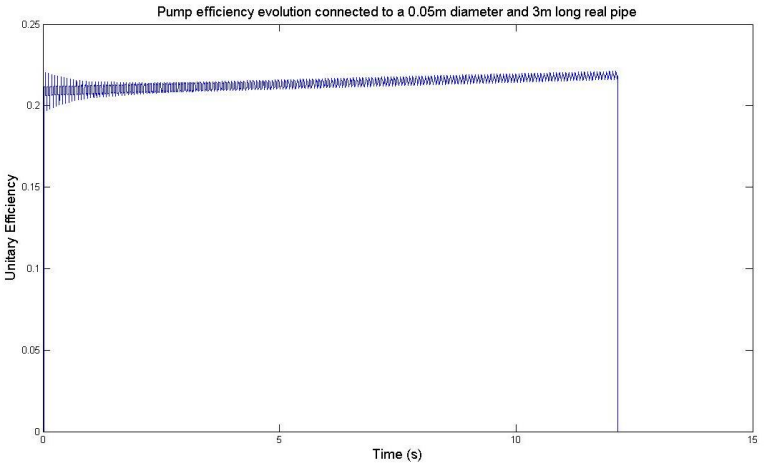

Figure 91: Pipe efficiency while transferring fluid from one tank to another

The efficiency is dependent on the pump RPM and the pressure difference between the input and output. The ringing is due to the pressure transients generated by the pipes, while its increasing mean is due to the higher pressure at the output due to the increasing level in the output tank. When there is no more fluid to transfer, it goes to zero, since it is still running but no fluid is moving.

Lund University
Department of Automatic Control
Box 118
SE-221 00 Lund Sweden

Document name
MASTER´S THESIS

Date of issue
June 2014

Document Number
ISRN LUTFD2/TFRT--5956--SE

Author(s)
Carlos Jorques Moreno

Supervisor
Ola Stenlåås, Scania
Tore Hägglund, Dept. of Automatic Control, Lund University, Sweden (examiner)

Sponsoring organization

Title and subtitle

Optimization and control of feed and transfer pumps

Abstract

A new low pressure fuel system implementation for Scania's trucks is being investigated. The main challenge consists in exchanging the mechanical pump with electrical pumps. The electrical pumps must then be controlled to supply exactly the demanded amount of fuel at the required pressure. System redundancy allows a lot of degrees of freedom influencing the final performance.

This thesis studies the factors influencing system's performance to design a controller that enhances its behavior. The physical basis of the elements in the system are investigated and stated with that purpose.

The system is analyzed and the output pressure and tank level are controlled by a LQG regulator giving successful results in reference tracking. Integral action is included for disturbance rejection and the states are estimated to overcome quantifications and noise from the signals. The disturbance rejection performance is improved by extending the regulator with a Smith Predictor for time delay compensation and including information about the engine mass-flow demand. The control actions are minimized by the tuning of the controller in order to extend component's life. The controller includes different modes for when an external action should be input e.g., when a diagnosis test must be run.

The optimization of free set-points is discussed and holistic criteria from experience is set. The result is that the system endurance is enhanced by running only two pumps when one does not provide higher efficiency. Results show that different pumps should be chosen in the final design for an improvement of the global efficiency.

Future work will consist in implementing the resulting controller in the real system built with actuators selected accordingly to the optimization results.

Keywords

Classification system and/or index terms (if any)

Supplementary bibliographical information

ISSN and key title
0280-5316

ISBN

Language
English

Number of pages
1-168

Recipient's notes

Security classification